Annual Report 2003

Center for Micro- and Nanotechnologies

ZMN

Technical University of Ilmenau

th

Front page (from left to right):

LTCC chip for microwave applications in satellite communications

Technical solution for an artificial Phloem cell

SiC/Si nozzles formed by ECR etching for MEMS applications

Surface analytic module

WC/C multilayer structure for tribological coatings

Schematic layer structure of a SiC transistor for GHz applications

Layout/press:
Klapproth and Koch, Weimar

Funding:
µ-Comp e. V.

Preface

The entire staff at the Center for Micro- and Nanotechnologies (ZMN) is dedicated to pursuing education, research, and innovation in micro- and nanotechnology. The research is focused on the development of smart materials, the patterning of novel micro- and nanostructures, the design and realization of devices, and the development of systems demonstrating possible applications for future industrial technologies.

In 2003, important goals were reached which contributed to the further improvement of the infrastructure of the Center for Micro- and Nanotechnologies (ZMN). This progress has increased the number of scientists that can benefit from the outstanding technological and analytical equipment within the ZMN and has allowed the number of projects running simultaneously in the ZMN clean rooms to grow in number. The key to the center's success is the interdisciplinary cooperation of several chairs belonging to three different faculties. Based on interdisciplinary cooperation between scientists with expertise covering the key fields of design, materials, technology, devises, and systems, the primary mission of the ZMN is to provide an intellectual and working environment that enables education through teaching and research in areas that require or may benefit from advanced silicon based microsystems, wide bandgap semiconductor nanostructures, ceramics for microperipherics, polymer heterostructures for electronic devices, novel positioning systems, or advanced tools for structural and surface analytics.

The evaluation procedure required before the Technical University (TU) was allowed to join the German Research Foundation (DFG) was located at the ZMN which obviously was one of the important reasons for its success. This event was one of many in which the ZMN and its members were able to improve the reputation of the Technical University of Ilmenau. In spring 2003, referees of the DFG approved additional funding for investments which will include an e-beam lithography system and a complex system for producing hetero- and nanostructures based on metal oxides and metal nitrides. Furthermore, since the inauguration of the ZMN in March 2002, the scientific teams in the ZMN have raised more that 10 M € which are distributed over about 30 projects.

One of the outstanding projects funded by the Thuringian Ministry is focused on the creation and analysis of nano- and picoliter droplets of water based liquids. The goal of this project, which involves all partners in the ZMN, is to build a system which allows the identification of organic substances by a combination of transparent electronic sensors for biotechnological and medical applications.

It is my pleasure to summarize some additional and exemplary highlights of 2003:

Feburary	Evaluation by the DFG resulting in additional funding.
March	Dipl.-Ing. Michael Fischer joins the ZMN staff.
March	First anniversary of ZMN.
April	Funding by the BMBF to map out a strategy for a *Center of Innovation competence*.
April	Kirsti Schneider becomes a permanent member of the ZMN staff in order to organize the financial aspects of a fast increasing number of projects.
June	First plenary ZMN meeting with invited speaker.
September	Workshop „MacroNano".
October	Representatives of the VDI/VDE-IT „microtechniques" visit the ZMN. This is the first step towards organizing a conference related to microsystems in 2004.
November	Submission of a completed concept for a *Center of Innovation competence* funded by the BMBF.
December	PD Dr. Frank Schwierz successfully finalizes his habilitation.

The 2003 Annual Report of the Center for Micro- and Nanotechnologies provides a much more detailed overview of the facilities, staff, faculties, and students associated with the ZMN, as well as a description of many of the ongoing research projects which make use of the ZMN facilities. These developments, which are based on close links with industry and cooperation with German, as well as international institutes, contribute to the advanced education for our students.

I would like to take this opportunity to thank all my colleagues, the scientific fellows, and technicians for all their dedicated work. We kindly acknowledge the support of the Federal Ministry of Research, the German Science Foundation, the Thuringian Ministry of Science, and the European Commission.

I look forward to participating in the promising development of innovative micro- and nanostructures, new devices, and concepts through the use of semiconductor technology.

Sincerely,

Oliver Ambacher

Contents

Scientific Activities - Titles 4

Development of the ZMN 5

Research Departments and Staff of the ZMN 7
- Materials Science 8
- Technology 10
- Design 14
- Devices 15
- Modules 16
- Systems 18
- Analytics 18

Infrastructure and Equipment 20

Finances 25

Scientific Activities
- Materials Science 26
- Technology 38
- Design 54
- Devices 56
- Modules 68
- Systems 74
- Analytics 78

Publications and Conference Contributions 92
- Materials Science 92
- Technology 93
- Design 95
- Devices 95
- Modules 96
- Systems 97
- Analytics 98

Theses 100

Invited Talks and Colloquia 101

Scientific Projects 102

Scientific Activities - Titles

Materials Science
Nanoscale multilayer WC/C coatings developed for nanopositioning

Bias-magnetron sputtering of tungsten carbide coatings on steel

Thin film materials and structures for microsensors

Low-emitting ceramic layers

Preparation and investigations of nickel zinc ferrite layers on copper foils for the processing of printed circuit boards

Preparation of hexagonal WSi_2 and tungsten silicide metallization with adjustable thermal coefficients of the electrical resestivity

Technology
Functional liquid-crystalline elastomers in microsystems

ECR-etching of 3C-SiC for MEMS

Education network for the maintenance of qualified employees in microsystems technology in Thuringia

Characterization of vertical regions of microstructures based on monochromatic speckle-techniques

Modification of GaN and AlGaN surfaces for nano- and picofluidic sensors

Modelling and alignment of SiC quantum dots

Forisomes in MEMS

A new type of heterostructures for SiC technology: 3C-$(Si_{1-x}C_{1-y})Ge_{x+y}$ /4H-SiC

Design
New materials and technologies for printed circuit boards - A development from the perspective of new demands for environmental-friendly products and production steps

Devices
Pt/GaN Schottky diodes for hydrogen gas sensors

The detection of oxygen at the electrode/polymer interfaces in polymer solar cells

Design development, technology optimization, and electrical characterization of silicon carbide MESFETs

The preparation of novel group III-nitride based micro- and nanomechanical devices

Submicrometer organic field-effect transistor

Electron mobility models for GaN and AlGaN/GaN

Modules
Advanced LTCC processes using Pressure Assisted Sintering

Ultrasonic and x-ray inspection of multilayer PBC and LTCC hybrid circuits - comparison and advantages of both methods

KERAMIS: 20 GHz LTCC applications for satellite communications - Challenges for design and technology

Systems
Experimental set-up and investigations for an integrated measuring station for the examination of biological material in the nano- and picovolume range

Investigation of the metrological characteristics of the nanopositioning and nanomeasuring machine with an integrated focus sensor

Analytics
Characterization of SiC/Si heterostructures and GaN films on sapphire by infrared spectroscopic ellipsometry

Structural investigations of cubic InN

Determination of dopands and polytypes of SiC by Auger Electron Spectroscopy

Organic field effect transistors: the molecule-metal interface

Defect related absorption and emission of AlGaN based UV photodetectors

Thermal stability of polycrystalline and epitaxial Indium Nitride layers

Plasma deposited fluorocarbon films as anti-wetting and structurable coatings for applications in nano- and picofluidic sensors

Development of the ZMN

In the mid 1980s, the initial idea surfaced for creating a center focussing on science and technology in the areas of microelectronics and micromechanics at the Technical University of Ilmenau. The plan resurfaced in 1990 with the aim of hosting multiple advanced technology and materials oriented research groups in one central laboratory building. Only by bringing together technological potential and high efficiency can quality research and education be guaranteed. Thus, in autumn 1990, the Electrical Engineering faculty installed a commission to create a concept addressing this subject.

Laying of the foundation in 1999

Moving of scientific equipment into the ZMN

This concept was realized in certain steps:

January 1991
Completion of a concept for a shared technological institution for teaching and research by the faculty of Electrical Engineering and Information Technology (5000 m^2).

June 1994
Suggestion for an expansion to other faculties.
Inclusion of microsystems technology and physics.
Focus on one research building for a reduced need of space and costs.

March 1995
Contract between the TU Ilmenau and Siemens AG on a formulation of a concept for a technological laboratory building.
Provision of the finances through the state of Thuringia.
Completion of the concept in August 1995.

August 1995
Project outline for a technology building for the faculties of Electrical Engineering and Information Technology, Mechanical Engineering, and Mathematics and Natural Sciences with the research focus „New materials, technologies and systems for applications in the fields of information and microsystems technology".

May 1997
Recommendation of the Wissenschaftsrates for the classification of the technology building in the 27th Rahmenplan Hochschulbauförderung as category I.

January 1998
Fixing of the costs with approx. 15 M € for the building and approx. 12 M € for the scientific equipment.

April 1999
Application for large equipment in the context of Hochschulbauförderung (HBFG) of approx. 10 M €.

August 1999
Laying of the foundation.

September 1999
Expert meeting of the German Research Council addressing the requirements of the technology building and larger equipment.

October 2000
Foundation of the Center for Micro- and Nanotechnologies (ZMN).

March 2002
Transfer of the technology building to the ZMN as the user of the building.

During the foundation of the ZMN nine departments contributed to the ZMN and brought in scientific equipment, most of which was new:

Faculty of Electrical Engineering and Information Technology:

Department of Solid-State Electronics
Department of Design and Technology of Electronic Compounds
Department of Microperipherics
Department of Nanotechnology
Department of Materials for Electronics

Faculty of Mechanical Engineering:

Department of Process Measurement
Department of Micromechanics
Department of Materials Technology

Faculty of Mathematics and Natural Science:

Department of Technical Physics.

The director of the ZMN is the head of one of the departments and elected by the Zentrumsrat.

The tasks of the Center for Micro- and Nanotechnologies consist of two main points:

(1) The ZMN is the central scientific facility of the TU Ilmenau for research and teaching in the fields of advanced technology. Departments from different faculties cooperate and work towards the realization of the ZMN research strategy „new materials, technologies, and systems for applications in the fields of information and microsystems technology".
(2) Aside from the specific duties of the departments in teaching, research, and further education, the ZMN serves as an interdisciplinary research center in the fields of micro- and nanotechnology for the complete university. The main emphasis of the research is on the cutting edge of nanotechnology.

Start-up time period
Insight was given by the Thuringian Ministry for Science, Research, and Art (TMWFK) concerning general support and a fast and comprehensive ramp-up of the highly equipped laboratories by special start-up projects. Thus, specific start-up projects were formulated and finally approved. Some of these are still effective:

The aim of this start-up time period was:

1. a fast and comprehensive implementation of the scientific equipment,
2. the testing and obtaining of the achievement limits of the equipment.

Start-up projects:

- Organische Schichten und ihre Grenzfläche zur Anwendung in Feldeffekt-Transistoren (OFET).
- Wachstumskinetik und elektrische Eigenschaften niedermolekularer organischer Funktionsschichten für die Anwendung in Feldeffekttransistoren.
- Neue Materialkombinationen für SiC-Feldeffekttransistoren (NEMASIC).
- Untersuchung zur Entwicklung von Polymeren und organischen Mischschichten für Solarzellen (ORSOL 1).
- Nanopartikelinduzierte Oberflächenmodifikation und Analyse (NANOVSS).
- Neue Technologievarianten von Mehrlagen-Keramikmodulen für Frequenzbereiche über 20 GHz.
- GaN-basierte UV-Detektoren für die Si-Technologie (UVSENS).

Research Departments and Staff of the ZMN

Administration

Faculty and Staff:

Oliver Ambacher
director, current
fon: -3402

Theodor Doll
director, former
fon: 06131-990-100

Heiko Thust
deputy director
fon: -2605

Herwig Döllefeld
abstractor
fon: -3400

Kirsti Schneider
financial management
fon: -3497

Katrin Dünkel
financial management
fon: -3497

Renate Röhner
office
fon: -3401

Torsten Sändig
head of technical engineering
fon: -3415

Olaf Marufke
network administration
fon: -3416

Michael Fischer
technical engineering
fon: -3413

Birgitt Hartmann
technical coworker
fon: -3426

Andreas Schober
scientific coworker
fon: -3486

Gerd Eichhorn
central services

Contact:
Renate Röhner, fon: +49-(0)3677-69-3401
email: renate.roehner@tu-ilmenau.de

Materials Science

Department of Metallic Materials and Composite Materials

With the appointment of Prof. Dr.- Ing. habil. H. Kern in 1996 as head of the department of Metallic Materials and Composite Materials Technology, the teaching and research activities related to materials at the Technical University of Ilmenau gained new momentum. The integration of the department into the Faculty of Mechanical Engineering reflects the significance of materials science engineering. The research areas in the department cover metallic, non-metallic, inorganic, and composite materials. The focus of the research is the improvement of available conventional materials, the development of new materials, and the creation of innovative material approaches.

Research Activities
- Tribological behaviour of materials and surface topography
- Characteristics of ceramic suspensions (rheology)
- Ceramic shaping
- Electrophoretic deposition
- Materials testing
- Metallography, microscopy and image processing techniques
- Special materials for mechanical engineering
- Composite Materials
- Metal-ceramic and ceramic matrix composites
- Glass matrix composites
- Interfacial characterization and interface design of composites

Faculty and Staff:

Prof. Dr.-Ing.
Heinrich Kern
head of department
fon: -2450

Kerstin Pfeiffer
technical coworker
fon: -1831

Contact:
Irina Hoffmann, fon: +49-(0)3677-69-2801
email: irina.hoffmann@tu-ilmenau.de

Department of Materials for Electronics

The department of Materials for Electronics is concerned with the development of new materials for nanopositioning, as well as the development of new metallization materials for wide bandgap semiconductor contacts. Furthermore, this department focuses on the analysis of liquid metals and the development of new adaptive materials which have low or negative thermal coefficients. These materials are produced via sputtering of thin films or by electrochemical or electrophoresis methods. Samples of different materials such as deposited layers and post annealed layers are provided also from other groups of the university, as well as industrial partners.

The main focus of this work is analysis with different methods:
- X-ray diffraction in different measurements setups,
- X-ray fluorescence spectroscopy, X-ray imaging
- analytical scanning electron microscopy (ESEM, EDX, EBSD)
- analytical transmission electron microscopy (EDX, PEELS, diffraction, high resolution)
- atomic force microscopy
- different electrical methods
- thermo wave inspection system
- classical mechanical testing of materials

Faculty and Staff:

Prof. Dr.-Ing. Dr. rer. nat. Christian Knedlik
head of department
fon: -3611

Lothar Spieß
scientific coworker
fon: -3403

Volkmar Breternitz
scientific coworker
fon: -3134

Andrey Chuvilin
scientific coworker
fon: -3486

Maik Gubisch
scientific coworker
fon: -3404

Thomas Kups
scientific coworker
fon: -3352

Henry Romanus
scientific coworker
fon: -3404

Friedhelm Scharmann
scientific coworker
fon: -3135

Elvira Remdt
technical coworker
fon: -3404

Jens Schawohl
technical coworker
fon: -3403

Without picture:

Manuela Breiter
scientific coworker

Gerd Teichert
scientific coworker

Contact:
Brigitte Weiß, fon: +49-(0)3677-69-3610
email: brigitte.weiss@tu-ilmenau.de

Technology

Department of Microsystems Technology

Microsystem technology combines actuators, sensors, and other electronic components on the smallest dimensions. Various principles from all areas of technology (mechanics, actuators, fluidics, optics, and chemistry) are included in this field. The research in the department of Microsystems Technology is focused on microfluidics, as well as sensors and actuators containing active piezo layers.

Certain functions and properties which are not achievable through the conventional combination of macroelectronic components are obtainable through miniaturization and functional integration. Technologies such as ink jet printing, arrays and plates for microreactions, and micromixing have been technically realized only through the use of micron sized structures. These systems have begun to approach biological systems in their complexity. In the meantime, first principles of nature are integrated in microsystem devices.

The department of Microsystems Technology deals particularly with the outline, design, and production of complex micro mechanical and micro fluidic systems through the execution of functional measurements on the micron scale. Through the integration of microsystem technology into the faculty of Mechanical Engineering, there is a symbiosis between the classic disciplines and microsystem technology, this also influences the new field of mechatronics.

Since 1986 a group of experts has dealt with the development of micro components under the direction of Prof. Helmut Wurmus. In 2002 the department moved to the Center for Micro and Nanotechnologies (ZMN).

Faculty and Staff:

Prof. Dr.-Ing.
Helmut Wurmus
head of department
fon: -2487

Matthias Kallenbach
scientific coworker
fon: -3424

Arne Albrecht
scientific coworker
fon: -3426

Julian Botiov
scientific coworker
fon: -3426

Jörg Burgold
scientific coworker
fon: -3425

Mathias Bründel
scientific coworker
fon: -3422

Faculty and Staff:

Tamas Fischl
scientific coworker
fon: -1295

Sigmar Hecht
scientific coworker
fon: -2479

Balázs Horváth
scientific coworker
fon: -1295

József Król
scientific coworker
fon: -1295

Mike Stubenrauch
scientific coworker
fon: -3422

Frank Weise
scientific coworker
fon: -3423

Christoph Kremin
diploma student
fon: -3426

Lothar Dressler
technical coworker
fon: -3421

Karin Friedel
technical coworker
fon: -3421

Gabriele Harnisch
technical coworker
fon: -3422

Birgitt Hartmann
technical coworker
fon: -3426

Christine Lohmann
technical coworker
fon: -3425

Without picture:

Feng Qiao
scientific coworker

Contact:
Annette Volk, fon: +49-(0)3677-69-2485
email: annette.volk@tu-ilmenau.de

Department of Nanotechnology

Nanotechnology, "the manufacturing technology of the 21st century", should allow us to build a broad range of complex molecular machines (including, not incidentally, molecular computers). This technology will give us the means to build fleets of computer controlled molecular tools that are much smaller than a human cell. Such tools allow medicine, for the first time, to intervene at the cellular and molecular level in a sophisticated and controlled way. They could remove obstructions in the circulatory system, kill cancer cells, or take over the function of subcellular organelles. Just as today, we have the artificial heart, so in the future we may have the artificial mitochondrion.
Equally dramatic, Nanotechnology will give us new instruments to examine tissue in unprecedented detail. Sensors smaller than a cell would give us an inside and exquisitely precise look at ongoing cellular functions. Tissue that was either chemically fixed or flash frozen could be analyzed literally down to the molecular level, giving a completely detailed "snapshot" of cellular, subcellular, and molecular activities.
For this purpose, the Chair of Nanotechnology and his members are concentrating on the development of novel materials and nanostructures for electronic devices especially dedicated to sensor applications. Our research topics include hetero- and nanostructures for light detection, extremely light NanoElectroMechanical Systems (NEMS), and piezoelectric sensors for nanolitre droplets which are optimized for the detection of small organic systems such as viruses or single molecules.

Faculty and Staff:

Prof. Dr. rer. nat.
Oliver Ambacher
head of department
fon: -3723

Jörg Pezoldt
scientific coworker
fon: -3412

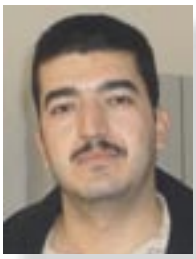

Majdeddin Ali
scientific coworker
fon: -1172

Maher Al Ibrahim
scientific coworker
fon: -3409

Carsten Buchheim
scientific coworker
fon: -1172

Dorin Cengher
scientific coworker
fon: -3352

Genady Cherkashinin
scientific coworker
fon: -3352

Irina Cimalla
scientific coworker
fon: -3352

Volker Cimalla
scientific coworker
fon: -3408

Gernot Ecke
scientific coworker
fon: -3407

Faculty and Staff:

Christian Förster
scientific coworker
fon: -3352

Ute Kaiser
scientific coworker
fon: -3404

Gabriel Kittler
scientific coworker
fon: -1172

Vadim Lebedev
scientific coworker
fon: -3410

Thomas Stauden
scientific coworker
fon: -3409

Ronny Wagner
scientific coworker
fon: -3408

Petia Weih
scientific coworker
fon: -3352

Charbel Zgheib
scientific coworker
fon: -3408

Oliver Schulz
diploma student

Ilona Marquardt
technical coworker
fon: -3230

Silvia Probst
technical coworker
fon: -3230

Dietmar Schäfer
technical coworker
fon: -3230

Willy Schliefke
technical coworker
fon: -3418

Jutta Uziel
technical coworker
fon: -3230

Without picture:

Rastislav Kosiba
scientific coworker

Contact:
Simone Gutsche, fon: +49-(0)3677-69-3724
email: simone.gutsche@tu-ilmenau.de

Design

Department of Design and Technology of Electronic Components

Research in the department of Design and Technology of Electronic Components is focused on Computer Aided Design (CAD) of thick film hybrid components including the simulation of thermal behaviour. This work includes the simulation of frequency and time domain behaviour of solid and gridded reference power/ground planes in Low Temperature Cofired Ceramics (LTCC) modules. Available software includes an extensive Computer Aided Engineering (CAE) system from Mentor Graphics® installed on a SUN compute server system.

Other topics include the development of new technologies and materials for environmental friendly production, as well as easy to recycle electronic devices and assemblies.

The laboratories of this group establish an interesting connection with the Microperipheric group (also in the ZMN) which provides technological equipment for production of Printed Circuit Boards (PCB) and LTCC modules. Furthermore, modern analytic facilities at the ZMN allow testing by ultrasonic and X-ray inspection systems.

Faculty and Staff:

Prof. Dr.-Ing.
Gert Winkler
head of department
fon: -2606

Gernot Bischoff
scientific coworker
fon: -1116

Aneta Sutor
scientific coworker
fon: -1119

Thorsten Mülln
scientific coworker
fon: -1118

Contact:
Regina Simon, fon: +49-(0)3677-69-2604
email: regina.simon@tu-ilmenau.de

Devices

Department of Solid-State Electronics

The research projects of the deptartment of Solid-State Electronics are focused on the development and investigation of advanced semiconductor devices. The department consists of four research groups dealing with

- Polymer devices (organic field-effect transistors, new organic materials for electron devices),
- RF and nanodevices (nanometer MOSFETs, SiGe HBTs, wide bandgap devices),
- Power electronics (IGBTs, reliability issues, control circuits),
- Sensors.

The work of the four groups includes the investigation of basic operation principles, device simulation, device design and optimization, fabrication, and characterization. Polymer and wide bandgap devices are fabricated in-house, while other devices, such as SiGe HBTs, are fabricated in the facilities of partners in the semiconductor industry. The research projects of the dept. are supported by the European Community, German federal agencies (BMBF, DFG), the Federal State of Thuringia, and by industry (e.g., Semicron, Atmel).

Faculty and Staff:

Ingo Hörselmann
scientific coworker
fon: -3406

Mario Kittler
scientific coworker
fon: -1550

Gundis Bauer
technical coworker
fon: -3423

Silvia Klaube
technical coworker
fon: -3222

Prof. Dr.-Ing.
Theodor Doll
head of department
fon: 06131-990-100

Susanne Scheinert
scientific coworker
fon: -3222

Ali Chaybon
scientific coworker
fon: -1589

Jörg Geßner
scientific coworker
fon: -3219

Frank Haase
scientific coworker
fon: -3219

Andrei Herasimovich
scientific coworker
fon: -3406

Frank Schwierz
scientific coworker
fon: -3120

Christian Fachmann
diploma student
fon: -3413

Contact:
Silvia Herda, fon: +49-(0)3677-69-3717
email: silvia.herda@tu-ilmenau.de

Modules

Department of Microperipherics

The Microperipheric group focuses on the examination of the microwave range properties of passive structures manufactured with thick film hybrid and LTCC (Low Temperature Cofired Ceramics) techniques. The microwave frequency area will be used in the near future for new applications such as telecommunication, satellite navigation, and automotive applications. Further applications of interest include sensor and micro system technologies (micro fluidics and micro optics). Therefore, it is necessary to study exact models of hybrid elements which can be developed as a result of advanced-technology research.

We have a fully equipped laboratory for manufacturing thick film circuits (screen printing, punching, sintering, and laser structuring) and LTCC tapes. Modern analytic equipment such as ultrasonic and X-ray inspection systems, as well as other measurement equipment (network analyser, impedance analyser, spectrum analyser) are also available. In addition, we have access to a complete technology laboratory for printed circuit boards.

One specific topic is the optimization of process steps for special materials and applications, as well as 3D applications in LTCC like sensors, packaging, and other MST components. Another main research focus is the RF (radio frequency) and microwave design of multilayer devices, MCM's (multichip modules), and packaging. Furthermore, another topic includes the thermal analysis and simulation of printed elements, materials, and connections.

Main research topics:

- Integration of new materials (ferrite, PZT, high-k and low loss- inks and tapes) and materials chracterization up to current experimental limits (regarding temperature, environment, and frequency).
- Optimization of process steps, design and technology for special applications and modified technologies (like photo defined inks or zero-shrinking methods).
- Further development of LTCC technology for packaging and for combination with other micro technologies (micro fluidic-, sensor- and micro system-elements).
- Development of models and simulation data for elements and structures.
- Development of design and technology specifications.

Faculty and Staff:

Prof. Dr.-Ing.
Heiko Thust
head of department
fon: -2605

Karl-Heinz Drüe
scientific coworker
fon: -3429

Waleed Ehrhardt
scientific coworker
fon: -1117

Michael Hintz
scientific coworker
fon: -3430

Ralph Münnich
scientific coworker

Ruben Perrone
scientific coworker
fon: -1360

Torsten Theleman
scientific coworker
fon: -1118

Uwe Genatis
technical coworker
fon: -3427

Ina Koch
technical coworker
fon: -3455

Regina Lenk
technical coworker
fon: -3440

Martina Sieler
technical coworker
fon: -3428

Contact:
Regina Simon, fon: +49-(0)3677-69-2604
email: regina.simon@tu-ilmenau.de

Systems

Department of Process Measurement

The department of Process Measurement, together with the department of Mechanical Engineering Measurement and Production Measurement, forms the institute of Process Measurement and Sensor Technology. At the Technical University of Ilmenau, this institute is in charge of teaching instruction in the areas of process measurement, production measurement, sensor technology for automation engineering, computer-aided processing of measuring values, measurement dynamics, laser and precision measurement, analysis and environmental measurement, and calibration techniques. The institute fulfils its teaching assignments not only in the stage-I- and stage-II-studies for the Faculties of Mechanical Engineering, Electrical Engineering and Information Technology, Computer Science and Automation as well as Business Administration, but, it is also responsible for academic training in the branch of study entitled "Process Measurement and Sensor Technology." The highly qualified and practical-oriented training of students is based on extensive research in cooperation with a number of partners from industry as well as the BMBF (Federal Ministry of Education and Research), the DFG (German Science Foundation), and the Thuringian Ministry of Science, Research, and Art.

Faculty and Staff:

Prof. Dr.-Ing.
Gerd Jäger
head of department
fon: -2824

Eberhard Manske
scientific coworker
fon: -1250

Rostyslav Mastylo
scientific coworker
fon: -1836

Contact:
Cordula Höring, fon: +49-(0)3677-69-2822
email: cordula.hoering@tu-ilmenau.de

Analytics

Department of Technical Physics

In the age of miniaturization and nanotechnology, our main research topics cover the very interesting field of surface science on the atomic scale. The main focus of this research is to investigate the possibilities of controlling the fundamental elements of condensed matter: atoms and molecules on solid surfaces. The concept of "customized" materials plays an important role in the optimization of the performance of electronic, optoelectronic, and mechanic devices.
The ability to produce structures atom by atom or molecule by molecule would allow the creation of a large array of specialized materials and functional structures; this is the long-term goal of nanotechnology. It is already possible to manipulate single atoms, for example, by using the tip of a scanning tunnelling microscope to influence the position of adsorbed atoms or to investigate chemical reactions of single molecules. The full potential of surface sensitive techniques offers promising possibilities for future research. In this context, our group investigates organic-inorganic interfaces, the mechanical contact between macroscopic and microscopic solid surfaces (including biological systems), as well as the growth and characterization of carbon layers, specifically C_{60}-molecules and carbon nanotubes.
Another focus of our group's research is the growth and characterization of compound semiconductors such as silicon carbide and the group III-nitrides. These materials show promise for use as high temperature and high frequency electronic devices for sensor applications. Furthermore, electrical contacts (such as those based on metal carbides) and epitaxially grown insulating layers have a strong influence on device performance.
Another growing field of research is the investigation of friction and wear. Fundamental processes on macroscopic and microscopic scales are currently being investigated by our group. Additionally, several analytical measurements are performed by our group for a variety of researchers inside the TU Ilmenau as well as for outside companies.

Topics

- Processing of ultrathin layers
- Surface and interface properties on atomic scale
- Structural, electronic and vibronic properties of semiconductors: SiC and group-III nitrides
- Doping profiles in semiconductors
- Structure formation of organic layers
- C_{60}, nanotubes, nanowires
- Interaction of hydrogen with silicon surfaces
- Microtribology in micromechanical systems
- UHV tribology
- Technical properties of fluorescent lamps

Faculty and Staff:

Prof. Dr. rer. nat.
Jürgen A. Schäfer
head of department
fon: -3609

Stefan Krischok
scientific coworker
fon: -3405

Andreas Opitz
scientific coworker

Rolf Öttking
scientific coworker
fon -3215

Vasil Yanev
scientific coworker
fon: -3417

Marcel Himmerlich
diploma student
fon: -3417

Annette Läffert
technical coworker
fon: -3417

Without picture:

Oleg A. Balykov
scientific coworker

Sebastian Oßwald
student

Contact:
Jana Spindler, fon: +49-(0)3677-69-3608
email: jana.spindler@tu-ilmenau.de

Infrastructure and Equipment

The science center, which holds an overall laboratory space of more than 1000 m², hosts a clean room facility of about 700 m² with various clean room classes. While about 400 m² are classified as clean room class 10,000, the remaining 300 m² of space is classified as class 1,000 or even as low as class 100 in the lithography area.
Outside the clean room there are facilities for different technologies such as the printing of circuit boards, a laser lab for the trimming and cutting of specimens addressing the packaging applications of devices, and the central application lab which addresses the construction of large and sophisticated complete systems. Furthermore, analytical devices on the nanoscopic scale, which require a very low level of vibration, are located in the basement of the building.

Technological labs and equipments inside the cleanroom:

Polymerelectronics lab

Evaporation system (Edwards Auto 306)

Glovebox used for preparation of polymer films (Braun)

Maskaligner (JUB 2104 Elektromat)

Spincoater (Convac)

Glove-Box

Thin film measurement lab

Optical surface profiler (UBM, UBC 16)

Measurement system for degradation of conductive layers (Karl Süss)

Diverse microscopes

Ellipsometer (SD 2300 - Plasmos)

Stress measurement system (TENCOR)

Tactile surface profiler (Ambios Technology)

Film thickness measurement system (Mister)

Ellipsometer

Optical lithography lab

Anodic bonding tool EV501 (EVG)

Automatic spincoater CEE 4000 (Brewer Science)

Double side maskaligner AL6-2 (EVG)

Semiautomatic spincoater CEE CB100 (Brewer Science)

Spraydeveloper Delta 20 (BLE)

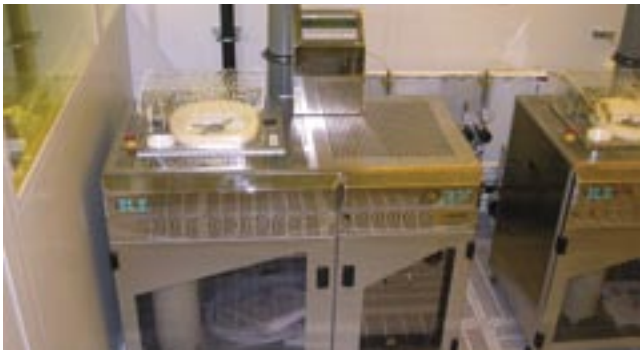

Spraydeveloper

Wet chemical processes lab

Quick dump rinser

Rinser dryer (Semitool)

RCA cleaning process

Wetbenches for several wet chemical etching processes (Kufner)

(metals, metal oxides, silicon, SiO_2, Si_3N_4 ....)

Wetbench

PVD/RIE lab
(physical vapor deposition / reactive ion etching)

Simple evaporation system for metallic layers (Edwards Auto 306)

Cluster system with ISE, sputtering chamber for metals, e-beam evaporation system (Ardenne LES 250)

Cool sputtering system for preparation of SEM samples (Emitec)

ECR dry etching process for siliconcarbide (Balzers PLS 500)

ICP dry etching process for silicon (STS - ASE)

Leybold sputtering system (LAB 500)

PECVD system for SiO_2 and Si_3N_4 (STS 310 PC)

Plasmastripper for removement of resists (TEPLA 200)

Scanning microscope (Hitachi SD 2700)

RIE dry etching process for SiO_2 and Si_3N_4 (STS 320 PC)

RTP system (Jipelec)

Sputtering system for tungsten carbide und silicide (Ardenne LA 440)

Sputtering system for ZnO-films (Nordiko)

ICP-ASE dry etching process for silicon

LPCVD

cluster system with ISE

Sputter system

High temperature processing lab

Atmospheric oxidation system for silicon substrates (wet oxidation)

4-stock LPCVD system for Si_3N_4, TEOS, poly-Si, doped poly-Si (Tempress Systems)

Mounting technologies lab
(mounting and connection technologies)

Cyberscan

Puncher for LTCC tapes („Punche“) (PTC)

Isostatic press

Screen exposure system

Screen printer (EKRA)

Screen washing system

Annealing systems (ATV)

Via filling system

Cyberscan

MBE/Surface analytics lab
(Molecular Beam Epitaxy)

MBE system for SiC, GaN, InN, AlN
(Balzers UMS 500)

Surface analytic modul with several technologies (OMICRON) (STM, AFM, XPS, UPS, AES, RHEED, PEEM, EELS, MBE)

Surface analytic module

Solid state analytics lab

Augerelektron spectroscopy (AES) (Riber)

Photothermal deflections spectroscopy (PDS)

IR ellipsometer (Sentec)

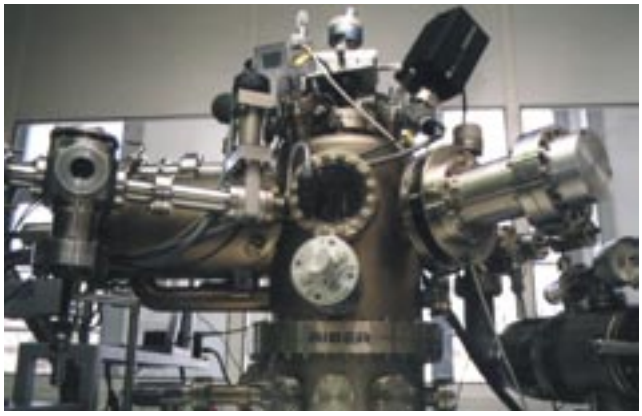

Augerelektron spectroscopy

Electrical characterization lab

Measurement system for gassensors

Hall measurement system (Agilent)

Wafer probe station with HP-tools for electrical characterization (Agilent)

Waferprober

Back end technologies lab
(lab for electronics and testing)

Chemical mechanical polishing system PM5 (Logitec)

Dicing saw DAD-2H/6T(Disco)

Wetbench for sample preparation

Dicing saw

Chemical mechanical polishing

Technological labs outside the cleanroom

Mounting technologies lab I
(mounting and connection technologies)

Heating press (Schmidt)

NdYAG laser (LPKF)

SMD mounter

Annealing system (ATV)

Trimming laser system (Aurel)

NdYAG-Laser

Mounting technologies lab II
(mounting and connection technologies)

Die bonding system (Delvotec)

Wire bonding system (Delvotec)

Fine placer for SMD components

SMD soldering station

Ultrasonic measurement system (Sonoscan)

Wedge bonding system (Delvotec)

Ultrasonic measurement system

Fluidics and bionics lab

Surface tension measurement system (Krüss)

Tribometer (Tetra)

Viscosimeter

Glovebox for experimentals with biological or chemical samples (Ganuk)

Laminar-flow box (Ganuk)

Dosing systems for liquids

Electronmicroscopy lab
(transmission and scanning electronmicroscopy)

Sample preparation for TEM/REM (Gatan)

Scanning electronmicroscope (Philips FEI)

Transmission electronmicroscope (Philips TECNAI)

Atomic force microscope

Transmission electronmicroscope

Scanning electronmicroscope

X-ray analytics lab

X-ray diffractometers (Siemens)

X-ray analytics (Feinfocus)

Diffractometer

Nanomeasurement technologies lab

Measurement system for nanometers (SIOS)

Vibration free lab benches

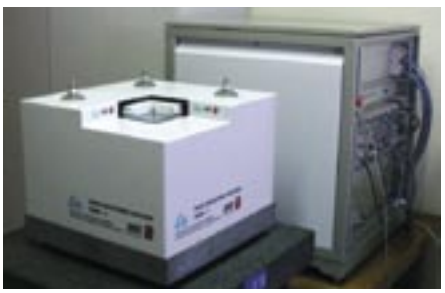

Nanometer measurement and positioning system

Finances

The basic funding for the ZMN is provided by the Technical University of Ilmenau. This covers the cost for the basic operation of the building and the equipment contained within. The total income for ZMN operation amounts to 21,000 €. This funding is provided by the following agencies:

- central funding of the university 7,000 €,
- different faculties 7,000 €,
- chairs active in the center 7,000 €.

The specific expenditures are listed in detail in Fig. 1.

Funding of about 10 M € was raised provided by a third means, i.e. external funding such as e.g. federal or state government or industry. Fig. 2 gives an overview of the different sources.

The development of the overall financial volume of the research projects in the time period of 2002 – 2004 is plotted in Fig. 3.

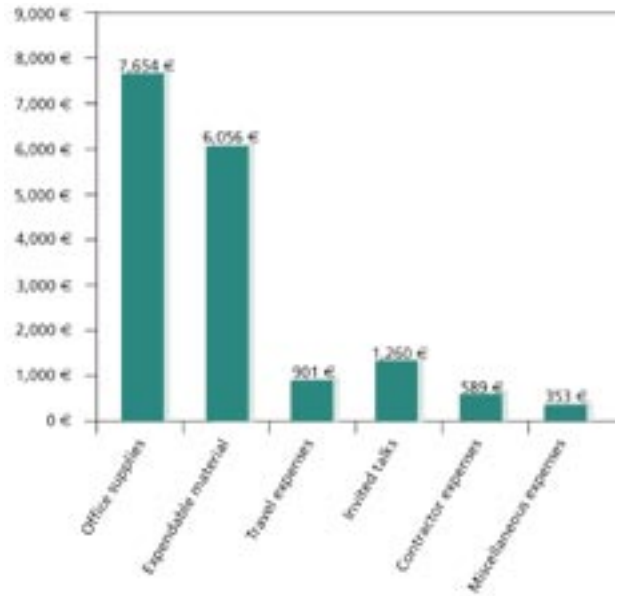

Fig. 1: Household expenses of the ZMN in the year 2003

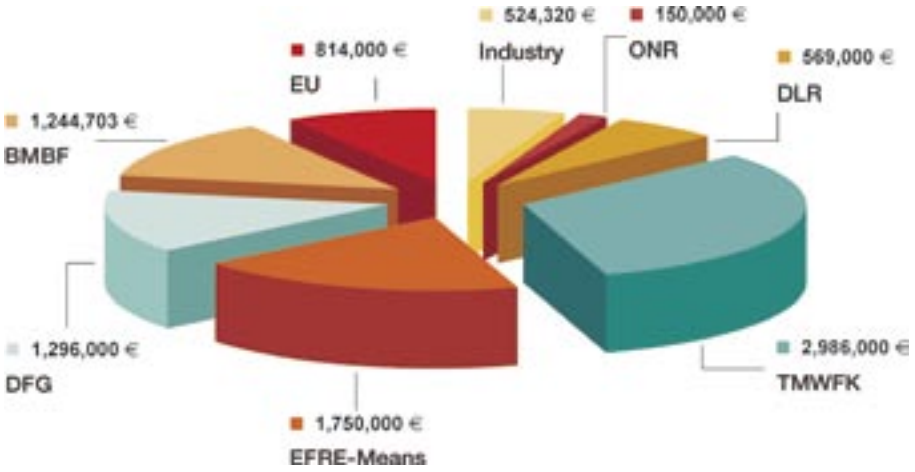

Fig. 2: Fundraising provided by a third means. The contributions of the different agencies are shown.

TMWFK	*Thuringian Ministry for Science, Research, and Art*
EFRE	*European Fond for Regional Development*
DFG	*German Science Foundation*
BMBF	*Federal Ministry of Education and Research*
EU	*European Union*
ONR	*Office of Naval Research*
DLR	*German Aerospace Society*

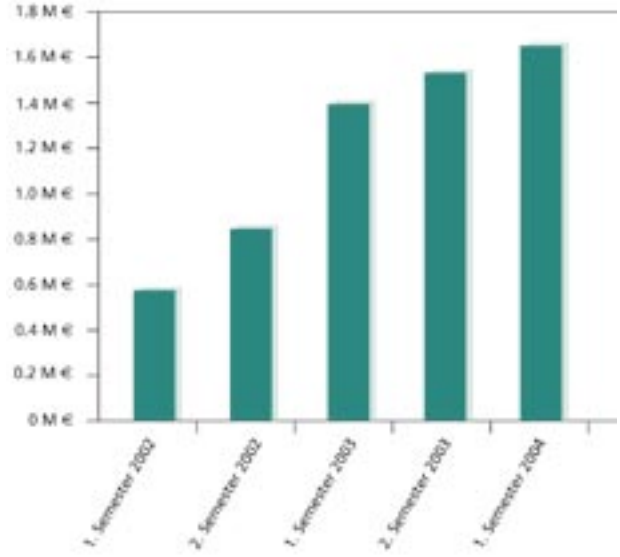

Fig. 3: Research project development 2002-2004

Nanoscale multilayer WC/C coatings developed for nanopositioning

M. Gubisch[1,*], Y. Liu[2], L. Spieß[1], H. Romanus[1], J.A. Schäfer[2], and Ch. Knedlik[1]

[1] Institute for Materials Engineering

[2] Institute for Physics

Introduction

Nanopositioning in wide working distances of several hundred millimeters raises many new requirements on materials, among which the elastic and dimensional stabilities are key issues. At constant temperatures, high elastic stability can be achieved by selecting materials with high Young's modulus in an optimized structure design. In addition, the friction and wear should be stable in the running process since friction instability can result in various problems such as tracking errors in the motion control. Tungsten carbide WC films have drawn considerable interest due to high hardness, extremely high modulus of elasticity above 700 GPa, high thermal conductivity and excellent thermal and dimensional stability, which make them attractive for several applications. A major draw-back for WC are the inadequate tribological properties in contact with steel. Another material with interesting properties for this application is diamond like carbon (DLC). Hard DLC films with rich sp^3 bonds are preferred since the higher amount of sp^3 bonds results in high hardness and high wear resistance. However, the dangling sp^3 bonds at the surface are not beneficial for reducing friction if they are not passivated by adsorption of water molecules, O, and H. A high friction coefficient was observed for sliding tests of diamond films in ultra high vacuum (UHV). The low friction and reasonably long life of DLC are more often attributed to a velocity accommodation mode, the build-up of the transfer film, and subsequent interfilm sliding. If the contact pressure and the sliding speed are high, graphitization of the film analogous to $sp^3 \rightarrow sp^2$ relaxation occurs and the friction coefficient decreases gradually. These results indicate that the two kinds of bonds, sp^3 and sp^2 in DLC films are responsible for the high wear resistance and low friction by providing a hard substrate and a soft interfilm lubricant, respectively, and the gradual $sp^3 \rightarrow sp^2$ transformation provides a continuous supply to compensate lubricant loss from wear. The velocity accommodation mode mentioned before, especially the $sp^3 \rightarrow sp^2$ transformation, might not be favoured by the low running speeds and the low working loads for nanopositioning. Nevertheless, it does give us a hint on the structure of tribological coatings, i.e., with hard substrate and a properly maintained low friction film at the interface. In fact, coatings with such structures have been proposed in the future design of composite coatings. Following this methodology, we developed a tribological coating aimed for nanopositioning. We provided crystalline WC as a hard substrate, amorphous carbon (sp^2 rich DLC) as low friction films (lubricant) in a multilayered structure to ensure a proper supply of lubricant. The microstructure and mechanical properties of the coatings were investigated.

Experimental Details

Nanoscale multilayer coatings with different periods (C5/WC5, C5/10 and C10/20) topped with a carbon layer were deposited in a sputtering chamber (LA440S, Ardenne Anlagentechnik Dresden GmbH) with 90 mm d.c. magnetron sources and an ion etching system. Silicon wafers, which were coated with 10 nm SiO_2 and 200 nm Si_3N_4 were selected as substrates. Targets of chromium (99.8 %), carbon (99.99 %), and sintered tungsten carbide (99.5 %), as well as argon as sputtering gas were provided. The targets were fixed approximately 50 mm underneath the substrate holder, which could be rotated. The pressure in the deposition chamber was maintained at 0.85 Pa.

An adhesion layer of Cr and an intermediate layer of WC were deposited on substrates in sequence with a fixed power density of 3.15 W/cm^2, which resulted in a depositing rate of 2 nm/s and 1 nm/s for Cr and WC, respectively. WC/C multilayers were deposited subsequently on top of the WC intermediate layers by moving the substrate under the WC and C targets. The multilayer period (thickness of neighboring bi-layer of WC and C) and the thickness of a single layer were adjusted by varying the deposition time under each target. The power density during depositing WC and C was maintained at 1.1-3.15 W/cm^2 and 7.86-8.25 W/cm^2, which resulted in a deposition rate of 0.3-1 nm/s and 0.2-0.3 nm/s for WC and C, respectively. The thickness of the Cr adhesion layer, the WC intermediate layer, and the WC/C multilayers was 200 nm, 250 nm and 210 nm, respectively, which resulted in a total film thickness of 660 nm.

The structure was analyzed by X-ray diffraction (XRD, D5000, Bruker AXS) with Cu$K\alpha$ radiation and a Goebel-Mirror in both conventional Bragg-Brentano and grazing incidence arrangement (angle of incidence was 3°). Additional structure

* fon: +49-(0)3677-69-3404, email: maik.gubisch@tu-ilmenau.de

investigations were performed by transmission electron microscopy (TEM, TECNAI S20 LaB6, FEI). Conventional cross section preparation using GATAN equipment was carried out to prepare samples for TEM. The setup and morphology of coatings was estimated using a scanning electron microscope (SEM, XL30 LaB6 ESEM, FEI) and an atomic force microscope (AFM, TOPOMETRIX TMX 2000™), respectively. The chemical composition was analyzed by energy dispersive spectroscopy (EDS). The hardness and indentation modulus were evaluated by a Fischerscope H100™ with a Vickers indenter.

Results

Fig. 1a shows the setup of the multilayer coatings consisting of three distinct phases – WC/C multilayers, WC intermediate layer, and Cr adhesion layer extending from the surface to the substrate. Fig. 1b shows the surface morphology of C10/20. All the multilayer coatings show a similar surface roughness with RMS (root-mean-square) ranging between 1.5 and 2.5 nm. The high surface roughness of multilayer coatings is caused by the columnar growth of the adhesion Cr layer and the intermediate WC layer.

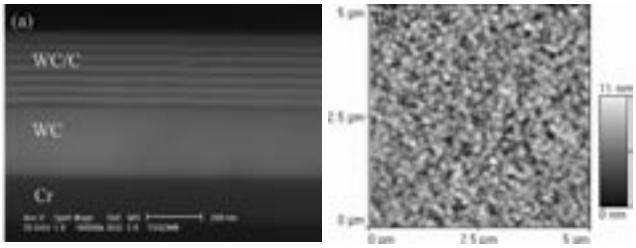

Fig. 1: Setup (a) and surface morphology (b) of the multilayer coating C10/20

The XRD spectrums for C10/20, C5/5, and a Cr/WC layer obtained in conventional Bragg-Brentano scan mode were presented in Fig. 2a. By comparing the diffraction patterns, two peaks at 2θ=42.2° and 44.5° can be determined. The former one corresponding to an average lattice spacing of 0.214 nm is indexed to the (200) reflection of β-WC_{1-x} with fcc NaCl structure. The latter one with an average lattice spacing of 0.204 nm is indexed to the (110) reflection of Cr. In Bragg-Brentano scan mode other peaks from WC_{1-x} and Cr from JCPDS file are not detected. In grazing incidence geometry, a broad peak of (111) and (311) WC_{1-x} with very low intensity was detected. These results indicate that WC and Cr are textured with WC_{1-x} (200) and Cr (110) parallel to the surface of the substrate. The carbon content of crystalline WC_{1-x} is ~39 at% due to resputtering of carbon. Fig. 2b presents the high resolution TEM (HRTEM) cross-sectional image of the multilayer C5/5. The WC_{1-x} appear as dark layers in the image because they have a higher scattering factor (mainly due to a greater atomic mass) than the adjacent carbon layer, which is amorphous. From the lattice image of WC grains we can determine the WC grain size and the layer thickness in this projection based on the lattice parameters from XRD. The grain size of WC_{1-x} is around 1-2 nm and the thickness of the WC_{1-x} and C layers is 4.7 nm and 4.3 nm, respectively, which is about 10% and 15% less than the designed thickness (5 nm). Ignoring any possible strain broadening contribution, an average WC and Cr grain size can be estimated from the Scherrer equation from Fig. 2a to be 15 and 30 nm, respectively. The estimated WC_{1-x} grain size is much larger than that in the multilayers determined by HRTEM (Fig. 2b), indicating that the XRD information was predominantly from the intermediate layer since the X-ray had a much higher penetration depth than the film thickness in the conventional Bragg-Brentano scan mode. The higher intensity of the WC_{1-x} (200) peaks observed (Fig. 2a) showed that WC_{1-x} layers in multilayer coatings also displayed preferred orientation similar to those of intermediate WC_{1-x} layers, i.e. parallel to the surface(200).

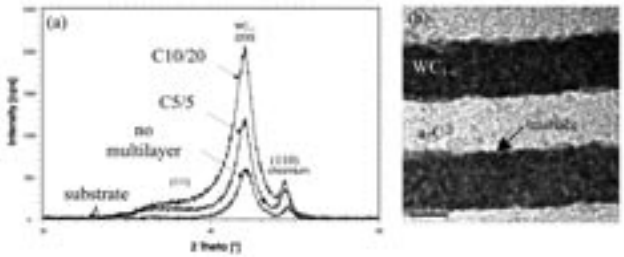

Fig. 2: XRD results (a) and HRTEM micrograph of multilayer C5/5 (b)

The interface between amorphous carbon and the crystalline WC_{1-x} covers only one or two atomic layers. The sharp interface between the WC_{1-x} and C layers (Fig. 2b) is typical for non-reactively sputtered layers at low temperatures. The advantage of this is the reduced primary and secondary wear of coatings and furthermore better mechanical properties of WC_{1-x}.

Both, the hardness and indentation modulus of the multilayers, which were determined to be 8-14 GPa and 200-300 GPa, respectively, were between the values for pure sp^2 rich carbon films (7.4 GPa and 161 GPa) and pure WC_{1-x} films (20 GPa and 685 GPa). It was expected that the WC_{1-x} layer act as a hard substrate while carbon layer as a soft lubricant presumed they behaved the same way in the multilayers as they do in the single-layer reference coatings. The maximum hardness and modulus was found for multilayer C5/10.

This work is supported by the German Research Foundation (DFG) under contract SFB 622/B3+B5 and Thuringian Ministry of Science, Research, and Art, TMWFK B407.0202.
The authors thank also Mrs. E. Remdt for TEM sample preparation.

Bias-magnetron sputtering of tungsten carbide coatings on steel

M. Gubisch*, L. Spieß, H. Romanus, J. Schawohl, and Ch. Knedlik
Institute for Materials Engineering

Introduction

In the research project nanomeasuring machine promoted by the German research foundation (SFB 622) the participating groups will develop a machine with a positioning accuracy of around 1 nm within a range of 450 x 450 x 80 mm³. The materials used for the moving parts require very small and well established surfaces with a high hardness and wear resistance. Furthermore, they must be produced economically on suitable substrates like steel. Tungsten carbide WC is an interesting and well known material in the tool technology due to the high hardness, extremely high modulus of elasticity above 700 GPa, high thermal conductivity, and excellent thermal and dimensional stability. WC films can be deposited by a variety of physical vapor deposition techniques (PVD). Magnetron sputtering of W in a hydrocarbon environment (acetylene, benzene, methane) was used to deposit WC films. Non-reactive sputtering of pure WC, WC-Co, or WC-Ni targets was also used. The structure and mechanical properties of WC coatings strongly depend on the target composition and process parameters. Ion bombardment during physical vapour deposition with substrate bias exerts a number of effects of thin films such as different crystallographic orientation, morphology and topography, grain size, chemical composition, and hardness. Additionally, other process parameters (mode, deposition pressure, temperature etc.) and their combination show a strong influence on the properties of WC coatings.

In this work, the influence of bias voltage between 0 V and -800 V on the properties of dc and rf non-reactive magnetron sputtered tungsten carbide coatings with 1 µm thickness on cold work steel 90MnCrV8 were determined. The coatings were deposited in a sputtering chamber (LA440S, Ardenne Anlagentechnik Dresden GmbH) with 90 mm magnetron sources and an ion etching system. Targets of sintered tungsten carbide (99.5 %) were fixed at a position approximately 50 mm underneath the substrate holder. The coatings were analysed with SEM, AFM, EDS, XRD, and nanoindenter. The morphology, the chemical composition, the structure, and the hardness of the deposited layers were analyzed. The investigations presented mark a starting point for processing and optimization of multilayers and nanocomposite coatings on WC basis and solid lubricant.

Results

From W-C phase diagram, several stable phase of crystalline tungsten carbide do exist, i. e. α-WC with a simple hexagonal structure, a metastable structure of hcp α-W_2C, a high temperature modification of W_2C denoted as β-W_2C, and β-WC_{1-x} with a fcc NaCl structure ($0 < x < 0.4$).

XRD was used to study the crystal structure of the WC films deposited. The XRD patterns are presented for dc and rf sputtered coatings recorded by conventional Bragg-Brentano scan mode (fig. 1). Figure 1a shows the XRD patterns for the WC film deposited in dc mode at a substrate bias of 0 V, -400 V, and -800 V, respectively. The non-stoechiometric cubic phase of tungsten carbide WC_{1-x} (JCPDS 20-1316) is evident. For the film deposited at a bias of 0 V, the center of the peak with highest intensity and a low FWHM is located at 42.2°. This peak corresponds to the (200) plane of the crystalline phase WC_{1-x} with a carbon content of ~40 at% determined by energy dispersive spectroscopy (EDX, Fig. 2a). The resputtering of carbon resulted in a composition of the WC coatings different from the stoichiometry of the targets. For WC_{1-x} another peak was detected at 74° (311) in Bragg-Brentano scan mode. Recordings in grazing incidence geometry showed a broad peak of (111) and (311) WC_{1-x} with low intensity. These results indicate that WC is textured with WC_{1-x} (200) parallel to the surface of the substrate.

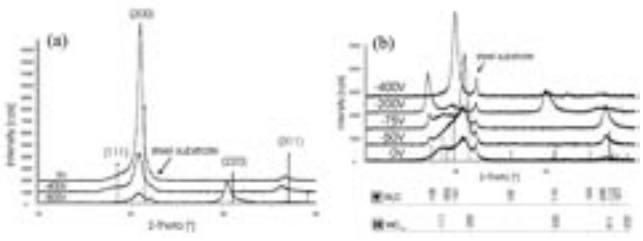

Fig. 1: XRD patterns of dc (a) and rf (b) sputtered WC coatings depends on bias voltage

Different bias voltages lead to changes in the crystallinity of the dc sputtered WC coatings. For the film deposited at a bias of -400 V and –800 V, respectively, a broad diffraction peak was observed for (200), indicating nanocrystallinity and lattice

* fon: +49-(0)3677-69-3404 , email: maik.gubisch@tu-ilmenau.de

defects in the coating. Additionally, at a substrate bias of -800 V a peak corresponding to the (220) plane of crystalline WC_{1-x} was detected at 61°. This changed orientation in WC_{1-x} films is related to the increased mobility of the adatoms which hit the substrate due to higher substrate bias. Additionally, in grazing incidence geometry a peak of (100) W_2C was detected, indicating a dominated WC_{1-x} phase with a fraction of W_2C in the coating deposited at a bias of -800 V. The resputtering effect was increased especially when sputtered in the presence of a bias due to additional bombardment of argon ions. With an increased bias voltage the carbon content of dc sputtered WC_{1-x} decreases from 40 to 33 at% (Fig. 2a). The centers of the diffraction angles all appear at smaller angles than the standard reflection angle (Fig. 1a). This indicates larger interplanar spacing pointing in the direction of high compressive stress in the WC films. However, this effect was not significantly dependent on the bias voltage.

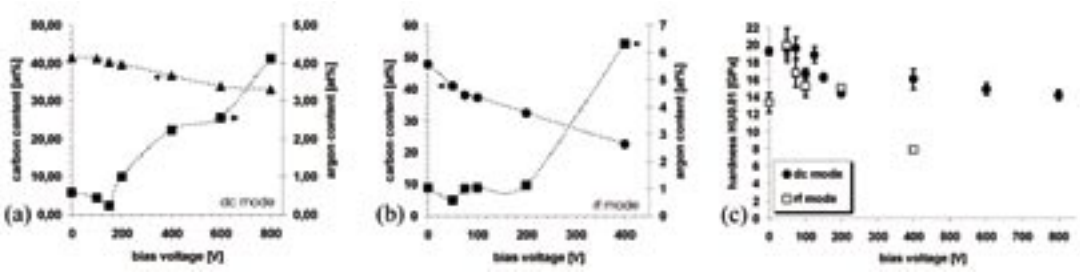

Fig. 2: Variation of chemical composition (a, b) and hardness (c) of sputtered WC coatings dependent on the bias voltage

Figure 1b shows the XRD patterns for the WC films deposited in rf mode at substrate biases of 0 V, -50 V, -75 V, -200 V, and -400 V, respectively. A rf sputtered WC coating was obtained with nanocrystalline structures comparable to the dc sputtered WC films. At a substrate bias of 0 V, broad diffraction peaks indicate the presence of a nanocrystalline or amorphous WC_{1-x} film. At a bias of -50 V, a dominant crystalline WC_{1-x} phase was obtained with a carbon content of ~41 at% which is comparable to the dc coatings without or with low ion bombardment. Increasing the bias voltage leads to an increased resputtering of carbon and to a phase transformation from WC_{1-x} to W_2C (JCPDS 35-0776) (Fig. 1b and 2b). Coatings with no significant preferred orientation were achieved by these process parameters. A phase transformation of WC_{1-x} to W_2C was obtained at a substrate bias of -200 V. However, in corresponding XRD pattern a very broad peak at 60° was detected. This peak can be identified as WC_{1-x} (220) or W_2C (110) phase of WC. The carbon content of this coating at 32 at% indicated a presence of both WC phases (Fig. 2b). In contrast a W_2C phase with carbon content of ~ 22 at% (C:W ~ 0.31) was obtained at a substrate bias of -400 V due to preferred resputtering of carbon by deposition in rf mode. However, high argon content was also measured in this coating.

The mechanical characteristics of the WC layers depend strongly on the chemical composition, crystallinity, and the phase transformation. We found that WC layers sputtered in the dc mode are crystalline, nanocrystalline, or amorphous with carbon concentrations between 40 at% and 33 at% dependent on the bias voltage. Therefore, with an increased bias voltage (Fig. 2c) the hardness was reduced from 20 GPa to 14 GPa. This dependence of structural and mechanical properties were significantly by the rf sputtered WC coatings. We found that WC_{1-x} films with nanocrystalline or amorphous structures have lower hardnesses as crystalline WC_{1-x} coatings. At a bias voltage of -50 V a dominant crystalline WC_{1-x} phase was obtained in rf mode. The hardness of these coatings of 20 GPa is comparable to the dc coatings without or with low ion bombardment. Furthermore, the phase transformation from WC_{1-x} to W_2C leads to a reduced hardness of the film (Fig. 2c). However, lower carbon contents in the WC films reduce the mechanical properties. A hardness of 8 GPa of W_2C coatings (-400 V) was the lowest value for all WC coatings manufactured.

The surface morphology of deposited WC coatings was also dependent on the substrate bias. By increasing the bias voltage an increased roughness RMS of 2 nm to 9 nm was obtained (Fig. 3).

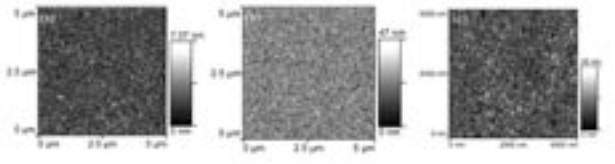

Fig. 3: AFM image of sputtered WC coatings on a steel surface depending on the bias voltage, (a) dc mode, 0 V (RMS ~2 nm); (b) dc mode, -800 V (RMS ~9 nm), and (c) rf mode, -400 V (RMS ~5 nm)

This work is supported by the German Research Foundation (DFG) under contract SFB 622/B3 and the Thuringian Ministry of Science, Research, and Art, TMWFK B407.0202. The authors also thank Fa. Lohnhärterei Faulhaber (Zella-Mehlis, Thüringen), Christian Müller, and Björn Schwenke.

Thin film materials and structures for microsensors

C. Knedlik[1,*], V. Tvarozek[2], I. Novotny[2], V. Rehacek[2], A. Jakubec[2], E. Vavrinsky[2], B. Borový[2], V. Breternitz[1], L. Spieß[1], and H. Tippmann[1]

[1] Department of Materials for Electronics

[2] Slovak University of Technology Bratislava, Slovak Republik

This work is the result of a co-operation between the Department of Materials Technology of TU Ilmenau and the department of microelectronics of Slovak University of Technology Bratislava.

Students and young scientists from the Slovak partner institution were actively involved in the project. For two PhD students it was a very useful help which significantly supported and improved their scientific results obtained in the frame of PhD theses. One diploma work was successfully defended in frame of this bilateral activity. The project supported also one PhD thesis done by research worker at the Microelectronics department of STU Bratislava.

1. Technological development and optimisation of preparation of thin film materials and structures

In the effort to miniaturize biosensors our interest has been focused on the fabrication of reliable microelectrodes based on thin film technology. Planar microelectrochemical chips with thin-film electrodes (Au, Pt, Pd, ITO, and Ag/AgCl) of different shapes and arrangements (compact, interdigitated array) on Si or glass substrates have been developed and fabricated. For the isolation thin film structures we developed the technology of preparation of Y_2O_3 and the electrochemical Hg deposition for amalgamization of microelectrodes.

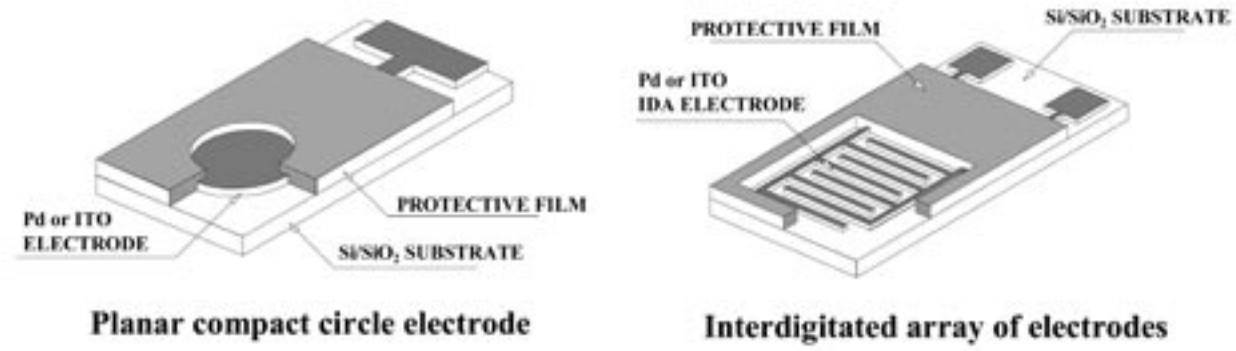

Fig. 1: Thin film microelectrode chips

2. Characterization of thin film sensoric interfaces

We controlled and analysed sensing interfaces which play a significant role in the design of biosensors and optimization of their properties. We used the following analytical methods: AFM, XRD, VOA, electrical and electrochemical characterisation (CV and ASV).

Well-defined geometric arrangements, reproducible and controlled thin film interfaces offer a predictable performance of biosensors. The use of microelectrodes modified by Hg was proven for heavy metal trace monitoring. We have developed a novel asymmetric ratio method which allows us to adjust the sensitivity of conductance sensor by setting up the frequency of supply voltage.

As part of the research on developing new biomedical devices prepared by thin film technology, we sputtered indium-tin-oxide (ITO) films used as the highly conductive and transparent microelectrodes. The optical and electrical properties of ITO thin films are dependent on the deposition parameters and we found the optimal conditions for sputtering: r.f. power 700 W, gas atmosphere of Ar + 5% O_2 of the total pressure 1.3 Pa, and substrate temperature of 350°C. The ITO films are polycrystalline with a strong preferred orientation of crystallites in [111]-direction. The sheet resistance was in the range of 100 Ω/❑ and the optical transmittance better than 80 %.

Our aim was to analyze and characterize thin electrochemically produced ITO microelectrodes which can be applied in biochemical sensing because they enable simultaneous electrical and optical measurements of analytes, e.g. blood and skin. From this point of view the chemical resistance of microelectrodes is a crucial parameter. Chemical resistance of the ITO thin films was evaluated

* fon:+49-(0)3677-69-3611, email: christian.knedlik@tu-ilmenau.de

by AFM measurements. The concentration of solutions used for chemical treatment is similar to concentrations of biological environment and so they represent the aggressive properties of the biological system. Chemical treatment in Phosphoric acid (0.1 M H_3PO_4), Hydrochloric acid (0.1 HCl) and Potassium (0.1 M KCl) for 10 minutes, 1 hour, 24 hours and 72 hours, respectively, increased the rma roughnesses from 5.59 nm up to 142.14 nm. Sputtered ITO films of all thicknesses were resistant against selected chemicals during 1 hour. These results pave the way for development of the ITO microelectrode chip applicable in electro-optical biochemical sensors.

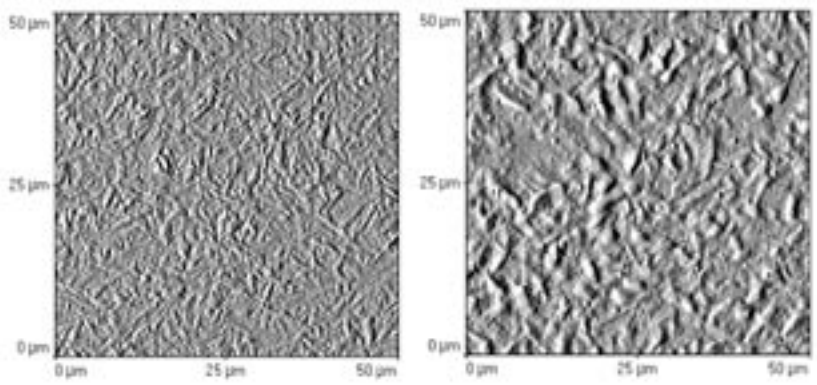

Fig. 2: AFM scans showing the influence of Hg electroplating potential on surface properties of Au amalgam, Au-Hg (surface area 50 x 50 µm²), electroplating time 3 min for - 800 mV and - 200 mV, resp.

Analyses of thin film roughness and surface morphology by Atomic Force Microscopy (AFM) and Cyclic Voltammetry (CV) have been performed. Both cleaning procedures, chemical and pulse electrochemical, are suitable for pre-treatment of microelectrode surfaces which was confirmed by AFM and CV analyses. Resulting from this we found an optimal cleaning procedure of Au and Pt microelectrodes.

We studied the selected mechanical and electrical properties of Y_2O_3 thin films prepared by planar r.f. diode sputtering for application in microelectrochemical biosensors. The electrical cross-resistivity of Y_2O_3 thin films was estimated by I-V measurements and its values are in the order of 10^{11} Ωm. The examined Y_2O_3 thin films have shown a low leakage current, max. 0,4 nA at 100 V which corresponds to an electrical strength of $2{,}5 \times 10^8$ V/m. The value of breakdown voltage (coming to destruction of Y_2O_3 structure) was up to 100 V in all samples. The properties of Y_2O_3 thin films prepared by r.f. sputtering are comparable to published data of bulk and Y_2O_3 films. They are suitable for insulation in the vertically arranged microelectrochemical cell.

Anodic stripping voltammetry (ASV) is one of the most sensitive techniques for heavy metal trace (such as Cd, Cu, and Pb) analysis and Au-Hg working electrodes are usually used. The modification of Pd and ITO microelectrodes by thin Hg film for application ASV was developed. Two types of microelectrodes arrays were fabricated by standard thin film technology. Depositions of Hg were carried out by electroplating.

The Pd-Hg and ITO-Hg microelectrodes were dipped into the solution (20 ml) with different content of ions Pb^{2+} from 5×10^{-5} to 2.5×10^{-4} M in 0.1 M KNO_3. The sensitivity of ITO-Hg circle array of microelectrodes is higher (280 nA/µM) in comparison to IDA Pd-Hg microelectrodes (60 nA/µM).

A novel asymmetric ratio resistance method has been developed to overcome the technological residual defects and imperfections. Accurate and reproducible monitoring of small differences of temperatures and concentrations is also important in biochemical sensors, e.g. calorimetric or electrochemical sensors. We have applied that new principle in electrochemical conductometry method. To minimize the polarization effect we have used Pt electrodes on alumina substrate. The configuration of the microelectrodes consists of three separate electrodes of interdigitated array or strip shapes with different areas, which give us unequal electrochemical cell constant. The improvement of ratio metric method is given by the possibility to adjust the sensitivity of combined sensor by setting up the supply voltage frequency.

This work has been supported by the German Academic Exchange Service (DAAD) in the framework of the Project Based Personnel Exchange Programme (PPP) with the Slovak Republic.

Low-emitting ceramic layers

A. Knote[1,*], H. G. Krüger[1], K. Pfeifer[1], H. Kern[1], and J. Manara[2]

[1] Department of Metallic Materials and Composite Materials

[2] Bavarian Center for Applied Energy Research

Introduction and Experimental

The aim of the present tests is to develop a surface coating for which the heat emission is significantly reduced at higher temperatures through a reduction in the emissivity. Ceramic layers with a powder mixture consisting of TiO_2 and Y_2O_3 were produced electrophoretically for these tests, and then sintered to the pyrochlore phase $Y_2Ti_2O_7$ in an open-porous layered structure. The total emissivity ε was ascertained on these layers for temperatures up to 800°C. By producing the electrophoretic layer and sintering to a porous layer, the total emissivity can be lowered by approx 40 % at 800°C in comparison with a plasma-injected layer.

The starting materials for the electrophoretic coating were the commercial powders yttrium oxide Y_2O_3 Grade C (H.C Stark GmbH) with an average granular size of 600 nm, and titanium oxide Kronos 1001 (Kronos Titan GmbH) with an average granular size of 400 nm. The coating was performed at a voltage of 60 V, a coating period of 3 - 15 s and an electrode spacing of 3 cm in a homogenous and constant electrical field. The stainless steel X10CrAlSi25 was used as coating substrate. After the layer had dried, the sintering was carried out at a heating and cooling speed of 6 K/min in unpressurised air (holding time of 3 h). After sintering was characterised the new phase formation by both X-ray diffraction means and difference thermo-analysis (DTA). The total emissivity ε was determined at the Bavarian Center for Applied Energy Research.

Results and Discussion

Examination of the sintered layers by scanning electron microscope reveals a very high porosity of 40 – 50 % (Fig. 1). At the same time, the degree of sintering is highly dependent on the sintering temperature. While only a formation of sinter necks between the smaller particles can be observed at 900°C (Fig. 1A), Figs 1B – 1D indicate an increasing sintering of the ceramic, represented by the clear formation of sinter necks at an increasing temperature.

This is associated with an increase in granular coarseness, the total porosity only altering slightly. However, an increase in the average pore size can be observed. Sintering of the Y_2O_3 and TiO_2 particles is associated with a new phase formation, as phase-analytical tests reveal. At the same time, the formation of the $Y_2Ti_2O_7$ phase from the pyrochlore type is dependent on temperature. The sinter tests indicate that the starting materials have undergone extensive conversion from a sintering temperature of around 1100°C upwards, with the result that a $Y_2Ti_2O_7$ ceramic with an open-porous structure arises. Below this temperature, even larger amounts

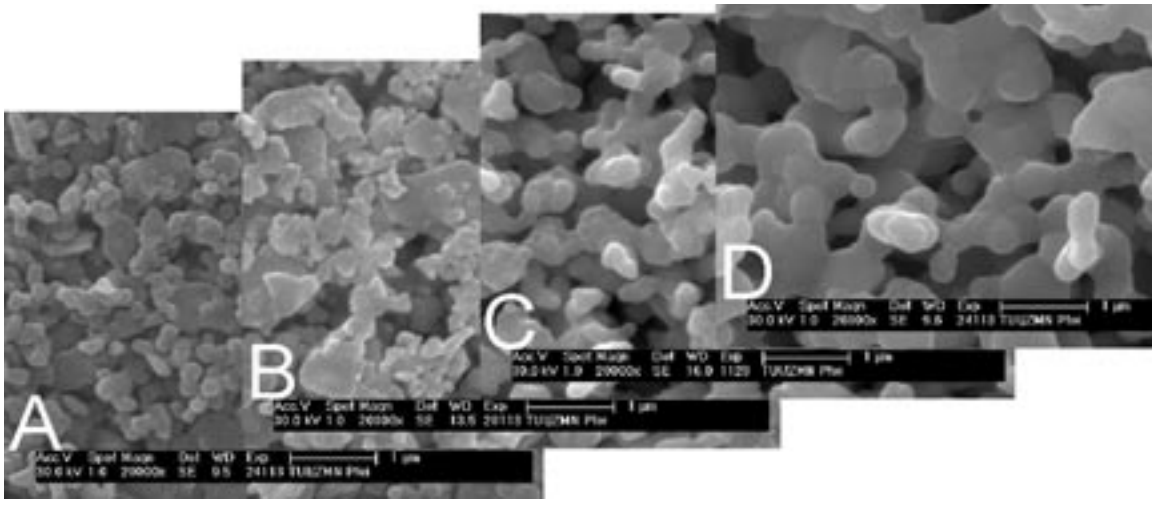

Fig. 1: Porosity and formation of sinter necks for Y_2O_3/TiO_2 ceramic, sintering at various temperatures: (A) 900°C, (B) 1000°C, (C) 1100°C, (D) 1200°C

* fon:+49-(0)3677-69-1664, email: andreas.knote@tu-ilmenau.de

of the starting powders Y_2O_3 and TiO_2 can be detected. Crystallisation of the $Y_2Ti_2O_7$ phase is also revealed by a DTA test (exothermic peak between 800°C and 1150°C).

The dependence of the total emissivity ε on the sample thickness revealed the expected behaviour (see Fig. 2). As a reason for this, it can be stated, that for thinner layers, the fact should not be excluded that part of the reflection results from the substrate. The values shown in the figure involve total emissivity at 800°C. It can be seen that the degree of sintering has a considerably greater influence on the emissivity than the layer thickness.

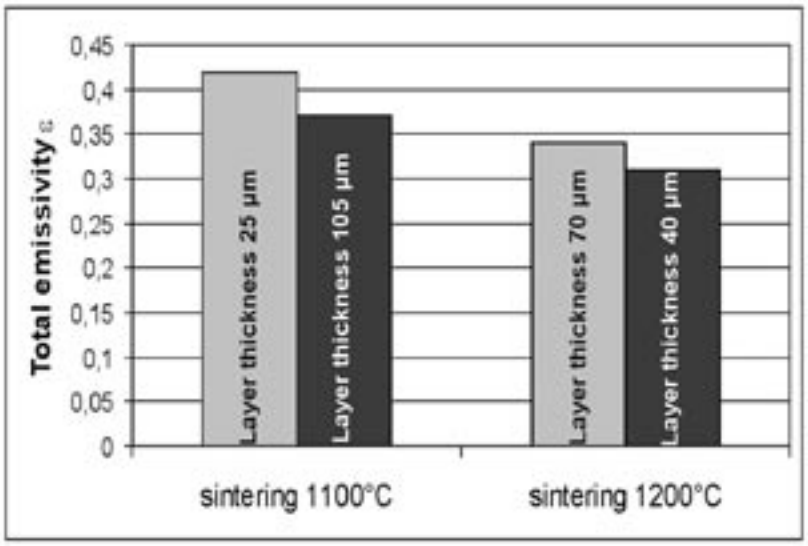

Fig. 2: Dependency of the total emissivity at 800°C on the sintering temperature and layer thickness.

As the thermally stable phase $Y_2Ti_2O_7$ predominates for the two sinter temperatures, influence of the materials on the total emissivity is to be ruled out. This indicates that the pore structure and grain size in the porous layer have a highly significant effect on the total emissivity. The 70 µm thickness with a porous layer sintered at 1200°C also indicates a 40 % lower total emissivity in comparison to a plasma-injected layer (Fig. 3). Further tests are envisaged in regard to the material composition and layer structure for reducing the emissivity.

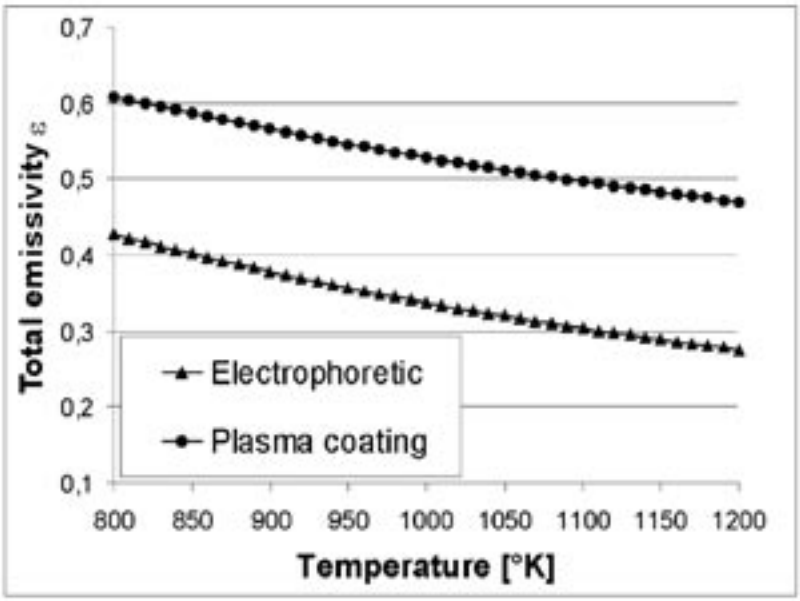

Fig. 3: Temperature dependency of the total emissivity of an electrophoretic and plasma-injected layer.

Conclusions

The investigations revealed the great potential of electrophoretic ceramic layers in reducing the total emissivity of surfaces. By producing an electrophoretic layer consisting of TiO_2 and Y_2O_3 powders and sintering it to an open-porous layer with the pyrochlore structure of the composition $Y_2Ti_2O_7$, it was possible to reduce the total emissivity at 800°C by 40 %.

This work is supported by the DFG under contract no. KE 359/7-1

Preparation and investigations of nickel zinc ferrite layers on copper foils for the processing of printed circuit boards

H. Romanus[1,*], K. Romankiewicz[1], B. Schwenke[1], V. Breternitz[1], Ch. Knedlik[1], and G. Teichert[2]

[1] Institute for Materials Engineering

[2] Materialforschungs- und Prüfanstalt Weimar (MFPA), Ilmenau department

Introduction

By introducing new technologies with rapidly growing transfer rates and pulse frequencies in all fields of science and technology (e.g. mobile networks, data processing, etc.) it is necessary to develop new and appropriate rf-materials and material combinations. In particular, this is important as conventional rf-materials with upper frequency limits of 1000 MHz fail the fast-growing requirements [1]. Thin magnetical soft layers are promising materials for rf-absorbers improving the electromagnetic compatibility. Such layers can be made of nickel-zinc-ferrite (Ni-Zn-ferrite), especial multi-layers of Ni-Zn-ferrite and silicon oxide, to enhance the absorption effect. These new rf-materials show almost linear increasing reflexion absorption of 0.6 dB from 1000 MHz to 77000 MHz. In the near future, they will be used as absorber materials, interference suppression materials, materials for case modules, and rf- printed circuit boards [2].

Experimental Details

The thin Ni-Zn-Ferrite layers and the silicon oxide layers were deposited by means of dc- and rf-magnetron sputtering, respectively, using the LA440S system *(Ardenne Anlagentechnik GmbH, Dresden)*. The target materials employed were sintered Ni-Zn-ferrite (*Kaschke GmbH, Göttingen*) and a SiO_2-target (*FHR*). Electro-chemical deposited copper foils (*ILFA GmbH, Hannover*) were used as substrates. With a thickness of 17 µm these copper foils are used in the fabrication of printed circuit boards. Before deposition in rf-argon-plasma, the 12 cm x 12 cm copper foil substrates were cleaned by means of inverse sputter-etching (ISE, 200 W, 3 min). The thickness of the Ni-Zn-ferrite layers ranged between 1 µm and 4 µm. Overall layer thickness of the multi-layers ranged from 300 nm to 2 µm. The multi-layers consist of a series of up to 4 individual layers of Ni-Zn-ferrite-/silicon oxide.

Structure, texture, and internal stress were determined using X-Ray Diffractometry *(XRD, D5000– Bruker AXS)*. Chemical composition was examined using X-Ray Fluorescence Analysis *(XRFA, Fischerscope X-ray XAN – Fischer)* and Energy-Dispersive X-ray Analysis (EDX, *EDAX*). Surface morphology was characterized employing Scanning Electron Microscopy (SEM, XL30 with LaB_6-Cathode – *FEI*) and Atomic Force Microscopy (AFM, TMX 2000 – *Topometrix*). A great deal of attention was given to the adhesiveness of the layers being significant for the following process of turning the copper foils into printed circuit boards. Adhesiveness was determined via bending-, deep drawing-, and compression tests, giving a good impression on this parameter which otherwise cannot be acquired directly. The mechanical strain induced was similar to the stress occurring in the production process of printed circuit boards.

Results

Analysis of the X-ray peaks proved the formation of a spinel-ferrite structure (PDF-Nr.: 08-0234). The Ni-Zn-ferrite layers were poly-crystalline showing weak or even none texture. X-ray stress analysis showed tensile and compressive stress within the layers. The grain size of the Ni-Zn-ferrite layers increases with increasing layer thickness, which could be proven with SEM and AFM. The copper substrate (Figure 1 a) strongly influenced the structure of the surface layer (Figure 1 b). This effect is typical with sputtered layers. The Root Mean Square (RMS) of the ferrite layers strongly depend on the peak to valley (R_t) which originates from the high roughness of the copper foil substrate. With increasing thickness of the Ni-Zn-ferrite layer no distinct tendency towards a higher RMS is recognizable. The RMS and the R_t of the multi-layers (Ni-Zn-ferrite/silicon oxide) decrease with increasing thickness of the layers. The process of co-sputtering interrupts layer growth and thereby grain growth. The small grains level the surface and therefore an increase in roughness does not occur.

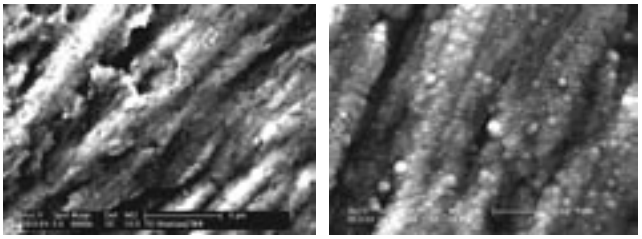

a) ISE etched Cu-foil b) Cu-foil with ferrite

Fig. 1: SEM images of ISE etched and coated copper foils

* fon: +49-(0)3677-69-3404, email: henry.romanus@tu-ilmenau.de

The dependence of the layer composition on the thickness of the layers was determined via EDX-Analysis. Apparently, the element concentrations in the Ni-Zn-ferrite layers remain constant for layers thicker than 2000 nm. The increased copper concentration within the 1000 nm sample is caused by the substrate. The small amount of copper within the other samples might as well be caused by the copper foil but presumably results from the target design. A fraction of copper is always sputtered off the base plate and is deposited in the layer, as well. According to the great penetration depth of the X-ray through the layer into the substrate and the built-in copper, XRFA turned out to be an inappropriate tool for quantification of the copper content.

The optical appearance of all examined samples after deep drawing tests is of similar type. A permanent deformation of the layer composites is clearly visible. A burst in the cup-like structure is the result of applied stress (Figure 2). Optically, no flaking of the layers is visible. Examinations of the fractured surface along the deformation imprints were conducted via SEM. Consistent with all samples, the copper foil showed a ductile deformation until finally breaking. An excellent adhesiveness was verified (Figures 2 and 3) and the columnar growth of the layers was clearly demonstrated *(Fig. 3b)*.

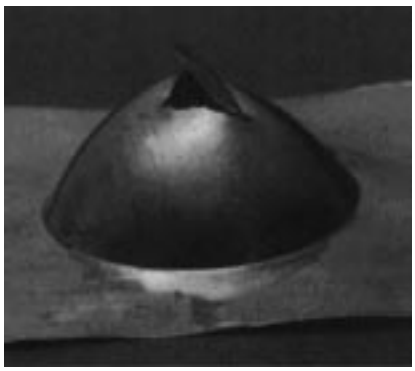

Fig. 2: bursted cup-structure

As a result of compression tests the Ni-Zn-ferrite layers showed inter- and trans-crystalline cracks. With increasing layer thickness an ascending crack initiation (in terms of micro-cracks) is noticeable, yet the adhesiveness is not affected. The results of bending tests demonstrated a similar behaviour.

Conclusion

The structure of the growing layers is predetermined by the structure of the copper substrate. With increasing layer thickness the grain growth is also increasing. The roughness of the ferrite layer increases in comparison to the basic roughness of the substrate. The multi-layer roughness decreases with increasing layer thickness compared to the basic roughness of the substrate (RMS: 336 nm and R_t: 2252 nm within working range of 50 µm x 50 µm). Element concentrations remain constant with increasing layer thickness. A formation of poly-crystalline Ni-Zn-ferrite layers appears. Stress analysis is pointing to tensile, as well as compressive stress.

The Ni-Zn-ferrite layers feature excellent adhesiveness on the substrate material as was demonstrated via bending-, deep drawing-, and compression tests. By applying mechanical load the ductile copper substrate is stretched, inducing inter- and trans-crystalline cracks within the layer. The sputtered Ni-Zn-ferrite layers withstand high mechanical load, thus qualifying them for the application in the processing of printed circuit boards. In conclusion, it will be possible to coat copper foil rolls in large scale, and therefore economically, as long as the bend radius is dimensioned accordingly.

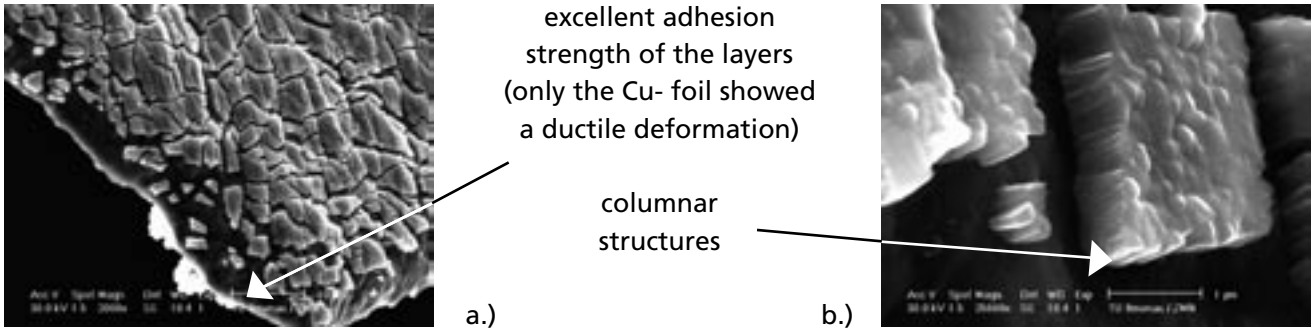

Fig. 3: SEM images of coated Cu-foils after deep drawing tests

[1] L. Michalowsky: Ferritwerkstoffe: Bauelemente f. d. Elektrotechnik u. Elektronik, Akademie Verlag, Berlin, 1985
[2] Forschungsberichte IMG Nordhausen, Deutschland

Preparation of hexagonal WSi_2 and tungsten silicide metallization with adjustable thermal coefficients of the electrical resistivity

H. Romanus[1,*], L. Spiess[1], Ch. Knedlik[1], and J. K. N. Lindner[2]

[1] Institute for Materials Engineering

[2] Institute for Physics, University of Augsburg

Introduction

In semiconductor technology tungsten silicide is a well known material for metallization suitable for high temperature contacts and high temperature sensors. Up to now, in many cases tungsten silicide layers have been used as low ohmic gate electrodes in FETs and as interconnects in VLSI technologies [1]. Tungsten silicides are being used for metallization and contacting of materials like Si [2], GaN [3], GaAs [4], InP [5], InGaN [6], InN [6], InAlN [6], AlN [7], and SiC [8]. Moreover, tungsten rich WSi_x-layers are efficient diffusion barriers against diffusion of Cu [9]. Tungsten silicide layers are suitable for fabrication of resistors with low thermal coefficient [10]. Furthermore, tungsten silicide can be used for mechanical structures, heating elements, and thermocouples [11]. Sputtering [3, 4, 6–8, 10], electron beam evaporating [12], CVD [9], interface- and solid-state reactions [12], ion beam synthesis, MBE and laser ablation are considered to be suitable tools for fabrication of tungsten silicide layers. In some cases, phase formation requires an additional *in-situ* or *ex-situ* annealing step.

Experimental Details

Formation of the tungsten silicide layers was accomplished by sputtering of a sintered stoichiometric WSi_2-target followed by annealing in a RTA system or a quartz tube furnace *(LA440S, Ardenne Anlagentechnik GmbH)*. The dependence of the phase formation on the substrate, the temperature of the substrate, and *ex-situ* annealing was determined. *Ex-situ* annealing temperatures ranged between 500°C and 1200°C. The different phases and layer characteristics were determined via XRD, as well as AFM, SEM, TEM, and electric measurements (linear van der Pauw method).

The heating of the substrates was performed from the back side and showed a strong dependence on different parameters [13], i. e. starting temperature, sputtering power, and sputtering time. With a sputtering power of 200 W, the substrate temperature starting from 20°C increased to 325°C and from 544°C to 582°C, respectively, within 15 min.

Results

Influences of different substrate materials like 3C-, 4H-, and 6H-SiC, n- and p-doped Si(111) and Si(100), SiO_2, and Si_3N_4, respectively, on the phase formation were analyzed. Arranged close to the heater, the substrates were heated up to approx. 544°C and then coated with tungsten silicide. The substrates were insulated to minimize the influence of the substrate holders. Formation of hexagonal WSi_2 on the different substrates was observed and no influence of the substrates on phase formation could be shown.

To analyze the influence of *ex-situ* annealing on phase formation, three SiO_2-coated Si-wafers were coated with tungsten silicide at different substrate temperatures (unheated, heated from the back side in standard position, as well as close to heater, and thermally insulated) and subsequently annealed in an *ex-situ* annealing step for 15 min between 500°C and 1200°C in a quartz tube furnace with argon atmosphere. The deposition of layers yielded the following results:

1. Layers on non-heated substrates ($T_{substrate}$ = 23°C) showed an amorphous behaviour with a resistivity of $\rho \approx 780$ μΩcm,
2. Layers on *in-vacuo* heated substrates were crystalline (hexagonal WSi_2),

- at $T_{substrate}$ = 508°C (substrate in standard position), ρ = 664 μΩcm,

- at $T_{substrate}$ = 544°C (substrate arranged close to the heater / insulated), ρ = 652 μΩcm, hexagonal WSi_2-crystallites showing increased grain size.

X-ray diffraction patterns of the sintered samples recorded from the unheated wafer indicated a phase formation of tetragonal WSi_2 and tetragonal W_5Si_3. Up to 800°C, the hexagonal WSi_2-phase is stable. From 850°C onwards, phase transformation into tetragonal WSi_2 and tetragonal W_5Si_3 occurs. At 900°C, the transformation process is complete. Above 900°C, both tetragonal tungsten silicide phases are stable. A higher temperature results in increasing grain sizes and decreasing resistivity. Analogous behaviour was observed on annealed samples heated in standard position.

* fon: +49-(0)3677-69-3404, email: henry.romanus@tu-ilmenau.de

The resistivity ρ_0 of the samples of the tungsten silicide coated wafers shows a dependence on the annealing temperature (Figure 1a). The strong decrease of the resistivity between 800°C and 900°C goes along with the phase transformation described above. From 1100°C upwards, the resistivity only decreases marginally. The lowest value of 159.3 µΩcm was reached by annealing at 1200°C. The resistance values of the unheated wafers are on the average approx. 120 µΩcm higher than those of the previously heated wafers. After annealing at 1100°C these values do not differ any longer from each other.

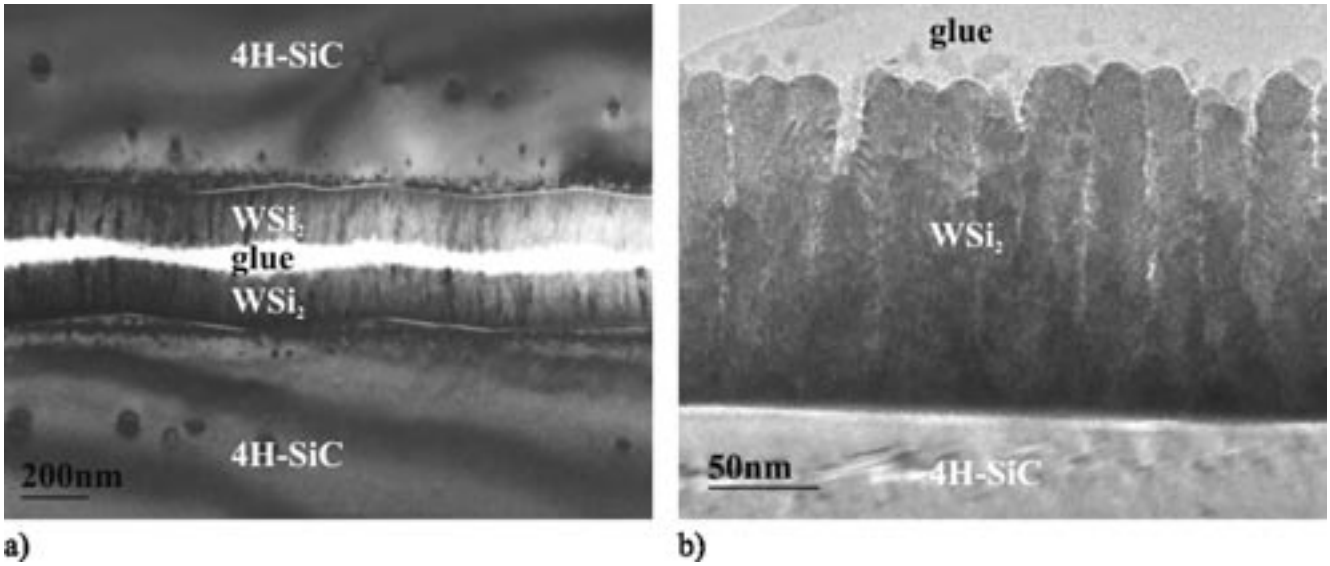

Fig. 1: TEM x-section images of hexagonal WSi_2 (deposited at 544°C) on 4H-SiC a) overview, b) section enlargement

The positive thermal coefficient α_0 on both wafers heated during sputtering (heated from the back side in standard position as well as close to heater, Figure 1b) points in the direction of metallic behaviour of the tungsten silicide. Up to annealing temperatures of 700°C, samples of the unheated wafer indicated semi conducting behaviour and above 760°C metallic behaviour. To obtain tungsten silicide with a thermal coefficient of 0 K^{-1}, one sample of the unheated wafer was annealed at 725°C. The resulting thermal coefficient of 0.00296 10^{-3} K^{-1} ≈ 0 remained constant in the temperature range measured.

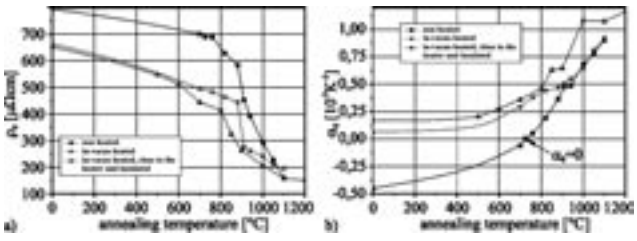

Fig. 2: Tungsten silicide – dependence on the annealing temperature of a) the electric resistivity ρ_0 and b) the thermal coefficient of the electric resistivity α_0 at different temperatures

From the X-ray diffraction patterns of the hexagonal WSi_2 on 4H-SiC the lattice parameters a = 0.4618 nm and c = 0.6537 nm were determined. Columnar growth of the layers is visible. In TEM diffraction images analogous to the XRD measurement recorded in θ-θ-geometry no evidence of any textures could be determined.

Conclusion

Preparation of hexagonal WSi_2 at a substrate temperature of 544°C was shown, as well as metallization of tungsten silicide metallizations with a temperature coefficient α_0 = 0 K^{-1} by an annealing procedure at 725°C. On standard atmosphere conditions, these layers are stable up to 400°C. Because of the possibility to individually adjust the thermal coefficient the metallization of tungsten silicide presented is suitable for different applications when high temperature stability is necessary.

[1] Saito, T. et al: Jpn. J. Appl. Phys. 33 (1994) 1A, p. 275-279
[2] Gambino, J. P.; Colgan, E. G.: Mater. Chem. and Phys. 52 (1998), p. 99-146
[3] Cao, X. A. et al: J. Vac. Sci. Technol. A 17 (1999) 4, p. 1221-1225
[4] Nebauer, E.; Merkel, U.; Würfl, J.: Semicond. Sci. Technol. 12 (1997) 9, p. 1072-1078
[5] Ren, F. et al: Appl. Phys. Lett. 74 (1999) 13, p. 1845-1847
[6] Ren, F. et al: J. Vac. Sci. Technol. A 15 (1997) 3, p. 802-806
[7] Savrun, E. et al: MRS Symp. Proc. 402 (1996), p. 561-566
[8] Erler, F.et al: MRS Symp. Proc. 572 (1999), p. 99-104
[9] Wang, M. T. et al: J. Vac. Sci. Technol. B 17 (1999) 2, p. 385-391
[10] Backhouse, C. J. et al: Thin Sol. Films 311 (1997) 1-2, p. 299-303
[11] Kreider, K. G.: MRS Symp. Proc. 322 (1994), p. 285-290
[12] Luby, S. et al: NATO ASI Ser. E 234 (1993), p. 545-549
[13] Romanus, H.: Diplomarbeit, TU Ilmenau, 1995 - 77 p.

Functional liquid-crystalline elastomers in microsystems

M. Bründel[1], M. Stubenrauch[1,*], A. Sánchez-Ferrer[2], and H. Wurmus[1]
[1] Departments of Microsystems Technology
[2] University of Freiburg

A new material for actuators

The search for new innovative materials plays an important role in microsystem technology research. There are various micro actuators containing piezoceramics or shape-memory-alloys[1]. However, those materials are often difficult to integrate or do not show a substantial ability for large deformations that are needed especially for use as artificial muscles. A promising approach could be compliant materials that contain mechanically active components, like elastomers enhanced by liquid-crystalline molecules (mesogens). Those molecules show a more or less uniform alignment when they are in a liquid-crystalline phase (a state of aggregation between solid and liquid). This alignment is lost when the LC undergoes a phase transition into the liquid state; the order of the molecules becomes isotropic. In combination with uniformly aligned elastomer networks, this effect can lead to a significant change of the shape of the elastomer.

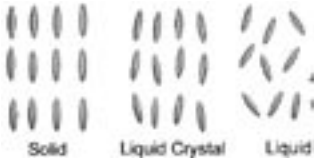

Fig. 1: Phases of liquid-crystalline materials

The synthesis and development of this kind of material, called "functional liquid-crystalline elastomer (FULCE)", has been a field of research in organic chemistry in recent years. The University of Freiburg, Germany, has developed elastomers that are able to reversibly change their length by 400% due to a change of the phase of the LC molecules, whereby stresses up to 27 kPa have been measured. Depending on the LC used, this change of phase can be caused by heating or irradiation with UV light[2,3]. These properties make FULCEs a promising material for the use in micromechanical systems with large deformations and small forces. To estimate the possibility for the implementation of this rather exotic material, the department of MST participated in the "European Research and Training Network FULCE", which was formed by some of the leading institutions in this area.

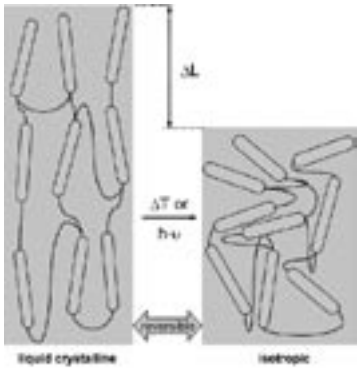

Fig. 2: Phase transition induced by temperature change or irradiation

Integration into microsystem technology

Besides the evaluation of the mechanical properties and the long-term-stability of the materials, it is necessary to show that they are compatible with standard materials used for MEMS, such as silicon or glass substrates, and with the processes used to manufacture the system, like photolithography, deposition of thin films and dry and wet etching.
Generally, the integration of the material can be done in two different ways. The first approach is to integrate the manufacturing of the elastomer into the production of MEMS, i.e. on wafer level. This can be done using a pre-elastomer-solution and photosensitive crosslinking of the polymer after forming a film on the wafer surface. In this case, one needs to perform the alignment of the mesogens on wafer level, too. As the pre-elastomer can be used in a liquid form, this monolithic approach has advantages in handling of the materials. If this is not applicable, the second method to integrate the material would be the hybrid assembly of preformed elastomer films, e.g. by using bonding processes or adhesives.
In our experiments, this pre-elastomer solution is a dichloromethane solution of polymethylsiloxane polymer with side-chain units like phenyl benzoate derivative, as mesogenic molecule, and benzophenon crosslinker. The preformed films consist of a similar material.

Experiments

To investigate how and under which conditions FULCEs can substitute other actuator materials, preliminary tests have been carried out. A typical bending beam structure was chosen to demonstrate the process steps for the utilisation of FULCE as an actuator. Even for this rather simple example, at least five different technology steps had to be adapted for the use of FULCEs (see fig. 3). The alignment of the mesogens within the network is a crucial step, because the ability of the material

* fon: +49-(0)3677-69-3422, email: mike.stubenrauch@tu-ilmenau.de

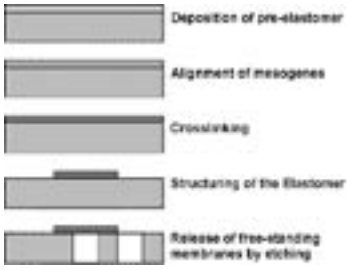

Fig. 3: Required processes steps for the monolithic integration of FULCE in MEMS

to operate as an actuator relies on a uniform alignment with a high degree of order. For the conventional production process of the materials as used in Freiburg, mechanical stretching was applied to align the network. However, this method can not be used with a film deposited on a rigid substrate. Alternatively, electrical and magnetic fields can be used to align the mesogens. For our tests, we deposited films of a pre-elastomer on glass substrates and exposed them to strong fields of 300 kV/m and 11 Tesla, respectively. Using XRD and polarisation microscopy, an effect on the alignment of the network could be shown, but not yet quantified. The results show, that an alignment of the material on the substrate is possible.

Essential for the integration is the deposition and structuring of thin films. Our experiments did show, that this can be achieved using standard photolithography. We spin-coated a pre-elastomer containing a photoreactive crosslinker on a substrate,

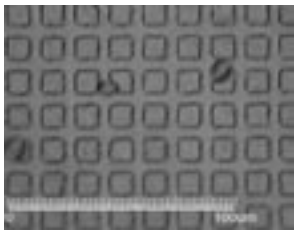

Fig. 4: FULCE patterned using standard photolithography

and crosslinked it after complete evaporation of the solvent using a standard photomask. The parts exposed to UV light were crosslinked to an unsolvable elastomer, while the rest of the pre-elastomer was not crosslinked and could be solved in toluene after the exposure. As shown in figure 4, structures down to 5µm could be patterned using this method. The thickness of the film is about 500 nm. Thicker films can be made by changing the viscosity of the pre-elastomer-solution or the method of application. The biggest problem while increasing the film thickness is the swelling of the elastomer structures due to the developing in toluene, which can affect the mechanical properties.

To be able to use the contraction of the material as displacement, we also needed to release free-standing elastomer membranes by etching. We choose advanced silicon etching (ASE) for this step because of its mechanically advantageous etching geometry, selectivity, and low process temperatures. The tests were carried out using a non aligned elastomer, that had been applied to the surface in a solution and was crosslinked using the mask aligner AL 6-2 prior to etching (see fig. 5).

Fig. 5: Free standing elastomer membranes released by ASE

To test the hybrid integration of preformed films, we needed to find a low-temperature method for assembly. As adhesives are likely to have negative effects on the elastomer, we adapted a technique for the assembly of polydimethylsiloxane on silicon[4]. The elastomer and the silicon surface were activated in oxygen plasma and brought in contact with each other. The oxidised FULCE sealed immediately and irreversibly to the silicon surface. Using this approach, we were able to manufacture a demonstrator that shows the remarkable actuator properties of the materials (see fig. 6).

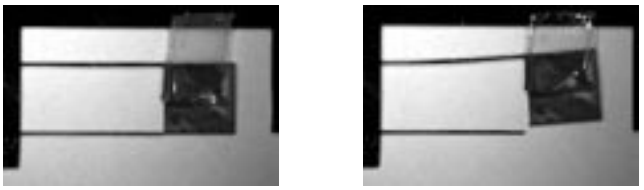

Fig. 6: Deformation of a silicon structure due to the shrinking of FULCE

Summary

We were able to show that all necessary processes for manufacturing a micromechanical system containing FULCE are compatible with existing technologies and materials. Full integration into batch processing and hybrid assembly have been investigated and found to be suitable for application. The next step in the ongoing research will be the combination of all processes described here on standard 4 inch substrates and the mechanical characterisation of the manufactured systems.

The project is funded by the European Union under contract no. HPRN-CT-2002-00169.

[1] Thielicke, E. ; Obermeier, E.: Microactuators and their technologies. In: Mechatronics 10 (2000), Nr. 4-5, p. 431-455
[2] Wermter, Hendrik ; Finkelmann, Heino: Liquid crystalline elastomers as artificial muscles. In: e-Polymers 013 (2001)
[3] Finkelmann, H. ; Nishikawa, E. ; Pereira, G.G. ; Warner, M.: A New Opto-Mechanical Effekt in Solids. In: Physical Review Letters 87 (2001), Nr. 1
[4] Duffy, David C. ; McDonald, J. C. ; Schueller, Olivier J. A. ; Whitesides, George M.: Rapid Prototyping of Microuidic Systems in Poly(dimethylsiloxane).

ECR-etching of 3C-SiC for MEMS

Ch. Förster*, V. Cimalla, O. Ambacher, and J. Pezoldt
Department of Nanotechnology

At the present time there is an increasing interest in wide bandgap semiconductor materials such as SiC. This material is excellent for high temperature (over 250°C), high frequency and high power applications. Silicon carbide can bee useful for some active electronic devices like field effect transistors, heterojunction bipolar transistors, and thyristors. Furthermore, optoelectronic devices such as wave guides and sensors for applications in harsh environments can be based on SiC. The physical properties of SiC make this material suitable for modern device applications like microsensors and microactuators in microelectromechanical (MEMS) systems and nanoelectromechanical (NEMS) systems with frequencies up to the GHz range.

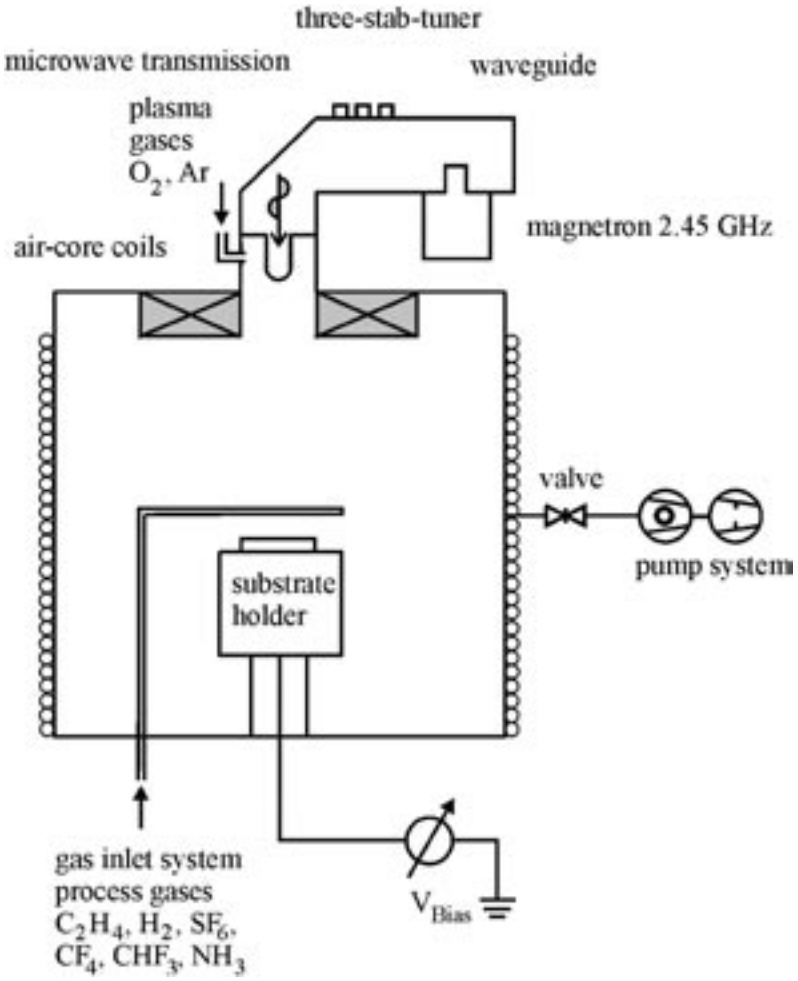

Fig. 1: Schematic illustration of the ECR equipment

Due to the high thermal and chemical stability, wet etching processes can only be performed at very high temperatures, in molten salts or electrochemically under UV light. Alternatively, plasma based dry etching processes can be used. For device and sensor applications, beside a sufficient etch rate, smooth surfaces and high anisotropy are necessary. ECR plasma based etching provides this opportunities. The first application of ECR plasma for etching of semiconductors was published by Suzuki in 1977. Compared to reactive ion etching (RIE) ECR plasmas have the advantage to generate a high ion density plasma at low process pressures, typically at 0.5 – 5 mbar. The plasma density can be further optimized by adjusting the distance between the ECR source and the sample. Furthermore, the ion flux rate and the incidence angle of the ions towards the surface can be adjusted separately. Additionally, the ion energy can be controlled by applying a defined bias voltage which is not possible in the case of RIE, where the bias voltage depends on the power, gas flow and pressure. Another important advantage of ECR plasma is an independent control of the ion current density by changing the ECR source power. The disadvantage of ECR processes are the lower through put and the more sophisticated microwave circuit matching. In the present study a comparative investigation of the applicability of two different fluorinated gases on the MEMS structure formation based on 3C-SiC and Si was carried out by using ECR-technique. The used equipment consists of a Roth & Rau ECR source mounted on a PLS 500 system from Balzers AG. The set up is shown in Fig. 1. The ECR source operates at 2.45 GHz and a magnetic flux density of 875 G. Two separate gas inlet systems were used for the experiments. The first gas system for the plasma gases Ar and O_2 and the second one for the process gases CF_4 and SF_6. The gas flows were varied within a range from 0 to 25 sccm and 0 to 20 sccm for SF_6 and CF_4, respectively. The fluorinated gases enter the chamber through a distribution ring close to the

* fon:+49-(0)3677-69-3352, email: christian.foerster@tu-ilmenau.de

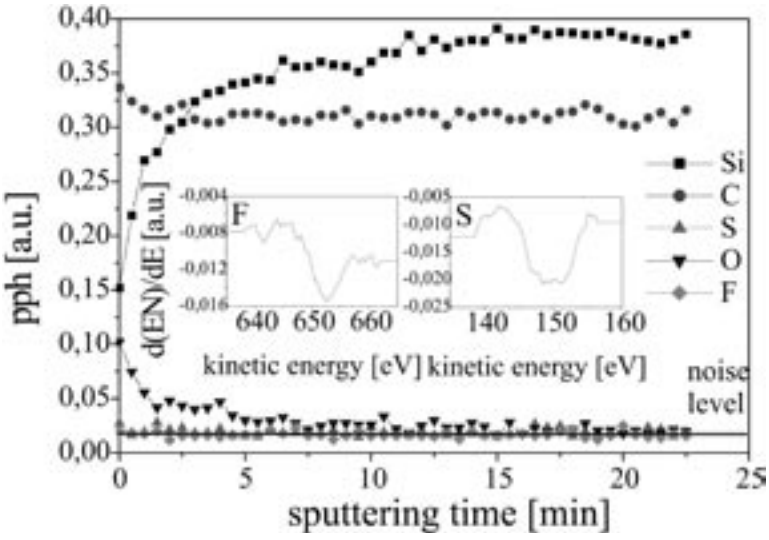

Fig. 2: AES measurement of 3C-SiC sample etched in case of SF_6

sample. This design allows the generation of radicals by the Ar/O_2 plasma directly above the processed sample surface. The Ar to O_2 ratio was kept at 8 at an overall flow rate of 45 sccm. The bias voltage was kept at 0, 50 or 70 V. The bias voltage was chosen in a way, that the ion damage in the near surface regions was as low as possible. For every set of the etching parameters SiC and Si samples were treated simultaneously to exclude the influence of process fluctuations. The etch rate was determined by measuring the step heights with an Ambios Technologies Profilometer and in the case of 3C-SiC by reflectometry. The surface composition was determined by Auger electron spectroscopy (AES).

The obtained results can be summarized as follows. In the case of SF_6 the etch rates of Si and SiC at a constant gas flow of 20 sccm are by a factor of 9.8 and 1.4 higher than in the case of CF_4. In all experiments the etch rates of Si compared to 3C-SiC achieved with SF_6 are much higher compared to CF_4. The maximum of the selectivity is around 2 for CF_4 and 11 if SF_6 is used. The value obtained for SF_6 shifts to higher gas flow rates. The etching rate increases with increasing bias voltage and plasma power. This is due to the increasing excitation of the etched surface by ion bombardment in the case of increasing bias voltage. The increase of the etching rate with increasing plasma power is due to a higher concentration of reactive species generated in the plasma and reaching the surface. The highest etch rates at the chosen conditions were for SiC 260 Å/min and 160 Å/min in the case of CF_4 and SF_6, respectively. For Si etch rates of 1570 Å/min (SF_6) and 260 Å/min (CF_4) were achieved. Smooth and residue free surfaces after the etching are important, because unwanted contaminations can have a strong negative impact on subsequent technological steps, device properties and device reliability. For this reason the determination of residual contaminations caused by plasma treatment after the etching process is of crucial importance. The chemical composition of the 3C-SiC and Si surfaces were investigated by AES. A typical depth profile is shown in Fig. 2. From this depth profile it can be deduced that only an adsorption layer of F and S exists in the case of SF_6, but a change in the surface stoichiometry was evident due to the reaction of F with Si. Nevertheless, the obtained chemical and morphological quality is suitable for the envisaged application. Based on the developed process different MEMS structures were fabricated. One of them is shown in Fig. 3 were the application of the etching in conjunction with an exposure process using a self adjusting process leads to submicron dimensions also micron resolution lithography is applied for nozzle formation. In conclusion, ECR etching of 3C-SiC and Si with SF_6 and CF_4 was investigated. By using SF_6 higher etch rates and a higher selectivity were achieved. At the maximum etch rates residue free 3C-SiC surfaces were obtained.

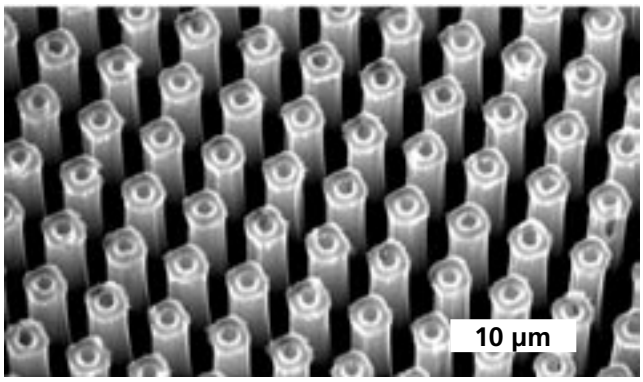

Fig. 3: SEM SiC/Si nozzles formed by ECR etching

This work has been supported by the European Union under contract G5RD-CT-2002-00704.

Education network for the maintenance of qualified employees in microsystems technology in Thuringia

I. Hirt* **and H. Wurmus**
Micro-Comp e. V.

FasiMiT is one of six education networks for microsystems technology (MST) in the Federal Republic of Germany supported in the context of the initiative MST 2000+ funded by the Federal Ministry of Education and Research (BMBF).
It is the aim of the network to contribute to the development of education and advanced professional training in microsystems technology in Thuringia. Young people shall be encouraged and motivated to education and training in the fields of technology and natural science to overcome the lack of qualified employees in this field.

University education in microsystems technology will be provided by both the ZMN and the Micro-Comp e.V. in cooperation.
Available competences shall be emphasised in the field of education and further professional training. Already existing activities of Mikrotechnik Thüringen e.V., OptoNet e.V., as well as MikroTec will be used for installing a wider training network.

The major aim is to develop a systematic training ensuring a high standard of qualified employees. In addition, the job market potential must also be considered, including pupils and students, as well as employees in enterprises and also unemployed people. In the context of the project, the activities will be coordinated with partners from education, science and industry, as well as political actions of the state of Thuringia.

Basic topics of the project are: determination and sensitization of the public for the need of qualified employees, development of strategies to ensure the availability of qualified employees, as well as organization and conducting of the basic education (school, vocational training, studies), further training on the job, and second-chance education (retraining). (See figure 1)

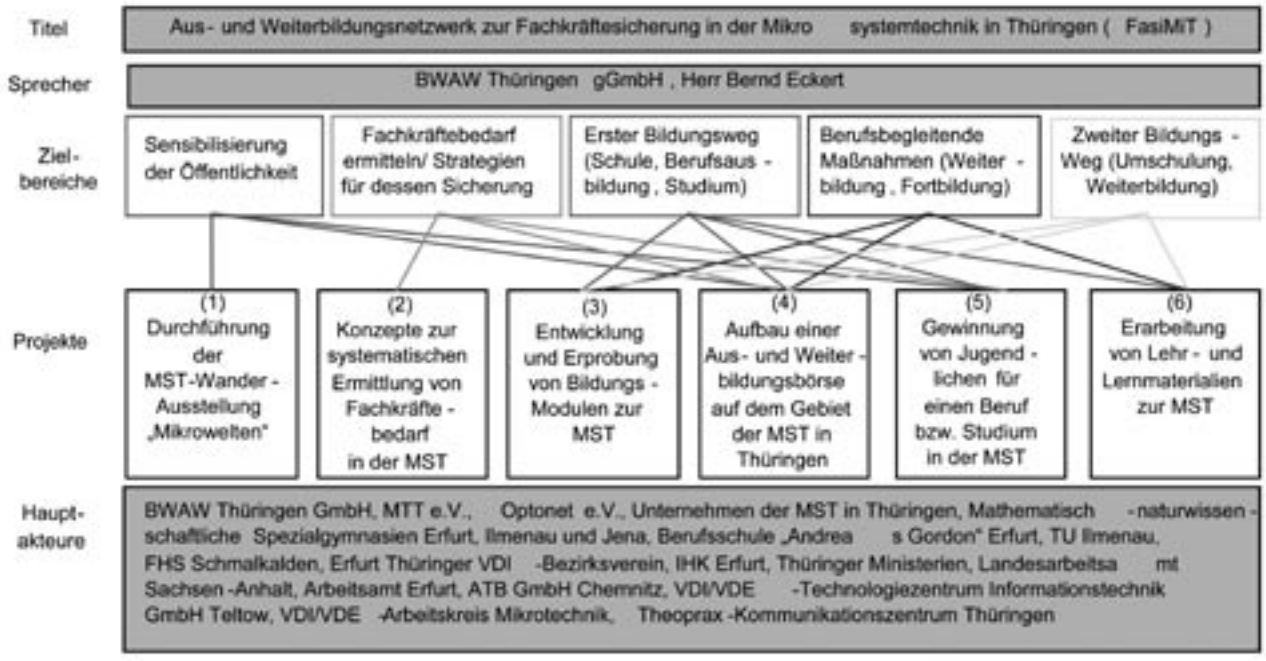

Fig. 1: Schematic overview showing the network of institutions involved in the program FasiMiT and the steps necessary to be accomplished.

* fon: +49-(0)3677-468386, email: info@micro-comp.de

First results (selection)

Coordination of the touring exhibition "Mikrowelten "

The exhibition "Mikrowelten" of the VDI/VDE was presented in the frame of the exhibition "Mikro-Optowelten" in the IHK Erfurt from Feb. 10 until March 15 2003, together with several exhibits of Thuringian companies.

Numerous visitors showed their interest in regional innovative developments and applications in the field of microtechnology and microoptics. In this context, infrared sensors and high-resolution measuring systems from Erfurt, as well as micro drives and fibre optics from Ilmenau were presented together with laser technology and chip systems for the detection of DNA.

About 2900 pupils used the exhibition to ask extensively about future demands in professional education in microsystems technology such as "Mikrotechnologe" and "Mechatroniker". The presentation was completed by seminars and additional events concerning spin offs and innovation funding, as well as opportunities for university studies in Thuringia. The award winners of the "Physikolympiade 2003" were honoured and information about the program "Berufschancen und Studien in Thüringen" was presented to pupils.

"Systematic qualified employee need inquiry"

A lack of qualified employees in the area of microsystems technology can already be recognized. An important field of the work of FasiMiT is the systematic and continuous determination of the need for qualified employees to derive measures suitable to guarantee the supply with qualified employees.

First results in the determination of the need for qualified employees in Thuringian enterprises were presented at a conference at the Fraunhofer IOF in Jena. Until now, relatively few MST enterprises deal with the future need of qualified employees in Thuringia. This is due to the fact that future developments and applications of MST products in industry are difficult to estimate because of the dependence on a broad range of external influences, especially in the semiconductor market.

"Development of education modules, preparation of teaching and studying materials"

Based on the information of the partner facilities on their demand in different education disciplines, the acquirement of education modules, as well as teaching and studying materials was started. An education module addressing the subject optics assembly / micro optics assembly was completed already by Fraunhofer IOF and tested in the teaching process at the FH Jena in the course "laser and visual technologies" and in mechanical engineering with the specialisation in MST.

Education modules are being prepared for future education at TU Ilmenau, including the technical spectrum of the different micro techniques as well as other subjects such as hybrid technology, nano-electronics, and material science based on glass and ceramics.

"Education and advanced professional training exchange forum"

The offers for education shall be published on the Internet in both new created and already existing portals. First concepts for a new portal with an exchange forum for MST education and advanced professional training is already being worked out. An important aspect is to find a future framework to continue the work initiated in this project. First contacts are established, i. e., with WIP portal, education portal Thuringia, and VDE/VDI.

The network FasiMiT is supported by the BMBF (16SV1847)

Characterization of vertical regions of microstructures based on monochromatic speckle-techniques

B. Horvath and H. Wurmus*
Department of Microsystems Technology

There are presently several 3D measurement procedures available for inspection of microstructures. These have in common that they can be applied only up to a well-defined surface inclination that is generally 15-20°. Thus, we cannot obtain any information from steep sidewall areas of structures. This has first of all physical reasons: either the scanning tip is not able to follow the surface, or simply the optical sensor does not receive any reflection signals. However, if form-tools have to be produced in microtechnical ways (for instance for microreplication technology), the quality of these "invisible" structure walls will become of critical importance. If the walls are too rough, the tool may cause damages to the finished plastic products by lifting out the implement. This problem has led to the demand for a method for quality inspection of steep microstructure surfaces [1]. An optical, coherent, parametrical technique was developed in this work for non-contact inspection of microstructure-sidewalls. The method is based on coherent scattering and evaluation of speckle patterns with laser illumination. Several properties of speckle phenomena are exploited in the measurement. The patterns found are filtered in the spatial frequency domain and analysed with various correlation- and statistical methods.

Fig. 1: The measurement setup

The principle of the measurements is as follows. That microstructure sidewalls can be illuminated under an adequate angle by a focused laser beam. A feature of the phenomena is that the average size of the generated speckles and the diameter of the illuminated surface-spot are in reciprocal relation. The device projects a convergent laser-illumination (HeNe 633 nm) directly onto the sidewall. Since the vertical surfaces lay in the collimator focus, a widespread speckle pattern appears on the screen standing behind the structure wall. The beam reflected from sidewall illuminates a lager area of the environmental surface. Thus, the secondary scattered patern appears with higher spatial frequency to the primary speckles. These disturbing high-frequency light components can be eliminated by a low-pass filter. The obtained stochastic intensity distributions can be evaluated by statistical methods (intensity, contrast) or by comparison of the speckle-images (cross-correlation, auto-correlation). The device is designed especially for non-destructive and simple roughness-analysis and features contactless testing, short measurement times, and user- friendly handling under Windows-systems.

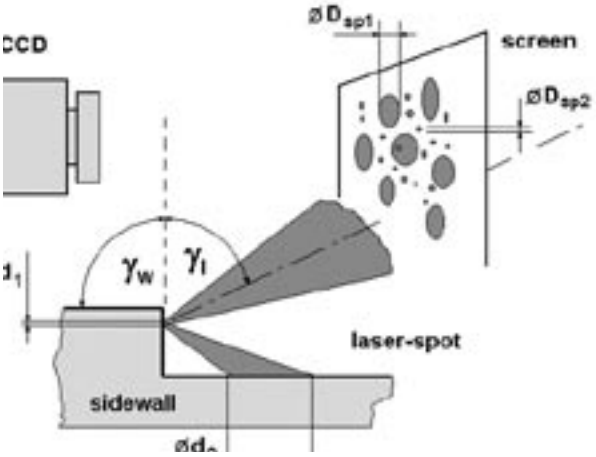

Fig. 2: Evolution of speckles at structure walls

The scattering properties of a surface depend, e. g. on the roughness. Because the speckle pattern presents the actual coherent scattered light, its intensity increases with increasing roughness. A rougher surface profile in turn causes a higher phase-deviation, which emerges as a higher

* fon: +49-(0)3677-69-2487; email: helmut.wurmus@tu-ilmenau.de

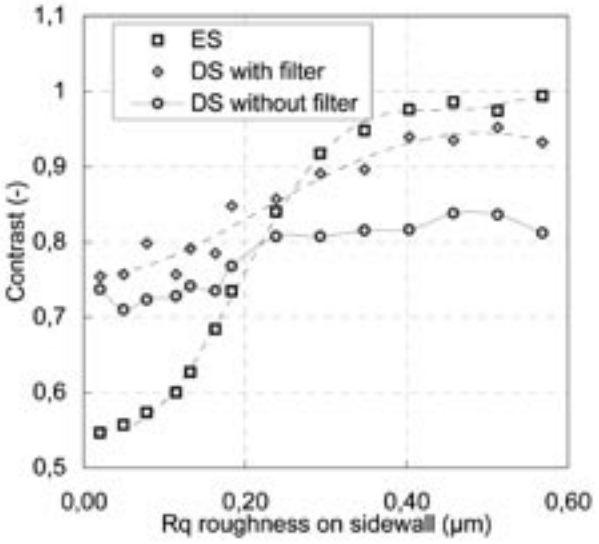

Fig. 3: Speckle-contrast as a function of sidewall roughness

intensity-modulation in the speckle structure, and the contrast increases. Both of these properties form the basis of the speckle-statistical measurements that can be used up to a certain roughness-limit of Rq=0.25-0.3 µm. Thus, the statistical evaluation can be applied only to specular reflecting surfaces. Figure 3 shows the contrast as a function of roughness for the evaluation of entire scattering field as well as for perpendicular sidewalls with and without the filter process.

In the case of higher roughnesses the comparison of speckle-structures under different illumination conditions can be utilized as a measurement effect. Traditionally, either the wavelength or the incident angle of light is changed. The decorrelation between the patterns rises with increasing roughness (spectral and angular correlation). The realized setup uses angular and spatial correlations. In the first case a slight offset of the laser beam in the object space of the lens appears as a change in the incidence angle at the surface plane. The correlation coefficient between both distributions is considered as an optical parameter for the roughness. In the latter case the speckle patterns are recorded with a slight shift of the sample and similarly the correlation of the distributions is calculated. However, the correlation processes can be adopted in a wider application range of Rq=0..1 µm, also over the maximal limit of speckle-statistics.

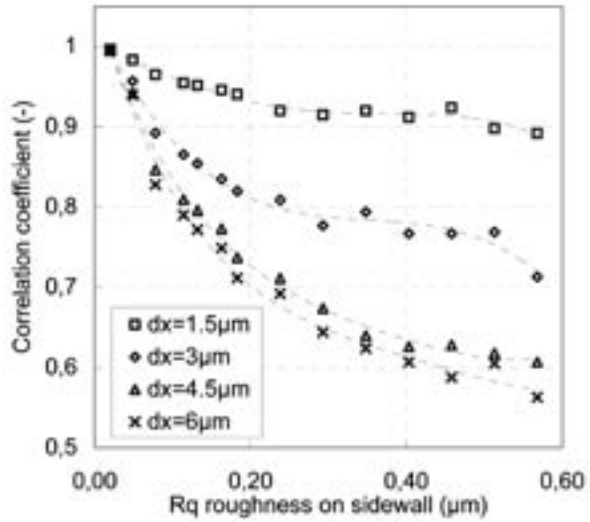

Fig. 4: Spatial correlation as a function of sidewall roughness

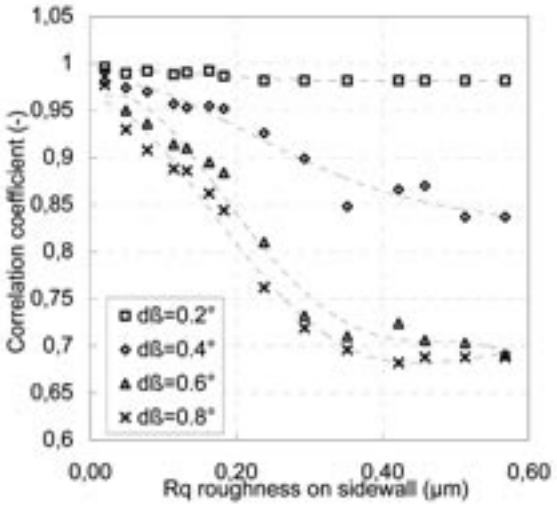

Fig. 5: Angular correlation as a function of sidewall roughness

This work has been financial supported by TMWFK

[1] M. Fischer, A. Albrecht: Prägewerkzeuge aus Silizium, Jahresbericht Zentrum für Mikro- und Nanotechnologien, 2002.

Modification of GaN and AlGaN surfaces for nano- and picofluidic sensors

G. Kittler[1,*], V. Cimalla[1], V. Lebedev[1], M. Fischer, S. Krischok[2], V. Yanev[2], J.A. Schäfer[2], and O. Ambacher[1]
Departments of Nanotechnology[1] and Technical Physics[2]

The modification and functionalization of GaN and AlGaN surfaces is an important part of the development of a sensor-system analyzing very small volumes of water based liquids in the range of 1 nl down to 50 pl. These small droplets can contain ions, rare substances, expensive pharmaceuticals, and organic substances like viruses. The fluidic system will enable a fast and cheap screening of these substances by electrical and optical measurements. In the first period of the project a sensor for analyzing the droplet volume of polar liquids like water will be developed. Group III nitrides are the ideal material system to realize the sensor structure. Because of the piezo- and pyroelectric properties AlGaN/GaN heterostructures can confine a polarization induced two dimensional electron gas (2DEG) close to the interface without the need of a modulation doped barrier. The carrier concentration and electron mobility within the 2DEG can be very high and build up an electrically conductive channel with low sheet resistivity. Because of charge neutrality the carrier concentration of the 2DEG is sensitive to any change of net surface charge. That means that the source drain current of an AlGaN/GaN based HEMT structure varies corresponding to a manipulation of surface charge or work function, e.g. caused by polar liquids. The scheme of a sensor is shown in Fig.1. The water droplet will be positioned on the active area and has to spread over the whole sensitive area to achieve a significant drop in source drain current. Therefore a hydrophilic active area and a hydrophobic surrounding are necessary. In addition the dynamic range increases by the proposed manipulation of surface wetting because the 2DEG underneath the whole active area is depleted by small volumes of liquid. The third positive effect is the self positioning of droplets over the active area in case of an insufficient droplet positioning.

Dry thermal and wet thermal oxidation processes were performed to get a hydrophilic active area. To achieve a hydrophobic surrounding different materials were deposited on top of the sensors. Surfaces were characterized by contact angle

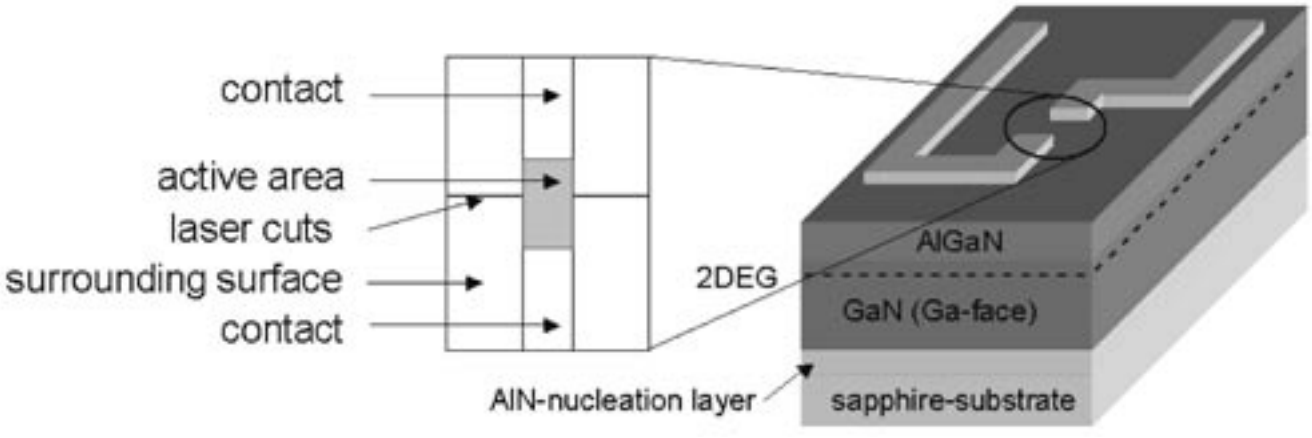

Fig. 1: Scheme of a fluidic sensor with enlarged active area and its surrounding.

measurements, atomic force microscopy (AFM), Auger electron spectroscopy (AES), and X-ray photoelectron spectroscopy (XPS). The dry thermal oxidation was performed by rapid thermal processing (RTP) at about 750°C for 3 minutes under oxygen atmosphere. In all cases the oxidation leads to a better wetting behaviour of the surface. The contact angle of deionized water on GaN decreases from almost 90° to 3° because of a thin oxide layer on top of the sample as revealed by AES. But the wetting behaviour of the oxidized GaN surfaces is not stable in time and as a consequence the contact angle almost increases to the initial value within a few hours. Probably oxygen containing adsorbates, e.g. water, are responsible for this behaviour. Oxidized AlGaN surfaces show a more

* fon: +49-(0)3677-69-1172, email: gabriel.kittler@tu-ilmenau.de

stable wetting behaviour (Fig.2). The contact angle increases within the first 48 hours, but than keeps stable at 42° as it is shown in Fig.4. For the wet thermal oxidation a new setup was realized consisting of a quartz tube, a furnace, and a bubbler. Experiments by wet oxidation of GaN samples revealed a similar characteristic like for dry oxidation. The wetting behaviour was drastically improved but degraded with time. SiN_x, oxidized aluminium, and fluorine carbon compounds (FC) were deposited on the sensor to realize a hydrophobic active area, but only fluorine-carbon (FC) compounds had hydrophobic properties as it is shown in Fig.3. FC layers were deposited by reactive ion etching (RIE) or by inductively coupled plasma (ICP) processes. The FC layers had different wetting properties in dependence of processing because of different chemical composition. The ICP layers had a higher content of CF_2-bonds (Figs.5 and 6). These bonds are responsible for the hydrophobic behaviour as it is known from PTFE (Teflon®) which consists of CF_2-bonds. FC layers also showed an instable wetting behaviour, but after 6 hours the contact angle remained stable.

The next step was the electrical characterization of the thin FC layers. After deposition on an insulating substrate (sapphire) gold contacts were evaporated on the FC layer. The specific resistance and conductivity were calculated by taking into account the film thickness and contact geometry. The specific resistance of the FC layers is in the range of

Fig. 2: Water droplet on hydrophilic oxidized AlGaN surface.

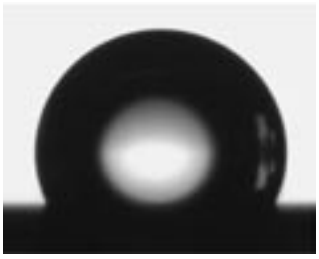

Fig. 3: Water droplet on ICP Fluorine-Carbon layer.

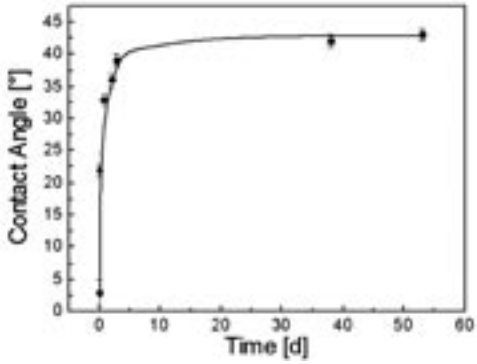

Fig. 4: time-dependent behaviour of the contact angle of water on AlGaN surface

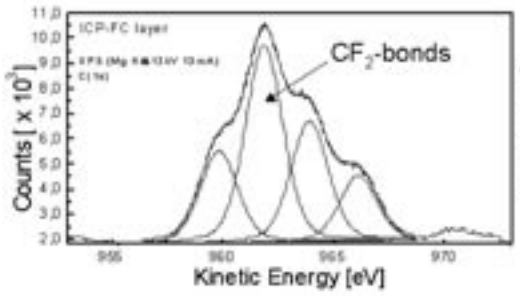

Fig. 5: XPS measurement for an ICP-FC layer.

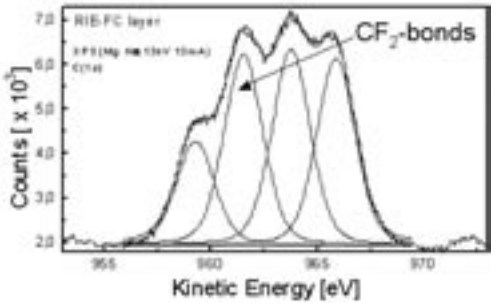

Fig. 6: XPS measurement for a RIE-FC layer.

1.6×10^9 to 8×10^{10} Ohm x cm and is two orders of magnitude higher than that of deionized water. So a current path through this layers is avoided. The last step was to check whether it was possible to create a window for the active area in the FC layers and to passivate the contacts by FC layers. The critical dimension is about 5 µm. It was successfully realized by a lift-off process. Dry thermal oxidation of AlGaN surfaces leads to an improved and stable wetting behaviour of the active area. Fluorine-carbon layers are used to successfully realize a hydrophobic surrounding. Further work will show the influence of surface modification on the electrical characteristic of the sensor and will lead to a better understanding of the oxidation process.

This work was supported by the Thuringian Ministry of Science, Research, and Art and the European Union (EFRE programm and 6th framework program).

Modelling and alignment of SiC quantum dots

J. Pezoldt[1,*], V. Cimalla[1], Th. Stauden[1], Y. V. Trushin[2], A. A. Schmidt[2], K. L. Safonov[2], E. E. Zhurkin[2], V. S. Kharlamov[2], M. N. Lubov[2], and S. A. Korolev[2]
[1] Department of Nanotechnology
[2] STU Sankt Petersburg, Russia

Self organized phenomena applied to produce quantum dot structures represents a new research area in epitaxial growth techniques. In contrary, antidot systems attracted much less attention. They are acting as non linear scattering centres and influence drastically the lateral conductivity, the photoconductivity or the magnetotransport in vertically confined layer structures like two dimension electron gases (2DEG). Previous studies concentrated on the formation of antidots inside a two dimensional electron gases (2DEG) using self-assembled islands of III-V semiconductor with a wider bandgap or using etched holes. Much less work is done for the integration of antidots into the Si technology. The wide band gap semiconductor SiC is a candidate for the creation of antidots in Si. It can be grown epitaxially on Si, however, only a few investigations of SiC nanocrystals on Si exist and no demonstration of an antidot alignment can be found in the literature. The large lattice mismatch of 20% stimulates a three-dimensional nucleation of SiC on the Si substrate. However, non uniformity in the size and the distribution of the islands strongly limit practical applications. Thus, the control of the nucleation sites of SiC is a precondition for a lateral alignment of the SiC nuclei. In the technology of the formation of Ge clusters on Si several ways to localize the nucleation sites are known, e.g., ordering on lithographically pre patterned substrates, on dislocation networks, and along step arrays on vicinal substrates. The latter method of two dimensional ordering has the advantage not to require additional processing steps. However, during the SiC nucleation on Si the substrate participates in the reaction to SiC by lateral Si diffusion. Consequently the surface is unstable during the growth which complicates an alignment control. In this work we describe a method to form regular arrays of SiC dots on Si based on the control of the nucleation sites by step arrays. We demonstrate how the growth temperature and time can be used to tune the size and distribution of the SiC nanostructures in order to align them regularly along step arrays.

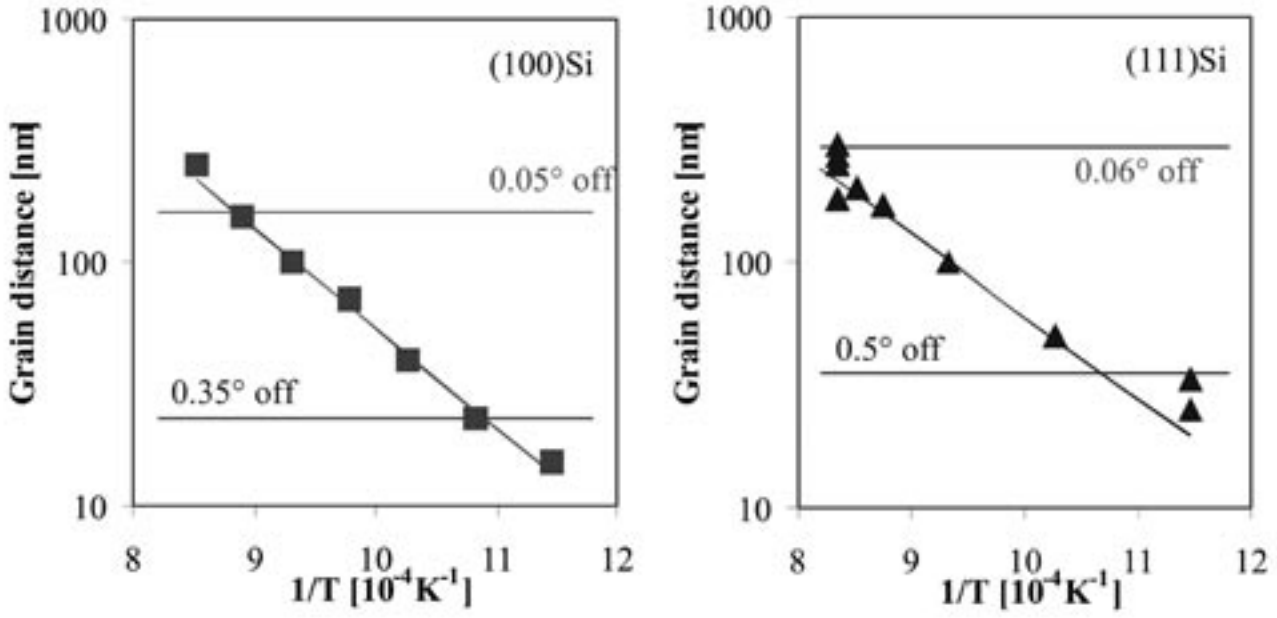

Fig. 1: Equilibrium distance of SiC nucleation sites as a function of the growth temperature at a carbon flux of 10^{13} $cm^{-2}s^{-1}$ on (100)Si and (111)Si. Horizontal lines indicate terrace widths for the vicinal substrates.

* fon: +49-(0)3677-69-3412, email: joerg.pezoldt@tu-ilmenau.de

The SiC dots were grown supplying only carbon by solid source molecular beam epitaxy [12, 13]. The grain size and the morphology were determined by AFM with an etched single crystal Si tip. Data were collected from area scans of (1x1) to (5x5) μm^2 with a 512x512-pixel resolution. The surface was characterized by power spectrum density (PSD) analysis [13], which deconvolutes the roughness as a function of surface lateral length. The off cut angle of the used substrates was estimated from AFM measurements and confirmed by x-ray diffraction with an uncertainty of 0.05°. If the growth temperature is increased the SiC island density decreases, i.e., the island separation increases. The nucleation density can be increased at higher temperatures at increased carbon fluxes. The terrace width is a function of the off cut angle of the substrate and the step bunching. For nominal surfaces with off cut angles below 0.5° monoatomic and biatomic steps, which are defining the terrace width, can be prepared on (100)Si and (111)Si, respectively. Examples of terrace width values for substrates, used in this study, are represented as lines in Fig. 1. Thus, if the growth and surface preparation conditions are tuned in a way that the terrace width matches the island separation distance, a linear ordering can be achieved and is demonstrated in Fig. 2.

The main difficulty to grow regular island arrays is the participation of the Si substrate in the reaction with the incoming carbon flux to SiC. It requires a lateral transport of Si to the growing islands resulting in a movement of the step edges during the growth. SiC islands are known to pin steps and the nucleation density increases in the very early stage of growth up to an effective SiC coverage of 10%. Thus, even if regular step or step band arrays can be prepared on the Si surface and the initial SiC islands nucleate regularly, the Si surface transport and the step pinning on islands create irregular step bands. Further nucleation cannot occur anymore on straight step band edges and the distribution of the nuclei will be irregular. This behavior was observed at high temperatures (around 1000°C), since at temperatures above 950°C (i) a remarkable sublimation of Si occurs, and (ii) the growth mode transforms from a quasi two-dimensional nucleation to a pure three dimensional mode with a higher need of Si. Both effects increase the velocity of the step wandering and consequently favor irregularities. To avoid these effects proper growth conditions were chosen. The nucleation behavior was modeled by the kinetic Monte Carlo and rate equation approach. Both gave good agreement of the nucleation size and density on different time scales with the experimental results. Lateral aligned self-assembled SiC dots have been grown for the first time on Si substrates by molecular beam epitaxy. The alignment was defined by the formation of well-ordered monoatomic and biatomic steps as well as step bands on (100) and (111) Si. The arrangement was controlled by three key parameter: (i) the temperature and the flux control the nucleation density, (ii) the processing time defines the size, and (iii) the terrace width has to be adjusted close to the average distance of the nuclei.

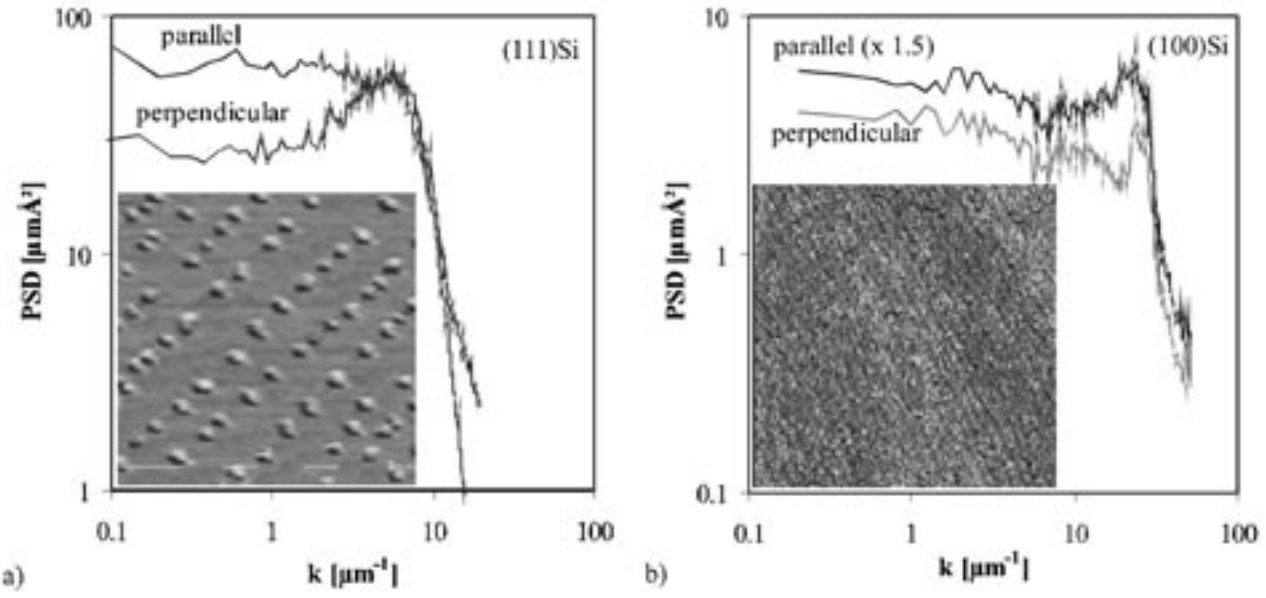

Fig. 2: PSD parallel and perpendicular to the step bands for SiC chains on (a) (111)Si, 0.06° off at 925° C and (b) (100)Si, 0.35° off at 700° C. Inlets are corresponding AFM images.

This work has been supported by DAAD within the Framework IQN project ICC

Forisomes in MEMS

M. Stubenrauch[1], D. Voges[1], C. Schilling[2], and H. Wurmus[1]
Departments of Microsystems Technology[1] and Biomechatronics[2]

In recent years more and more bio related requirements and applications have emerged in microsystems research. One of the key factors for the future success of biomedical and biochemical MEMS will be the integration of biocompatible, biogenic or biomimetic elements in the same size as the functional structures of the systems. In the near furture there will be a demand of valves without noticeable dead volumes, micropumps that do not harm molecules or cells by inducing mechanical stress, and integrated control loops using smart actuators. The traditional approach would be to search for existing solutions in other fields of application and their integration into bio MEMS. The alternative is the evaluation of biological actuators and their use in MEMS as shown here.

In close cooperation with the University of Giessen (Department of General Botany) we use crystalloid p-proteins as actuators in MEMS. These proteins can be found in the phloem system of plant cells in all *Fabaceae*. They were discovered and named "Forisomes" by the group of Prof. Aart v. Bel [1]. Forisomes are large molecule assemblies (about 5µm in diameter, 10-20 µm long) that form a security valve in combination with the sieve cells in the phloem to prevent the loss of fluid after injuries of the plant stem. As they are not part of a living cell structure, their activity does not depend on ATP like all other motor proteins. They are operated by a change of the ion concentration in the environment (mainly Ca^{2+}) and thus called entropic actuators [3].

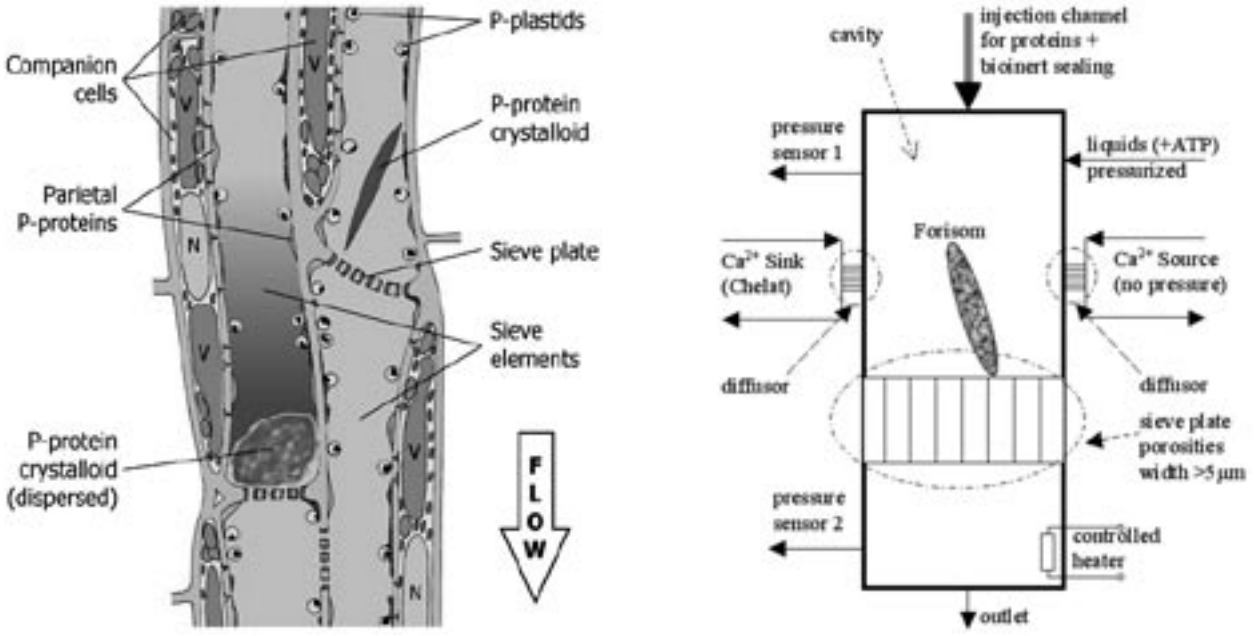

Fig. 1: Phloem system in plants [2] and proposed artificial phloem cell

So far, the working principle, internal structure, genetic sequence, and active behaviour of these proteins are still under intensive investigation. Tests with Forisomes have been carried out in vivo and in vitro (see figure 2). To allow further tests with controlled environmental conditions artificial cells are needed. Standard micromachining technologies were used to create a microfluidic systems as a first approach in silicon. Other materials that coulb be used are glass or special ceramics.
Figure 3 shows the actual setup of the artificial phloem system. The silicon chip is patterned using deep reactive ion etching (ASE) and then bonded with Pyrex® glass. The chip is connected to the liquid

[1] fon: +49-(0)3677-69-3422, email: mike.stubenrauch@tu-ilmenau.de

reservoir with the biological components in a special adapter suitable for microscopy. Silicon barriers with a pitch of 4 µm form the sieve elements. The detailed picture on the right shows the separation unit used to select a forisome or a single cell from a constant flow. A short pressure impulse from the control channel will push the required object into the collecting channel and likewise to the sieve structure. The function of the forisomes will then be tested with different ion concentrations in the flow and detection of any changes in the fluidic resistance. For recording the actuator properties it is also possible to use a reflected light microscope with attached image acquiring system.

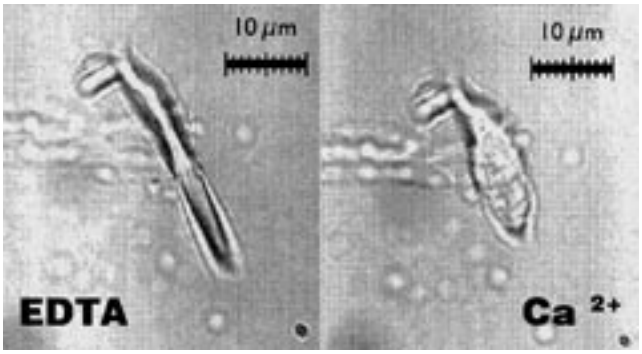

Fig. 2: In vitro test with Ca^{2+} change [1]

Instead of forisomes protist cells were used to show the capabilities of the systems (see figure 4). Forisomes tend to stick to almost every technical surface. Further investigations are necessary to be able to insert these proteins in artificial systems. FC layers used in standard MEMS could be a suitable solution. The deposition technologies have to be modified to get layers into a closed system or to deposit material only on the desired places to allow following bonding processes. Then more functions have to be implemented, like heaters for control of the test conditions, microinjection structures for fast ion concentration changes without pressure interference and electrodes for electrical influence tests. After the evaluation of all properties (mechanical, chemical, electrical) the systems can be easily changed to operate as a valve without any pinch-off effect. After assembly, the system has to be shock frozen and kept frozen until usage due to the limited lifetime. This first demonstrator will be a starting point for a variety of other applications in MEMS.

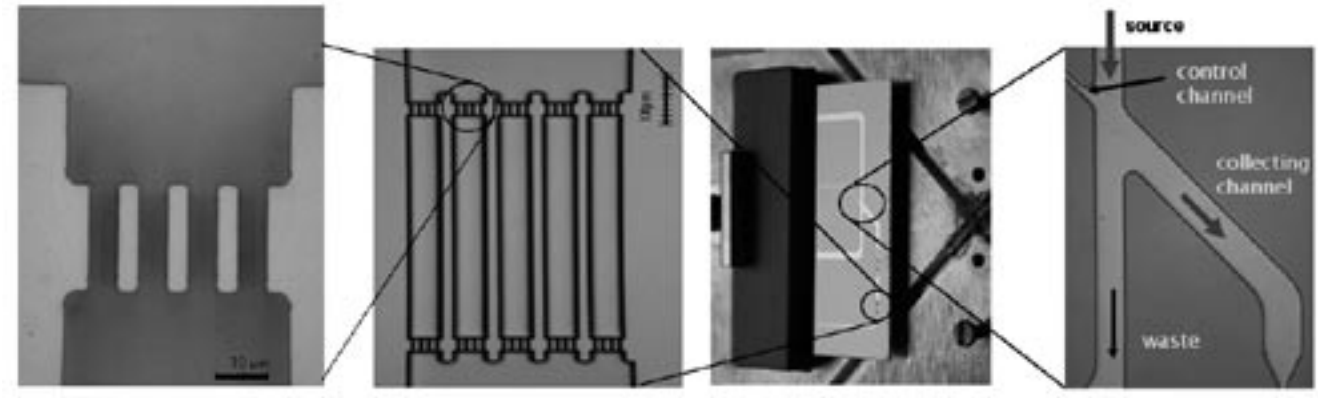

Fig. 3: Sieve elements in a microfluidic system for separation of forisomes from a flow

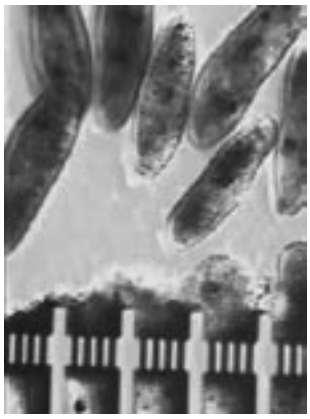

Fig. 4: Paramecium in the demonstrator

This work has been supported by the BMBF under contract no. 0312014C

[1] Knoblauch, M. et. al.; ATP-independent contractile proteins from plants; Nature Materials Sep. 2003
[2] Eckhardt, N.; Plant Cell, Vol. 13; 989-912; 2001
[3] Urry,D. W. Physical chemistry of biological free energy transduction as demonstrated by elastic protein-based polymers. J. Phys. Chem. B 101, 11007–11028 (1997).

A new type of heterostructures for SiC technology: 3C-$(Si_{1-x}C_{1-y})Ge_{x+y}$ /4H-SiC

P. Weih*, Th. Stauden, H. Romanus, O. Ambacher, and J. Pezoldt
Department of Nanotechnology

Silicon Carbide (SiC) is a wide band gap semiconductor that offers many advantages over conventional materials like Silicon or Germanium. Because of the high electron saturation drift velocity, high break down field, high thermal conductivity and chemical and radiation hardness this material is suitable for applications in electronic devices, operated at high temperatures, high power and harsh environment conditions. For the realization of many devices such as Hetero Junction Transistor (HJT) and High Electron Mobility Transistor (HEMT) the formation of heterostructures is required. In case of SiC the draw back is that there are no well developed methods and materials for heterojunction formation. Up to date the only realized intrinsic SiC heterostructure is based on a β-SiC/α-SiC heterojunction, which benefits from different band gaps of the two polytypes. The creation of $(Si_{1-x}C_{1-y})Ge_{x+y}$ alloys provides the opportunity to realize advanced SiC/$(Si_{1-x}C_{1-y})Ge_{x+y}$ heterostructures for band gap and strain engineering.

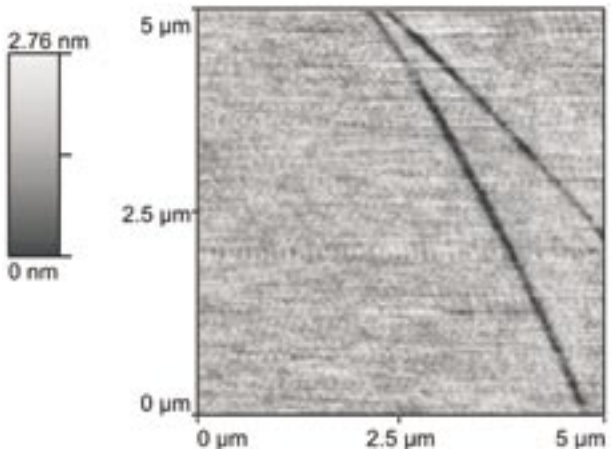

Fig. 1: Untreated 4H-SiC substrate.

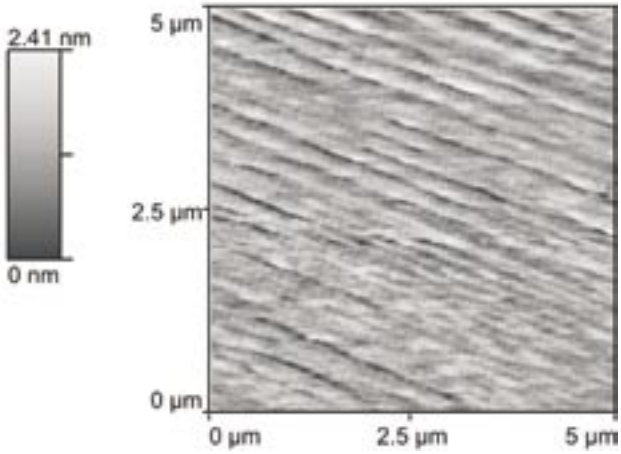

Fig. 2: 4H-SiC substrate after in situ cleaning.

In this work we present the realization of a new type of heterostructure based on the epitaxial growth of $(Si_{1-x}C_{1-y})Ge_{x+y}$ solid solutions on SiC substrates. For the structural quality of the epitaxial layer the control of the initial surface is of great importance. The critical issues in cleaning SiC is to remove the damages and imperfections caused by mechanical polishing (Fig. 1) as well as oxides and contaminants from the surface. The preparation of a specific reconstructed substrate surface and subsequent depositions of SiC layers are carried out in an ultra high vacuum molecular beam epitaxy (MBE) chamber (p = 10^{-10} mbar) on 4H-SiC (0001)Si on-axis substrates. The commercial available SiC substrates provided by Stearling are loaded in the MBE chamber without any chemical treatment. After an out gassing procedure for 1 hour at 500°C the native oxide is desorbed at 900°C for 3 minutes under a week Si flux. A well defined, reproducible (3x3)-Si reconstructed SiC surface is prepared by using a special in situ Si etching procedure. As a result of the cleaning process a step like surface morphology is observed with step heights of one unit cell (1 nm for 4H-SiC, Fig. 2). The preparation of the initial surface and the following epitaxial process are monitored in situ and controlled by reflection high energy electron diffraction (RHEED).

In order to grow epitaxial $(Si_{1-x}C_{1-y})Ge_{x+y}$ layers attention has to be paid to some challenges arising from the specific properties of the Si-C-Ge ternary alloys. The immiscibility of Ge in the SiC lattice, the low desorption temperature of Ge on the SiC surface and the tendency of Si- and Ge- to cluster formation are draw backs resulting in various difficulties during the epitaxial growth. To our knowledge there are only two publications present in the literature about epitaxial growth of $(Si_{1-x}C_{1-y})Ge_{x+y}$ alloys [1, 2]. With the attempt of Ge incorporation into the SiC lattice two different growth techniques were applied, namely (a) continuous fluxes of Si, C and Ge and (b)

* fon: +49-(0)3677-69-3352, email: petia.weih@tu-ilmenau.de

atomic layer epitaxy (subsequent deposition of C and Si/Ge). Several experiments were performed by varying the substrate temperature between 750°C and 950°C. The surface morphology, the chemical composition and the structural quality of the layers were investigated by a combination of atom force microscopy, secondary ion mass spectrometry and transmission electron microscopy, respectively. The structural investigations revealed that independent on the applied growth technique a polytype transition occurs. The grown layers exhibit a high quality cubic 3C-SiC single crystal structure and a perfect interface between the layer and the substrate (Fig. 3). The epitaxial relationship corresponds to a (111) plane of the cubic structure which is oriented parallel to the (0001) 4H-SiC plane. Transmission electron microscopy investigations revealed that the layers grown by atomic layer epitaxy are nearly free of defects and twinning and exhibit a higher crystalline quality in comparison to layers grown at continues fluxes. Energy dispersive X-ray analysis (EDX) could not detect Ge in the layers grown at continues fluxes. If controlled atomic layer epitaxy was applied Ge incorporation into the 3C-SiC layer was observed (Fig. 4). These results were supported by secondary ion mass spectrometry investigations.

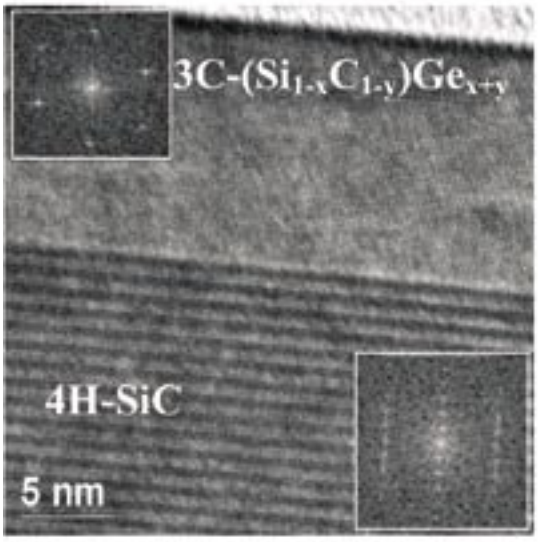

Fig. 3: Cross section transmission electron microscopy micrograph of the 4H-SiC substrate and the 3C-SiC:Ge epitaxial layer as well as the corresponding electron diffraction pattern.

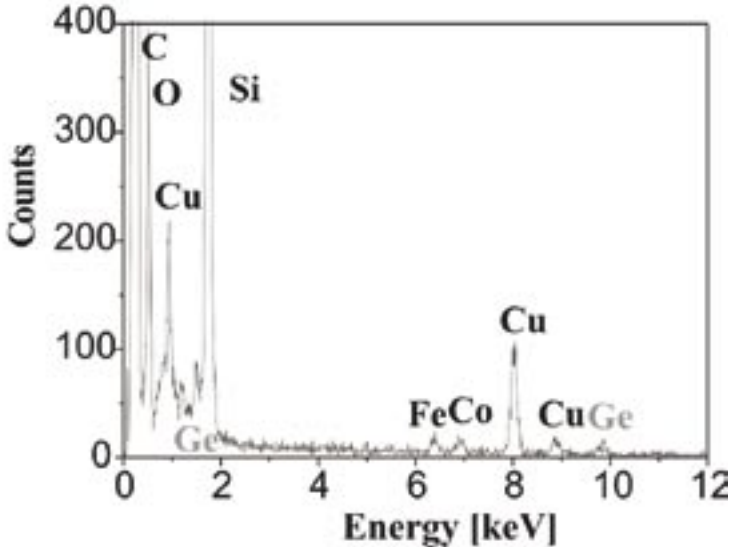

Fig. 4: Energy dispersive X-ray analysis of the grown layer.

In conclusion, a new type of heterostructure was realized by growing $(Si_{1-x}C_{1-y})Ge_{x+y}$ alloys by molecular beam epitaxy on 4H-SiC (0001)Si on-axis substrates. High quality 3C-$(Si_{1-x}C_{1-y})Ge_{x+y}$ layers were achieved using atomic layer epitaxial growth technique at low temperatures. About 0.1% Ge was incorporated into the layers by applying subsequent deposition of C- and Si-/Ge-fluxes without any annealing steps. For the applied growth techniques an optimum in the growth conditions between the higher temperature regime necessary for the growth of high quality 4H-SiC layers and the lower temperature regime promoting Ge incorporation has to be found in future approaches. Furthermore, subimplantation molecular beam epitaxy experiments will be carried out in order to increase the concentration of Ge atoms in the SiC lattice.

The authors would like to thank the TMWFK (B 607-02006) for the financial support and Mrs. Remdt for the TEM sample preparation.

[1] P. Weih, et al., phys. stat. sol. (c) 1 (2003) 347.
[2] M. Diani, et al., Phys. Rev. B, 67 (2003) 125316.

New materials and technologies for printed circuit boards - A development from the perspective of new demands for environmental-friendly products and production steps

G. Winkler*, G. Bischoff, and A. Sutor
Department of Design and Technology of Electric Components

Regulations
International instruments to manage the environmental issues are the „Eco-Audit", which is validated in the European Community and the ISO 14000 from the International Organization for Standardization.

An important requirement for environmental-friendly recycling is to sort the material of electronic devices in various classes. The draft of an order in Germany, called „Elektronikschrottverord nung", specifies the devices in various classes. The elimination of harmful chemical substances in base materials is also an important requirement. Perhaps it is the most important issue!

Bare printed circuit boards (PCB) as main carrier for electronic components
To achieve best results from the perspective of recycling and environmental-friendly production steps, the entire system of bare PCB, technology and components has to be considered. Different materials for bare boards, structuring and assembly will be described. Economic and ecologic evaluations help to show the obtained results.

The question was what possibilities exist for the electrical interconnections. Some possibilities are:

- FR-2 Al or Cu bonded on steel sheet
- FR-4 Al or Cu bonded on steel sheet
- Printing technologies for dielectrical and conductive layers on steel
- Ceramic on steel sheet (Thick Film Technology)
- New materials (still to be selected and developed) on steel sheets

With exception of FR-2 all substrates have nearly comparable mechanical and thermal properties. Ceramics show better thermal and FR-4 better mechanical properties. The thermal conductivity for FR-4 is 0.1 – 0.3 [W/mK] and for standard ceramics (Al_2O_3) 20 – 25 [W/mK].

The high costs for ceramics make the utilization possible only for high-end application.

A new material under the precondition of splitting the electrical functionality and the mechanical support system had to be found, called compound substrate.

If the electrical layer is simplified simultaneously by the mechanical construction, e.g. thin layers bonded on a metal substrate, the thermal management can be optimized, as well.

As the main objective of the investigation was the elimination of harmful chemicals in circuit boards, a conceivable solution is a mechanical construction in accordance with Fig. 1. Thermal management is simpler because the vertical heat dissipation is much lower than the one of the metal sheet. This solution can be improved by utilizing Silicone filled with Aluminium oxide, which is a well-known solution in industry for heat transfer foils. Such materials can also be filled with glass fabrics for stabilisation and produced as flexible copper-clad foil. The construction as a sandwich structure meets the need for easy separation: The metal layers do not only reinforce the flexible Silicone but also improve the thermal management of the whole system.

A typical Silicone foil used in tests was found as KERATHERM-foil 86/77 from KERAFOL GmbH Germany. This substrate was produced by KERAFOL in different modifications as copper-clad material. The basis material is well known as heat transfer foils in the automotive, electronic and electrical industry and does not contain flame-retarding substances. The excellent heat transfer properties are due to filling (> 50%) with Al_2O_3 (Alumina).

Heat management
Experiments showed the expected improvements in heat management. Some test configurations were produced and measured. Printed resistors were heated till they reached a stable temperature of 120^0C. The electrical power necessary to reach this temperature for different configurations is shown in Fig. 2.

Cables and connectors
In some cases, the use of flexible materials makes it possible to integrate cables directly into the

* fon: +49-(0)3677-69-2602; email: gert.winkler@tu-ilmenau.de

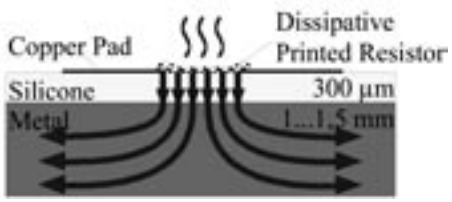

Fig. 1: Heat Dissipation in Compound Substrates

design. The "integrated cable trees" are cut, bent and connected to the different plug connectors as shown in Fig. 3.

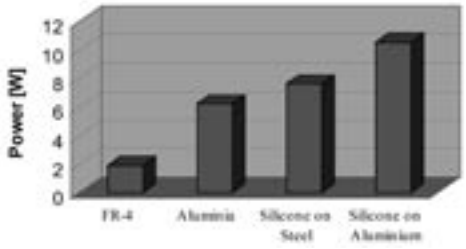

Fig. 2: Comparison of Heat Management for Different Configurations

New applications for polymer-thick-film technology

The promising results achieved in the project described above led to the decision to proceed with further investigation to make this material and technology available for a wider range of applications. The results achieved regarding recycling and ecology should encourage further research.

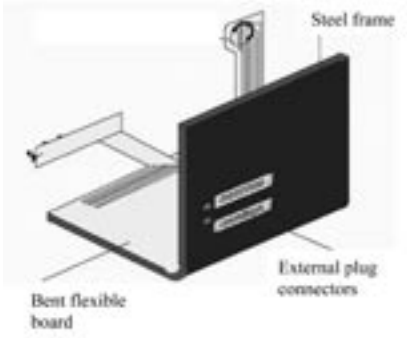

Fig. 3: Integrated cable trees

To achieve this goal, new partners for joint research had to be brought together. Some of the partners are:

- KEW Konzeptentwicklung GmbH, Kronach
- Creavac Creative Vacuumbeschichtung GmbH, Dresden
- Loewe Opta GmbH, Kronach
- Technische Universität Ilmenau
- KERAFOL Keramische Folien GmbH, Eschenbach

The applicable technology is similar to LTCC-Technology. To realize multilayer boards plated via holes are necessary. Holes in Silicon can be generated by punching, mechanical- or laser drilling. Punched and drilled holes showed suitable results, while laser drilling was not investigated due to the expected costs. A problem was the requirement of plating through the material should be realized without chemical processes. Suitable methods have been found.

The experiments revealed that dispensed vias show the lowest resistivity followed by vias filled with LTCC via filler.

Screen-printed filled vias showed an eight times higher resistance. Layer structuring was done by etching and printing. A screen printable adhesive developed by the Institute of Material Research of the University Bayreuth has been used to laminate the different layers.

New technologies for improved Silicone materials

In cooperation with the project partners Creavac and Kerafol improved Silicone materials were investigated to overcome some drawbacks of conventional etching. The technologies in question are PVD and vacuum deposition of Copper for the first conductive layer and selective galvanic reinforcement of this layer.

Conclusions

Forthcoming new regulations and environmentally aware consumers are setting pressure on the electronics industry to adopt more ecological production methods and materials. The prospective EU-directives place environmental demands for the design, production, and recycling of electronics products. It is a challenging task to develop compensatory technologies that will outperform the current ones in terms of quality and yet be affordable in mass production .

Other materials in conjunction with polymer thick film technology can replace the contemporary standard material in printed circuit boards. In this paper the process and results of development of electronic modules based on Silicone material filled with Alumina and glass fabrics on the basis of Keratherm® material from Kerafol GmbH has been described. So far the achieved results are promising to show a way to fulfil the posed objectives.

1 Fischer, Th.: Abschlußbericht „Beiträge zur Entwicklung einer Kreislaufwirtschaft am Beispiel eineskomplexen Massenproduktes TV-Gerät Teilvorhaben 4: Metallvariante" BMBF-Förderkennzeichen 01 ZV 9404/0, Projektlaufzeit: 01.04.1994 – 31.03.1995
2 Fischer, Th., Braun, A.: Passive Bauelemente in Polymer-Dickschicht-Technik für umweltfreundliche elektronische Baugruppen, Deutsche ISHM Konferenz 1996 München 14.-15.10.1996
3 G. Bischoff, G. Winkler, T. Tuschick, H. Landeck: „Polymer Thick Film Technology: New Possibilities for the New Millennium?", Proceedings of the 32. International Microelectronics and Packaging Society, Chicago/Illinois/USA 1999, pp. 131-136
4 G. Bischoff, G. Winkler, H. Landeck: "New Feasibilities for Multilayer Boards Polymer-Thick-Film Technology on Silicone Polymer Substrates", Proceedings of the 33. International Symposium on Microelectronics and Packaging Society, Boston/Massachusetts/USA 2000, pp. 346 – 350
5 G. Bischoff, G. Winkler, H. Landeck: "Fine Line Technology for BGA-Applications on Silicone Polymer Substrates", Proceedings of the 34. International Symposium on Microelectronics and Packaging Society, Baltimore/Maryland/USA 2001, pp. 693 – 696
6 Kerafol: Katalog KERATHERM, Keramische Folien GmbH Eschenbach, 2002

Pt/GaN Schottky diodes for hydrogen gas sensors

M. Ali*, V. Cimalla, and O. Ambacher
Department of Nanotechnology

Recently, the use of hydrogen gas has gained a considerable attention in industrial fabrication processes, medical installations, laboratories and fuelled motor vehicles. For safety reasons the monitoring of hydrogen molecules has become an important issue. One up-to-date technical solution to realize sensitive sensors for hydrogen and hydrocarbon gases in air is the combination of catalytic metals (Pd or Pt) with wide band gap semiconductors like GaN. At the Pt surface molecular hydrogen is dissociated into atomic hydrogen atoms which are able to diffuse very fast towards the Pt/GaN interface. Hydrogen accumulation at the interface changes the work function of the metal gate and therefore the barrier height of the Schottky contact which can be proven by measuring I-V curves.

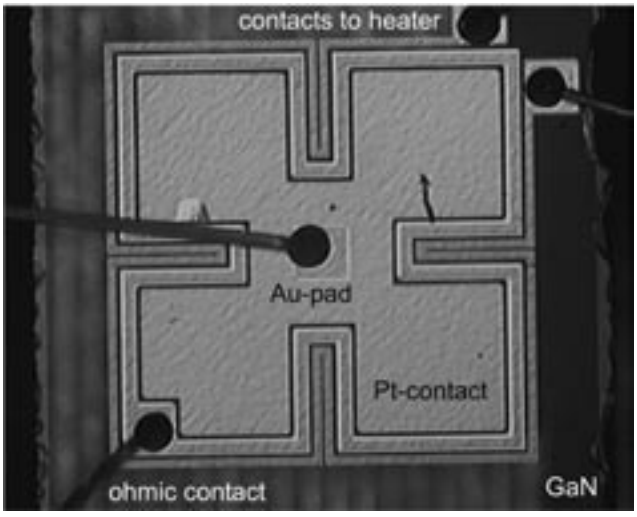

Fig. 1: Top-view micrograph of the Pt/GaN Schottky Diode processed by General Electric.
The active area of the device is about 1 mm².

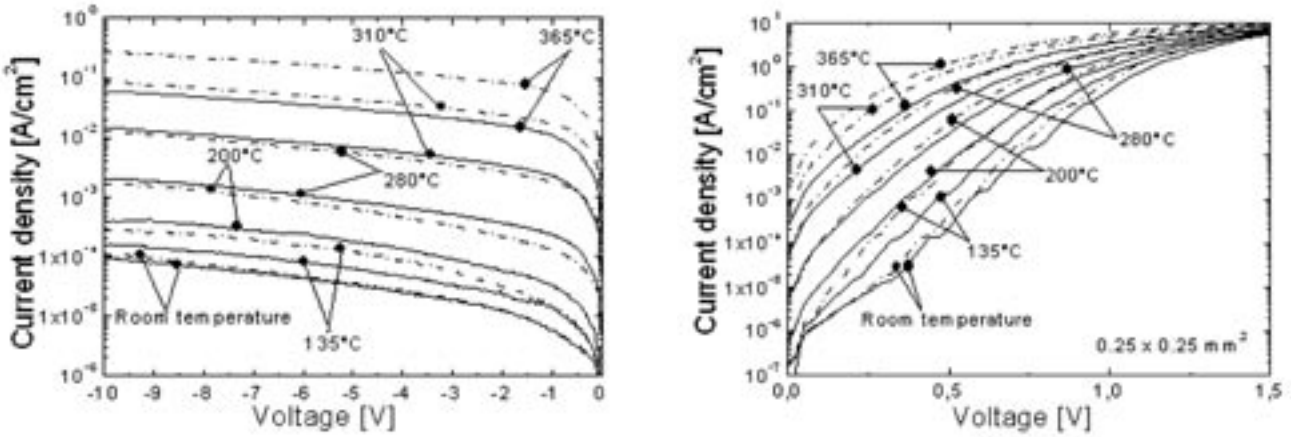

Fig. 2: I-V curves of the Pt/GaN Schottky diodes operated at different temperatures and in synthetic air (solid lines) or in synthetic air with 1 vol% hydrogen gas (dashed curves, (d_{Pt} = 24 nm)).

The sensors were prepared on GaN layers grown by metal organic chemical vapor deposition (MOCVD) on sapphire substrates. The thickness of the epitaxial GaN layer was about 3 µm, the n-type doping concentration around ~1 x 10^{17} cm^{-3}. The thickness of the Pt-Schottky contact was varied between 8 and 40 nm and the size of the active sensor area between 0.25 and 1 mm^2 (Fig. 1). The sensor structure was placed into a TO transistor package with an integrated heater. The sensitivity, response and recovery times have been measured for the different designs of Pt/GaN sensors as follows. I-V curves were recorded in dependence on the operating temperature in synthetic air as well as in synthetic air containing 1 vol% hydrogen gas. As shown in (Fig. 2) exposure of Pt/GaN Schottky diodes to H_2 causes an increase of both the forward and reverse current which can be attributed to a decrease in the Schottky barrier height. In a constant current operation mode this reduction of the Schottky barrier height results in a shift to lower bias voltages, which constitutes the sensor signal.

* fon: +49-(0)3677-69-1172, email: majdeddin.ali@tu-ilmenau.de

The sensitivity to H_2 was investigated in dependence on the active area, Pt thickness and the operating temperature. The change in the voltage of the diode at a fixed current was monitored as the diode was exposed to 1% H_2 in synthetic air and for comparison to dry synthetic air in order to determine the voltage difference as a measure for the sensitivity towards hydrogen gas. A significant increase of sensitivity by increasing the temperature of operation to ~365°C and by decreasing the Pt thickness down to 80 Å has been observed (Fig. 3). An expected voltage drop after the sensor is exposed to hydrogen has been measured due to the reduction in Schottky barrier height. We have also found that the sensitivity increases non linear with an increasing concentration of H_2 in air starting from 0.1 vol% to 1 vol% for all Pt contact thickness.

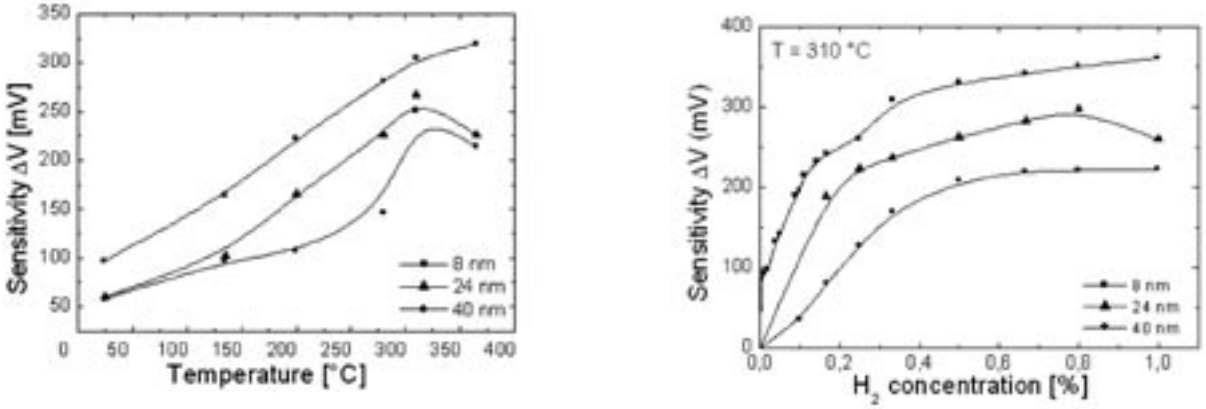

Fig. 3: Sensitivity of the Pt/GaN Schottky diodes in constant current density mode (J = 3.2 A/cm²) for different thickness a) at different operation temperatures. b) for different concentrations of hydrogen gas. (A_{Pt}= 250 x 250µm²). The sensitivity of the detector is given by $\Delta V=V_{air}-V_{hydrogen}$.

The micro-structure of Pt contacts was studied by means of electron microscopy (in terms of grain boundary density and average grain size). As expected, the higher sensitivity films have also a higher grain boundary density proving that hydrogen molecules dissociate on the Pt surface and diffuse along the grain boundaries reaching the Pt/GaN interface. A transient behaviour of electrical response of 0.5 x 0.5 mm² sensors operated in constant voltage mode (U = 1 V) and exposed to a 1 vol% H_2 in synthetic air pulse is observed at different temperatures (Fig. 4).

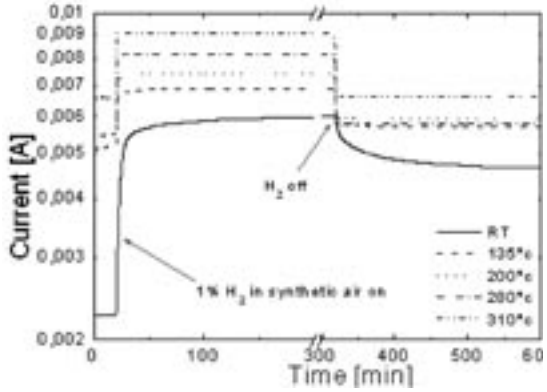

Fig. 4: Transient behaviour of electrical response of a sensor with an active area of 0.5x0.5 mm² exposed to 1 vol% H_2 in synthetic air at different temperatures, d_{Pt} = 24 nm.

The response (diffusion) times at room temperature were more than 1 hour and the recovery times were also very long, typically several hours. The long recovery time of Pt/GaN Schottky contacts after exposure to H_2 at room temperature indicates a strong trapping of hydrogen atoms at electronically active adsorption sites. We observed a significant decrease of response and recovery time by decreasing the Pt thickness down to 8 nm and by increasing the operation temperature to 365°C (Fig.4).

Conclusions:

(1) The sensitivity to hydrogen gas was observed down to room temperature.
An effective sensor operation at room temperature is possible.

(2) The sensitivity significantly improves with increasing operation temperatures. An excellent stability of the catalytic layer and the interface up to 400°C was proven.

(3) For thinner catalytic contact layers (down to 8 nm) the sensitivity is increased. A significant decrease in response and recovery time (up to several seconds) by the decreasing the Pt thickness and by increasing the operation temperature to ~365°C has been realized.

Funding by the Office of Naval Research (NICOP-Project) is grateful acknowledged

The detection of oxygen at the electrode/polymer interfaces in polymer solar cells

M. Al-Ibrahim[1,*], O. Schulz[1], G. Ecke[1], S. Sensfuss[2], and O. Ambacher[1]
[1] Department of Nanotechnology
[2] TITK Institute, 07407 Rudolstadt

Polymer solar cells made on flexible substrates are welcome for all photovoltaic applications onto curved surfaces. Cells of so called donor-acceptor (D/A) type based on conjugated polymers as electron donors and fullerene (or its derivative) as electron acceptors were successfully developed. Polymer solar cells with an external AM1.5 power conversion efficiencies of 3.5% based on poly(3-hexylthiophen) (P3HT)/([6,6]-phenyl-C61-butyric acid methyl ester) (PCBM-C61) on rigid glass substrate and of 3% based on poly[2-methoxy-5-(3',7'-dimethyloctyloxy) -1,4-phenylene vinylene] (MDMO- PPV)/[6,6]-phenyl-C61-butyric acid methyl ester (PCBM-C61) on flexible PET-foil substrates have been recently reported by Padinger et.al. (QSEL/Linz) and Al-Ibrahim et. al. (TITK/Rudolstadt), respectively. Besides the requirements for increasing energy conversion efficiency, the stability (or lifetime) of the polymer solar cells is a very important issue to be improved for this type of solar cells. Fig.1 shows the structure of a D/A polymer solar cell. For device preparation (at TITK/Rudolstadt) substrate (polyester foil coated with indium tin oxide ITO) was cleaned in an ultrasonic bath in methanol and isopropanol. After drying of the substrate, a thin layer (~100 nm) of PEDOT-PSS (poly(3,4-ethylenedioxythiophene)-poly(styrenesulfonate)) (Fig.2) was spin-coated and dried. Subsequently, the photoactive layer (MDMO-PPV:PCBM-C61 (1:3 wt. %)) was spin coated on top of the PEDOT-PSS layer. The aluminum cathode was thermally deposited through a shadow mask. The cells were prepared under ambient conditions in clean room. The chemical structures of the used materials are shown in Fig. 2.

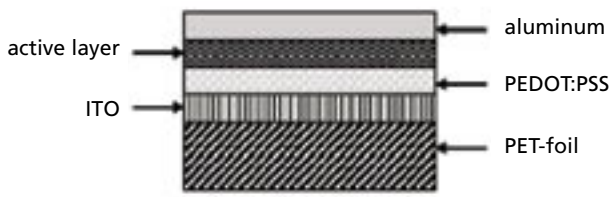

Fig. 1: Structure of the photovoltaic device.

During the study of the stability of this kind of polymer solar cells it was found that the degradation of cells stored with the top electrode Al is faster as of those without Al. Four samples were prepared under ambient conditions in clean room in order to investigate the stability of these cells based on MDMO-PPV:PCBM-C61 (1:3 wt.%) as photoactive layer.

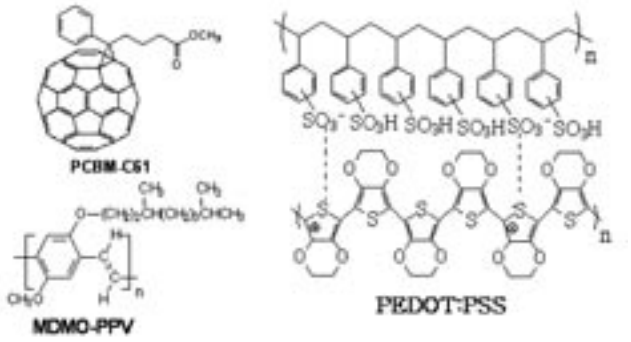

Fig. 2: Conjugated Polymers and Fullerens

To characterize the cells, I-V characteristics under illumination with white light (AM1.5 conditions) were recorded. The first cell was characterized immediately after the deposition of Al, the second after storage for two days in air/dark conditions and the third after storage for tow days in argon/dark conditions (experiment was performed inside a glove box). The fourth cell was stored without Al for two days in air/dark then it was coated with Al and immediately characterized. Fig.3 shows the I-V characteristics of the four cells in the fourth quadrant. In comparison to the first cell there is a great change, small change (between 0.55 and 0.8 V) and no change in the shape of the I-V curves

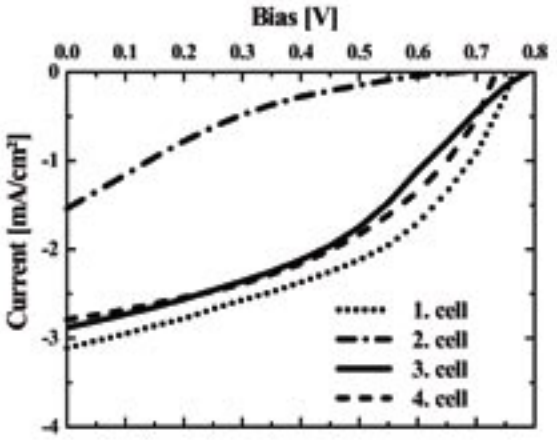

Fig. 3: I-V curve (in 4. quadrant) for the four cells (see text).

* fon: +49-(0)3677-69-3409, email: maher.al-ibrahim@tu-ilmenau.de

of the second, third and fourth cell, respectively. The second cell has showed no diode behavior after one week. Thus, while there is no change in the shape of I-V curve of the fourth cell there is a change in the shape of the I-V curve for the second and third cells. It can be concluded that these changes are caused by the change of the nature of the electrode (Al), of the interface photoactive layer/Al or of the interface photoactive layer/ITO. In order to study the interface electrode/polymer three samples were prepared as described above. The first sample has been measured by Auger depth profiling one day after the preparation of the cell, the second sample, after a storage in air for 10 days and the third after storage for one day in air and then 9 days in N_2 atmosphere. Auger depth profiling has been carried out with a ASC 2000 Auger spectrometer, measuring all relating elements (Al, O, C, S, In, Sn) by several characteristic Auger transitions, which are marked in the figure by their kinetic energies. Sputtering by Ar^+ ions of 1keV under 60° was applied for receiving the depth profile. The sputtering time scale is a measure of the sample depth.

Fig. 4 shows the Auger depth profile of the first sample. As it is seen clearly, there is a distinct oxide layer at the interface of Al to the polymer, which can be responsible for the shape change of I-V curves of the Al covered solar cells (cells 3. and 4. are shown in Fig. 3). Storage of the sample in air for longer time does not influence this oxide layer at the Al/polymer interface noticeable (second sample). But additional Auger depth profiles of this sample show a degradation of the polymer/ITO interface, which can be responsible for the full degradation of the polymer solar cell. The degradation of the interface organic/ITO was not found for the sample stored one day in air and 9 days in N_2 atmosphere (cell 2, Fig. 5).

Future investigation should clarify the origin of the oxygen. Possible sources are the diffusion of oxygen from air, humidity in the spin coating process or from the ITO contact.

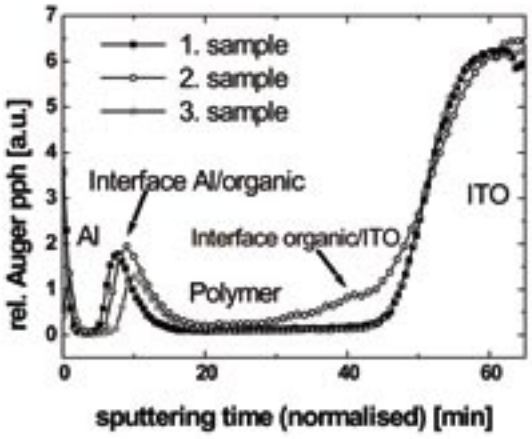

Fig. 4: AES depth profile of the solar cell structure of Fig. 1, the inset shows the oxygen profile at the Al/polymer interface.

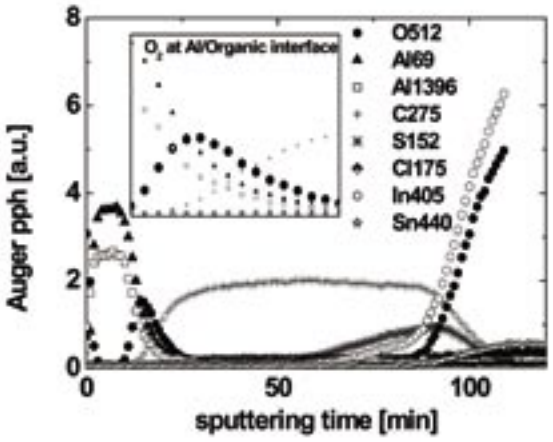

Fig. 5: Comparison of the oxygen Auger depth profiles of samples 1 (one day/ air), 2 (ten days/air), 3 (one day/air, nein days/N2)

The work was supported by the TMWFK (ORSOL)

Design development, technology optimization, and electrical characterization of silicon carbide MESFETs

C. Fachmann[1,*], T. Doll[1], M. Fischer[5], C. Förster[2], K. Friedel[3], H. Romanus[4], O. Marufke[5], J. Pezoldt[2], T. Sändig[5], F. Schwierz[1], L. Spiess[4], and P. Weih[2]
Departments of Solid-State Electronics[1], Nano-technology[2], Microsystems Technology[3], Materials for Electronics[4], and ZMN[5]

Silicon Carbide (SiC) Transistors are very attractive for mid-range RF-Power applications. Especially SiC-MESFETs (**M**etal **S**emiconductor **F**ield **E**ffect **T**ransistor) may have a promising future as power amplifier (PA) for the next generation of wireless communication systems above 5GHz or broadband bidirectional satellite communication systems up to 12GHz.

The establishment of the ZMN laboratories and the new and existing equipment as well as the trained, experienced staff provided the possibility to develop a full coordinated technology chain to fabricate operating semiconductor devices.
The purpose of the project NEMASIC (**N**ew **M**aterials on **Si**licon **C**arbide) is to develop the design and extend the existing technology to realize SiC-MESFETs for RF applications.

The first technology steps were performed on 1.5" high-conductive n-type 4H-SiC wafers. The processing was continued on 2" high-conductive n-type 4H-SiC wafers of Cree™ on which a 30µm $10^{15}cm^{-3}$ n^- buffer layer was deposited followed by an 300nm to 400nm $3x10^{17}cm^{-3}$ doped active n-type top layer (external partner). The final processing is performed on 2" high-conductive n-type 4H-SiC wafers on which a 5µm $1x10^{15}cm^{-3}$ p^- buffer layer was deposited followed by an 250nm $2x10^{17}cm^{-3}$ doped active n-type top layer. (Cree™)
The design and technology is also applicable for n^+ cap layers to improve the ohmic contacts and to reduce the parasitic source and drain resistances. However, such cap layers have not been processed, yet.

During first tests, the mask design was optimised to increase the contrast and the positioning accuracy of the lithography. Adjustment marks are placed on both sides for each lithography step. They are symmetrical and consist of differently sized lines and spaces. This optimises the required mask adjustment to achieve the required accuracy of less than 0.5 µm.

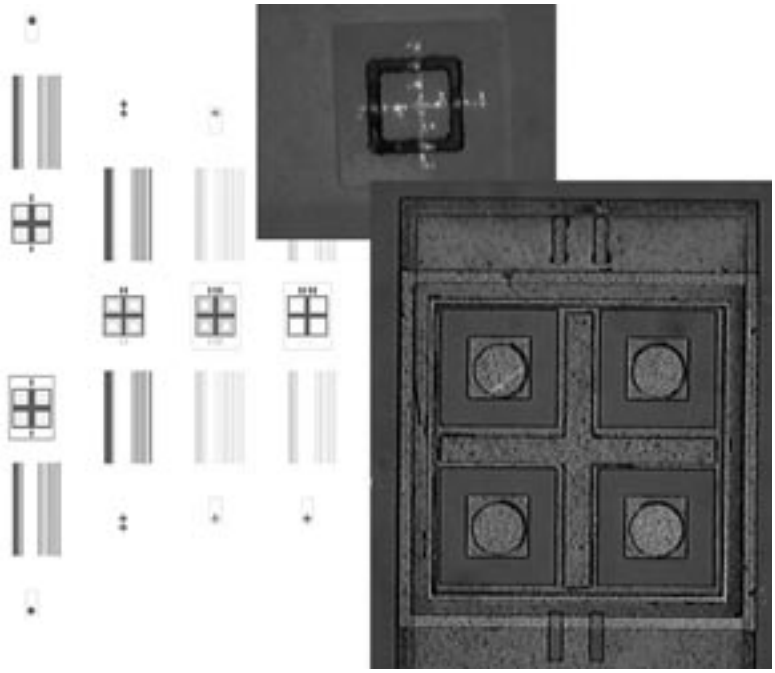

Fig. 1: Lithography mark field (left); quality mark (top); adjustment mark (bottom)

Additionally, special marks were introduced to monitor and log the adjustment during the processing of each technology step with the aim to improve the quality management and to increase the yield of the process, see Fig. 1. These marks are placed on all four sides of the wafer. To check the critical dimensions test fields containing lines were placed around the wafer.
Technology tests in combination with Auger electron spectroscopy have shown that an additional surface cleaning step is necessary antecedent each metallization. An Ar sputter etch process was performed under steady vacuum condition to improve adhesion and reduction of contamination of the previous lithography step. In Fig. 2 the Auger spectrum of an untreated sample (Nr.1) and a treated sample (Nr.2) are shown. The difference in organic contamination is obvious.

* fon: +49-(0)3677-69-3401, email: christian.fachmann@tu-ilmenau.de

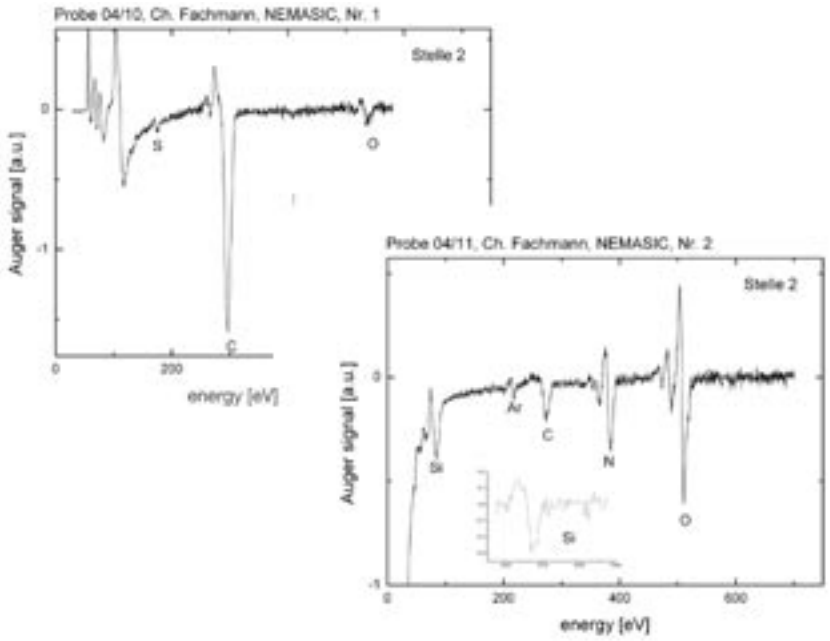

Fig. 2: Spectrum of the Auger-Electron-Spectroscopy before (Nr.1) and after (Nr.2) of an Ar-Sputter-Etch process

A compromise has to be found for the process condition of the ar sputter etch to prepare adherent contacts and a high schottky barrier, simultaneously

The technology chain was optimized to integrate a silicon nitride isolation layer into the SiC mesa etch step. This was achieved by using a top aluminium layer for masking. Later this layer has been removed by wet etching without interfering with the Nickel contact metallization. The silicon carbide etching process based on a CHF_3/CF_4 plasma at a Balzers ECR PLS 500P was optimized to obtain steep vertical side walls and smooth surfaces without micro masking for an etch depth of more than 600nm, see Fig.3. An rms-roughness of 26nm was determined by AFM measurements.

Considerating our contact lithography system and the resulting resolution of approximately 2µm we established an additional spacer technology to reduce the gate length. This technology shortens the gate down to 1µm depending of the gate recess. A layer of silicon nitride was deposed and anisotropically etched to build side wall spacers at the gate recess, see Fig.4. This spacer step fits well into the existing process chain. For this technology we designed self-aligned submicron gates to increase the RF performance of the transistor.

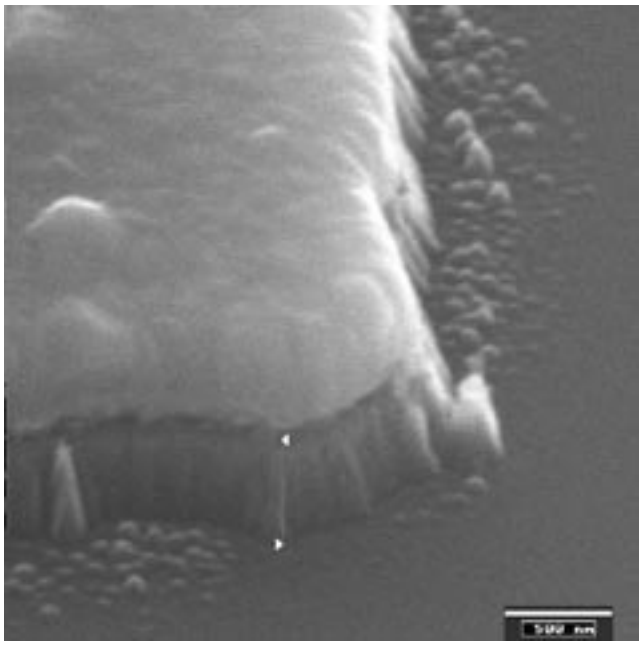

Fig. 3: REM picture of a MESA edge with an Aluminium mask and 620nm etch depth

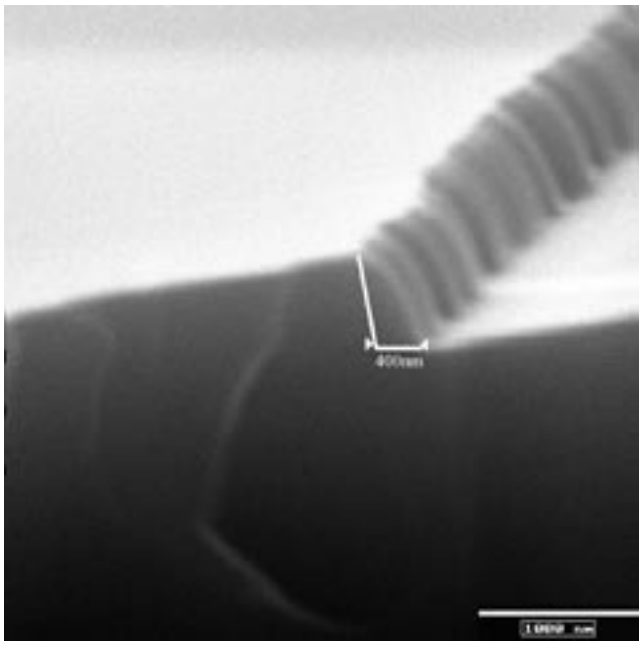

Fig. 4: 400nm Silicon Nitride Side wall Spacer

The work presented here is partially funded by the Thuringian state ministry TMWFK, grant B607-02006 NEMASIC

The preparation of novel group-III nitride based micro- and nanomechanical devices

Ch. Förster[1,*], V. Cimalla[1], V. Lebedev[1], R. Wagner[1], I. Cimalla[1], O. Ambacher[1], K. Brückner[2], R. Stephan[2], and M. Hein[2]

Departments of Nanotechnology[1] and RF and Microwave Techniques[2]

During the last years strong activities have been performed in the field of microelectromechanical systems (MEMS) to scale them into the submicron range, leading to the new category of nanoelectromechanical systems (NEMS). They consist of a combination of micromechanical structures with electrically active elements for the actuation and the read-out of the signals. The research on NEMS is focussed mainly on nanoresonators in order to achieve very high frequencies up to the GHz range. This opens the door for new applications like low-power high-frequency devices for mobile communications, or the detection of single molecules on the basis of functionalised NEMS surfaces. Resonators in the submicron range have been demonstrated already using Si and SiC. The focus on SiC reflects its chemical stability, but more importantly its significantly higher ratio of the Young's modulus, E, to mass density, ρ, yielding higher resonator frequencies.

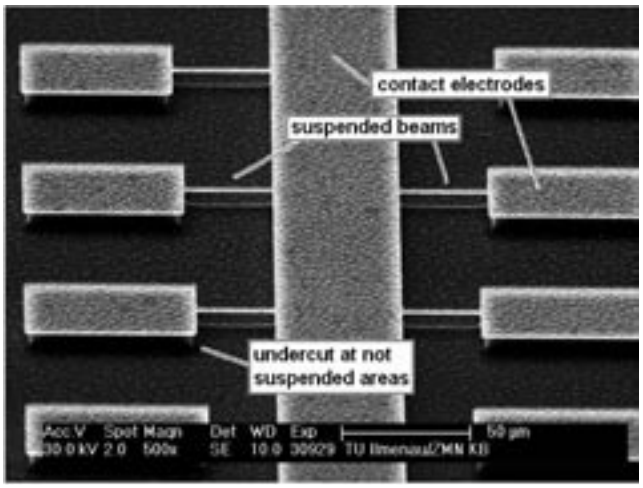

Fig. 1: SEM image of selected suspended SiC-beams

SiC layers were grown on (100) silicon substrates with a thickness of 200 nm, and suspended doubly clamped SiC beams were manufactured using photolithography and dry etching techniques. Some typical examples are shown in Fig. 1. The beams have a thickness of 200 nm and vary from 1 to 4 µm in width and from 2 to 250 µm in length. The beams were covered with a 50 nm thick Au or Ni film allowing the magnetomotive detection scheme to be applied. In that scheme the Lorentz force, caused by driving an RF current through the beams that were placed in a static magnetic field, is used for actuation. The movement of the beams results in an induced electromotive force which is proportional to the displacement. The simulation of the mechanical behaviour was done using a FEM software to determine the effective masses and spring constants of the beams.

Equivalent-circuit diagrams of these properties allowed electrical simulation. The fundamental resonant frequencies of the beams reach from 20 kHz to 20 MHz. For detection of these resonances, reflection measurements were done within the expected frequency range. To increase sensitivity, a transmission measurement scheme has been employed. In this bridge measurement set up, the inverted driving voltage is additionally applied to a non vibrating reference beam and finally superimposed by the original driving voltage (Fig. 2). The output voltage is therefore zero for all frequencies, except for the resonant frequency, where the mechanical motion of the beam is accompanied by a change of its electrical impedance.

However, further miniaturisation requires increasing efforts in the design and the technology of the NEMS. In particular, to keep the complexity of the NEMS and the manufacture technology on a reasonable level, the actuation and the read-out need the development of new principles and designs. The goal is to achieve integration to the resonator itself, which requires special attention to the selected material system with respect to the desired functions. In the ideal case just one material or material system should be used to realise the resonator, the actuator and the read-out. The group-III nitrides represent such a system. The wurtzite group-III nitride system combines piezo- and pyroelectric effects with semiconducting properties.

* fon: +49-(0)3677-69-3352, email: christian.foerster@tu-ilmenau.de

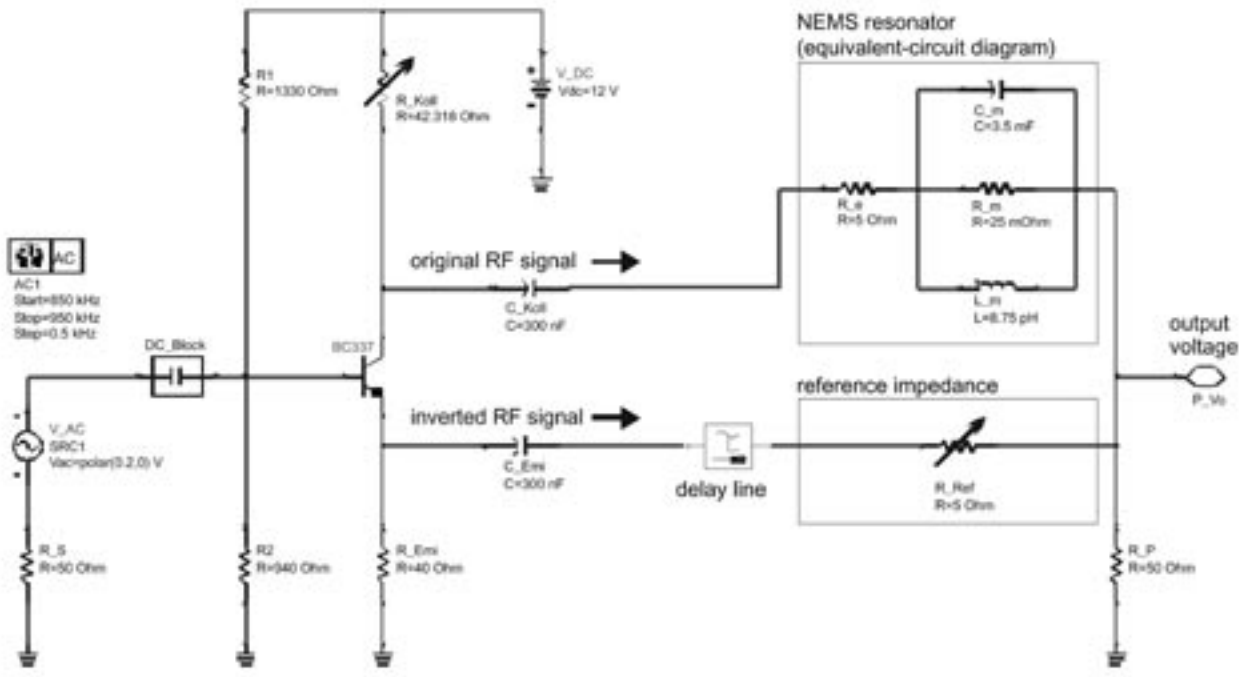

Fig. 2: Transmission measurement scheme

In addition to the high chemical and mechanical robustness, these properties make the group-III nitrides an outstanding material system for MEMS and NEMS. First, the piezoelectricity allows an easy integration of actuators for the nanoresonators. Second, piezoelectric polarisation induced sheet-charges of hetero-interfaces between alloys with different composition are highly sensitive to mechanical deformation and can be used for pressure sensors as well as for the detection of the resonator oscillation. Finally, for nitrides on silicon, the combination with the high developed processing technology for silicon micromachining allows the fabrication of resonator structures using established lithography and etching techniques. AlN and AlGaN alloys and heterostructures were grown on (111) silicon substrates by plasma induced molecular beam epitaxy with a layer thickness around 200 nm. Conventional optical lithography was used to define bridgelike resonator structures with dimensions of 1 to 4 µm and 2 to 200 µm in width and length, respectively. The main focus has been directed towards the development of a chlorine free etching process for the nitrides and the selectivity between pure AlN and AlGaN alloys. Both dry and wet etching techniques were investigated. In the case of the dry etching, an ion beam etching was applied, and an excellent reproducibility was achieved. Both metal and oxide masks were used with comparable results. The selectivity between AlN and AlGaN was found to be negligible. With a linear dependence of the etching rate on the time and the applied power, an easy adjustment of the process conditions to the layer thickness can be realised. This dry etching can be applied in vacuo with the in depth etching of the silicon as well as the lateral under etching to create the bridgelike resonators, reducing the contamination of the structure to a minimum.

The wet chemical etching was performed in hot phosphoric acid as well as in KOH solutions. A stable selectivity was found only for the KOH etching at room temperature. Only AlN was etched, while the process stopped completely on the AlGaN. In addition, the etching of silicon was negligible. This offers the possibility for self-adjusting etching of the AlN top layer to the AlGaN interface to realise contacts without the creation of radiation defects.

In summary, the technological advances in the preparation of group-III nitride based NEMS set up the basis for a new category of devices with integrated electrical transduction. The next steps of our investigation will be to optimize the design and to characterise their resonant properties experimentally.

This work has been funded and supported by the Deutsche Forschungsgemeinschaft, SPP 1157: "Integrierte elektrokeramische Funktionsstrukturen", contract no. AM 105/2-1.

Submicrometer organic field effect transistor

S. Scheinert*, A. Scherer, T. Doll, G. Paasch, I. Hörselmann, and A. Herasimovich
Department of Solid-State Electronics

Organic field effect transistors (OFET) are of interest for many applications including organic displays, complementary circuits and all-polymer integrated circuits. Low-cost fabrication requires the use of solution-processible polymers instead of vacuum deposited low-molecular weight organics. However, in such materials the charge mobility is very often smaller than $10^{-3}cm^2V^{-1}s^{-1}$. Consequently, using the simple Shockley equation one can estimate an upper limit for the channel length of L=1µm for a lower limit of the cut-off frequency of 100 kHz at a operation voltage of 10V. Since additional parasitic capacitances cannot be avoided, only submicrometer transistors lead to applicable circuits. Organic short channel pentacene transistors with L=30nm have been described in [1]. However, the used electron beam lithography for structuring is too costly for cheap organic electronics. In [2] a simple embossing technique is used to realize channel length in the submicrometer range, but there is no saturation for the transistor with a channel length of 900nm.
We applied also a simple technique for the preparation of short channel transistors [3,4]. However, down-scaling comprises also the gate insulator thickness in order to avoid short-channel effects. Since organic materials are not yet available for the realization of thin insulators, we used a hybrid structure as shown in Fig.1a. Here, the

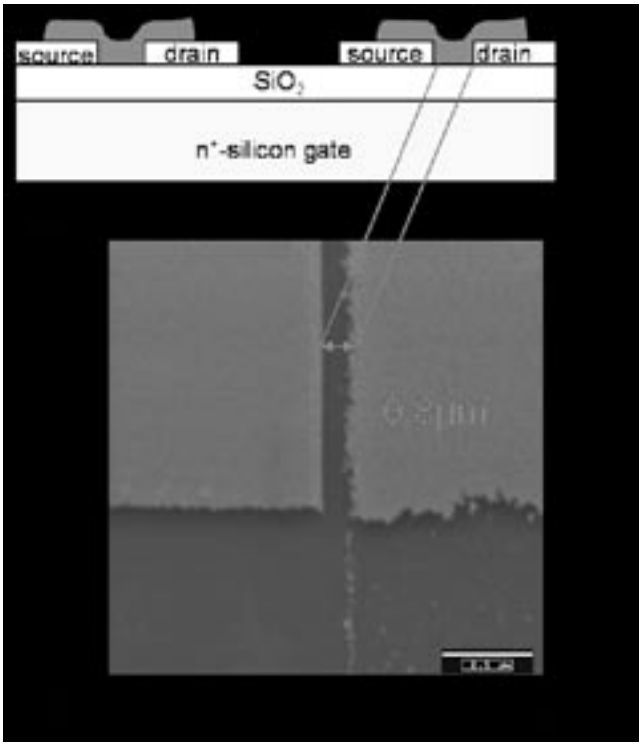

Fig. 1: Schematic cross sections (a) and scanning electron micrograph of prepared thin film transistors.

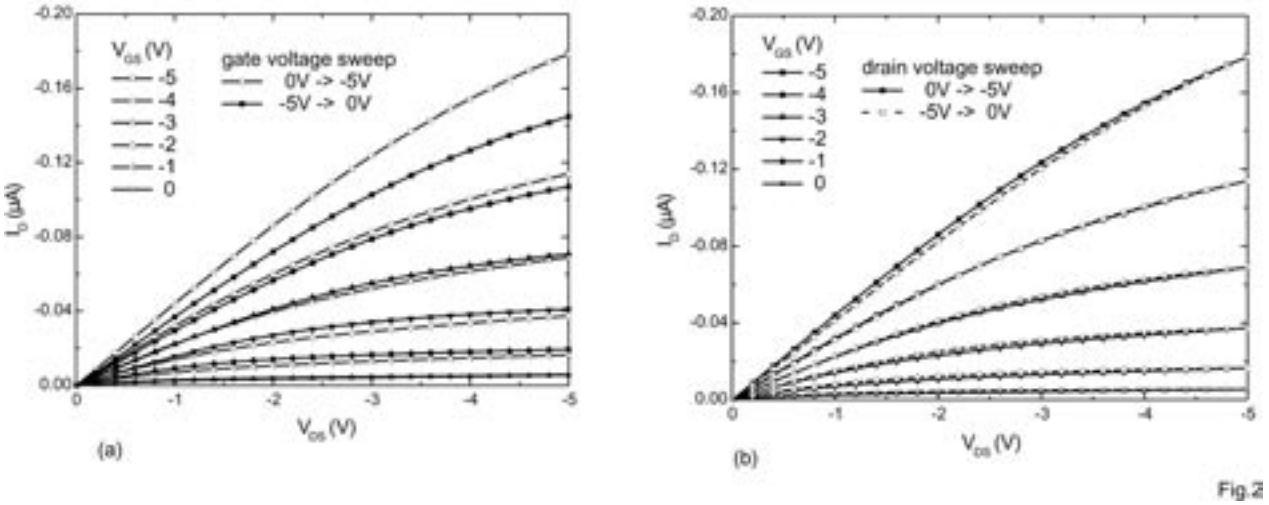

Fig. 2: Output characteristics of a P3HT transistor with L=740nm and w=1000µm at different gate voltages and for different sweep directions of the gate voltage (a) and the drain voltage (b).

* fon: +49-(0)3677-69-3222, email: susanne.scheinert@tu-ilmenau.de

gate insulator is a 30nm silicon dioxide layer on a silicon wafer serving as the gate electrode. The short channel (0.8µm in the case of Fig.1b) was prepared by sputtering of gold followed by a low-resolution photolithographic step, underetching and a lift-off process. Finally, the active organic layer is deposited by spin coating. We used soluble poly(3-octylthiophene) (P3OT) and poly(3-hexylthiophene) (P3HT) which are uninten-tionally highly doped. From capacitance-voltage measurements we obtained an acceptor concentration of $N_A \approx 10^{17} cm^{-3}$. Since the layer thickness has to be smaller than the depletion length, we prepared a thickness as low as 30nm.

In Fig. 2 the output characteristics of a transistor with a channel length of 740nm are depicted. In spite of such a short channel there is a pronounced saturation region since the gate insulator is thin enough. Comparing the two diagrams of the figure it becomes clear that there is only a hysteresis for different gate voltage sweep directions (Fig. 2a) but not for a variation of the drain voltage sweep direction (Fig. 2b). Hysteresis is known for organic devices but the reasons for this effect are not clear until now.

The transfer characteristics of the same transistor are shown in Fig. 3. From the linear dependence in the active region we conclude that there are no problems caused by series resistance. Therefore, despite of the short channel the polymer should fill in the space between source and drain without cavities near the contacts. Indeed, the estimated mobility of 5.8 x $10^{-5} cm^2 V^{-1} s^{-1}$ is still low so that a pre-treatment of the interface will be necessary in the future. The characteristics in a logarithmic scale show a small inverse subthreshold slope of 0.73V/dec indicating negligible short channel effects, and a high on-off ratio of approximately 10^4. The hysteresis for the gate sweep is 1.7V. All these data indicate a rather good performance of the transistor. As the next step, for the application in circuits, one has to realize the transistor on a plastic substrate with an organic insulator and reduce the parasitic capacitances.

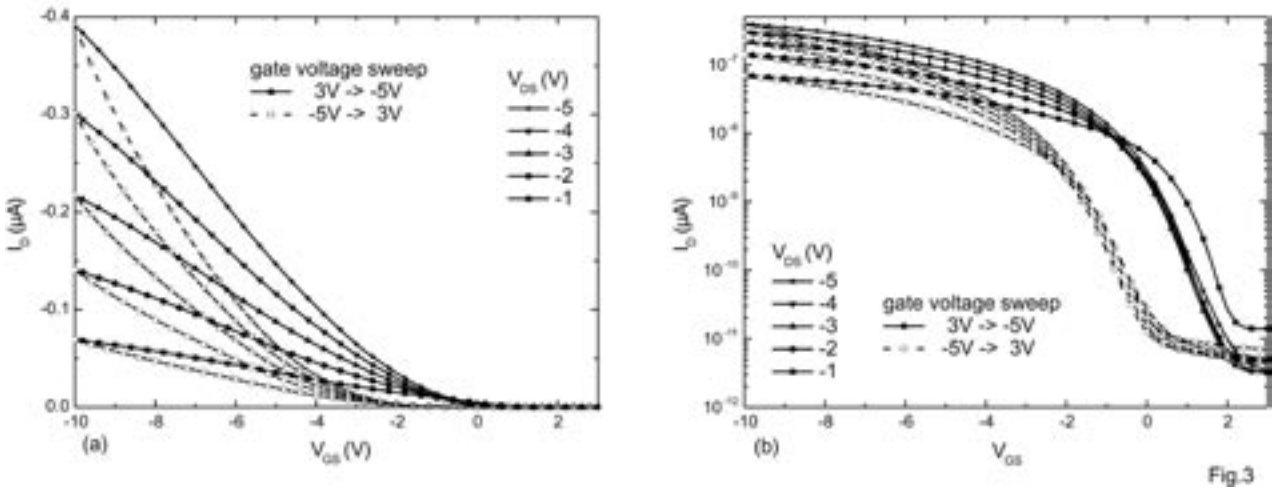

Fig. 3: Transfer characteristics of the transistor of Fig. 2 for different drain voltages and sweep directions (a) - linear scale, (b) - logarithmic scale

[1] Y. Zhang, J.R. Petta, S. Ambily, Y. Shen, D.C. Ralph, G.G. Malliaras, Adv. Mater.15 (2003) 1632.
[2] N. Stutzmann, R.H. Friend, H. Sirringhaus, Science 299 (2003) 1881.
[3] S. Scheinert, A. Scherer, T. Doll, G. Paasch, and I. Hörselmann, submitted to Appl. Phys. Lett.
[4] S. Scheinert and G. Paasch, submitted to phys. stat. sol.

Electron mobility models for GaN and AlGaN/GaN

F. Schwierz*
Department of Solid-State Electronics

Introduction

During recent years the wide bandgap semiconductors AlGaN and GaN have attracted a lot of attention. An important application of these materials is high-power high-frequency transistors. Both AlGaN/GaN HEMTs and GaN MESFETs are currently under development in labs around the world. To simulate the electrical behavior and to optimize the design of such transistors, reliable low-field electron mobility models are needed. In spite of the considerable efforts in fabricating GaN transistors, such mobility models are currently not available.

The aim of this work is to develop low-field electron mobility models for bulk GaN (important for the simulation of GaN MESFETs) and for the mobility in the two-dimensional electron gas (2DEG) occuring in AlGaN/GaN heterostructures. The 2DEG constitutes the channel of AlGaN/GaN HEMTs. Both models developed are based on experimental data collected from the literature.

Electron mobility model for bulk GaN

Up to now, two low-field electron mobility models for bulk GaN have been reported. One model [1] is based on experimental data from 1973 to 1996 and underestimates the mobility for electron densities below $10^{16}cm^{-3}$. The second model [2] applies results from Monte Carlo simulations and considerably overestimates the mobility high for electron densities.

We collected a large number of mobility data from the technical literature [3]. Based on this data the mobility is modeled by the well known Caughey-Thomas mobility formula

$$\mu_0 = \mu_{min} + \frac{\mu_{max} - \mu_{min}}{1 + \left(n / n_{ref}\right)^{\alpha}}$$

where μ_0 is the low-field mobility, n is the electron density, and μ_{min}, μ_{max}, α, and n_{ref} are parameters obtained by a fitting procedure. Figure 1 shows the experimental data together with the modeled mobility using the new mobility model (solid line). The thick dashed line is our upper limit fit to model high-quality GaN layers. Also shown are the mobilities obtained using the models from [1,2].

Clearly the new model describes the experimental mobilities much better than the previously published models.

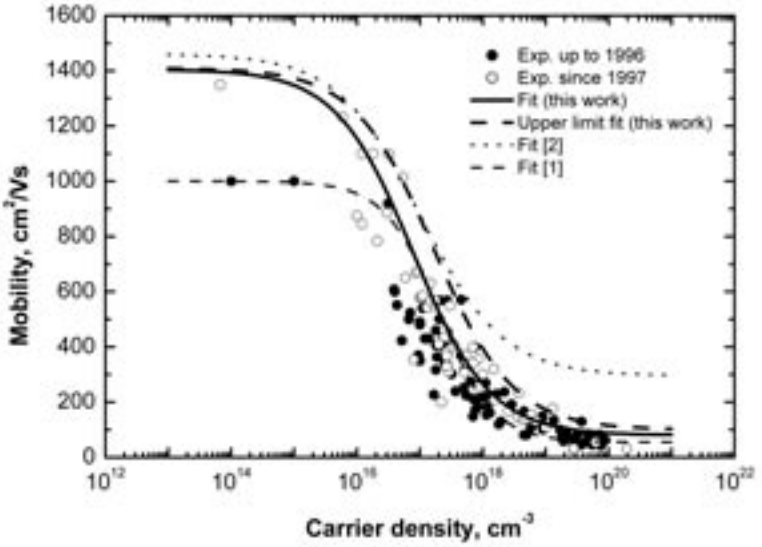

Fig. 1: Modeled GaN electron low-field mobility using μ_{min} = 80 cm²/Vs, μ_{max} = 1405 cm²/Vs, α = 0.71, and $n_{ref} = 7.78 \times 10^{16} cm^{-3}$.

* fon: +49-(0)3677-69-3120, email: frank.schwierz@tu-ilmenau.de

AlGaN/GaN 2DEG mobility model

The 2DEG mobility in AlGaN/GaN structures depends on a variety of factors related to the design of the structure, such as Al content, doping and thickness of the AlGaN, etc. Most of these factors also affect the electron sheet density of the 2DEG, n_s. Therefore it is convenient to plot the 2DEG mobility as a function of the sheet density and then to develop a model of the form $\mu_0 = f(n_s)$. For this purpose we used the expression

$$\frac{1}{\mu_0} = \frac{1}{\mu_{phon}} + \frac{1}{\mu_{red1}} + \frac{1}{\mu_{red2}} = \frac{1}{\mu_{phon}} + \frac{1}{a\, n_S^b} + \frac{1}{c\, n_S^d}$$

where n_s is the sheet density in 10^{13} cm^{-2}, μ_{phon}, μ_{red1}, and μ_{red2} are mobility components related to different scattering mechanisms. μ_{phon} is the phonon-limited mobility (independend on n_s), μ_{red1} is a mobility component related to scattering mechanisms whose effectivity decreases with increasing n_s, and μ_{red2} is a component describing the scattering mechanisms whose influence increases with increasing n_s. A value of 2300 cm^2/Vs has been chosen for μ_{phon} while the parameters a, b, c, and d have been obtained by fitting. In Fig. 2 the modeled 2DEG mobility together with the collected experimental data is shown. The thick solid line is our average mobility fit. Because of considerable scattering of the experimental data we developed a second fit (high mobility fit) to model the mobility in high-quality AlGaN/GaN structures.

The model can be easily incorporated in numerical device simulators by translating the sheet density into the perpendicular field in the GaN layer adjacent to the AlGaN/GaN interface.

In summary, two models for the electron mobility in bulk GaN and in 2DEGs at AlGaN/GaN interfaces have been developed. In the future, these models will be used to simulate the electrical behavior of GaN MESFETs, AlGaN/GaN HEMTs, and other AlGaN/GaN devices.

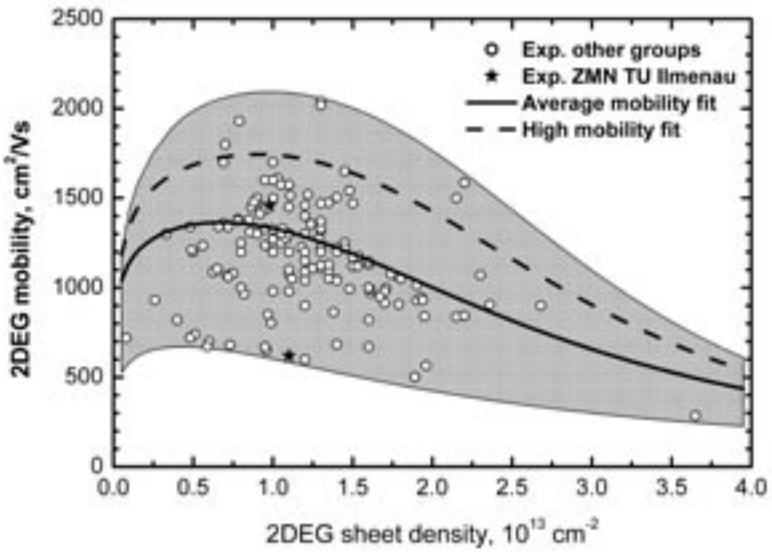

Fig. 1: Modeled 2DEG mobility in AlGaN/GaN structures. Average mobility fit: a = 4150 cm²/Vs, b = 0.262, c = 13200 cm²/Vs, d = -2.26. Shown are also measured mobilities from samples fabricated at ZMN [4].

This work has been supported by DFG under contract no. Schw729/2-3.

1. T. T. Mnatsakanov, M. E. Levinshtein, L. I. Pomortseva, S. N. Yurkov, G. S. Simin, and M. A. Khan, Carrier Mobility Model for GaN, Solid-State Electron. 47, pp. 111-115, 2003.
2. M. Farahmand, C. Garetto, E. Belotti, K. F. Brennan, M. Goano, E. Ghillino, G. Ghione, J. D. Albrecht, and P. P. Ruden, Monte Carlo Simulation of ElectronTransport in the III-Nitride Wurtzite Phase Materials System: Binaries and Ternaries, IEEE Trans. Electron Devices 48, pp. 535-542, 2001.
3. F. Schwierz, Electron Mobility in Bulk GaN and in AlGaN/GaN 2DEGs: A Compilation of More Than 200 Top References, TU Ilmenau 2003, Unpublished.
4. O. Ambacher, Private Communication.

Advanced LTCC processes using Pressure Assisted Sintering

M. Hintz[1,*], H. Thust[1], and A. Albrecht[2]
Departments of Microperipherics[1] and Microsystems Technology[2]

Low **T**emperature **C**ofired **C**eramics (**LTCC**) offer a wide range of possibilities to realize multilayer circuits with an almost unlimited number of layers. It permits the integration of passive components like conductors, resistors, capacitors and inductors into the circuit carrier. Together with the low dielectric losses, good thermal conductivity and stability, the LTCC technology is eminently qualified for many applications. However, freely sintered LTCC substrates are often limited in their dimensional accuracy. The overall x/y-shrinkage and tolerances during sintering might be responsible for problems in component assembly and complicates the specification of the electrical properties.
That is why in the last years zero-shrink techniques have been introduced more and more in LTCC-processes. These techniques use different constraining mechanisms to limit the x/y-shrinkage during sintering. Consequences are lower tolerances and the possibility to integrate full metal structures like foils or platings. Different constrained sintering processes are known, such as the **S**elf **C**onstrained **S**intering (**SCS**), the **P**ressureless **C**onstrained **S**intering (**PLAS**) and **P**ressure **A**ssisted **C**onstrained Sintering (**PAS**).
The Pressure Assisted Sintering process is the complexest method. During this process a uniaxial force assists the constraining effect of the release tapes. Therefore, a special hot pressure furnace is needed.

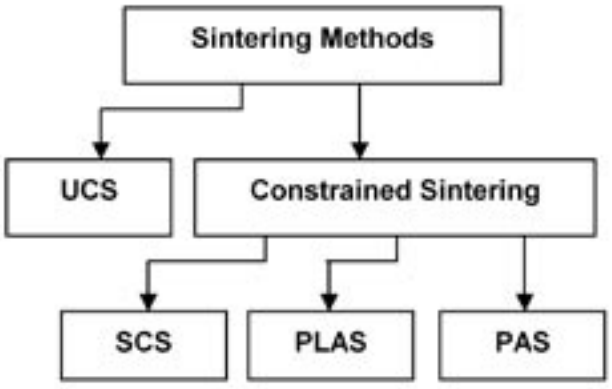

Fig. 1: Sintering methods

Shrinkage behavior
The investigation shows that with Pressureless Constrained Sintering the absolute shrinkage in x/y-direction is restricted to around 0.3%, (material A/B). Pressure Assisted Sintering allows to control the shrinkage between 0.3 - -0.1% (expansion) (material A) and 0.3 - 0.1% (material B). The optimal pressure depends on the material used. With some materials 0.0% shrinkage and also expansion of the modules are possible but in this case the tolerances rise rapidly. Best results regarding low tolerances are obtained by pressures allowing a shrinkage of 0.1 - 0.2%. The self constrained material shows a shrinkage of 0.2 - 0.4% (material C). When freely sintered, the shrinkage of the other materials was 12 - 14% (material A) and 18 - 21% (material B).
The tolerances of the constrained processed modules are between 0.1% (PLAS) and 0.05% (PAS and SCS). This allows the use of LTCC materials in larger dimensions than in the UCS process without assembly problems.

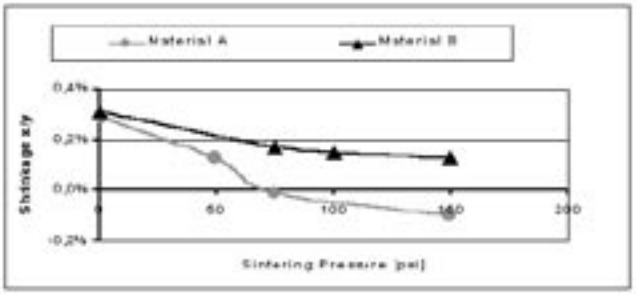

Fig. 2: PAS- Shrinkage behaviour

Mechanical behavior
The covering of the surface during the PAS and the uniaxial pressure during sintering influence the mechanical behaviour of the substrate. Some investigations were carried out to show the effects of these influences.
The surface roughness determination shows a lower roughness of PAS processed (Ra = 0.42) compared to freely sintered substrates (Ra = 0.67). Release tape and sintering pressure limit the growing of crystal needles on the surface (Fig. 3). Another effect comes from the needed sand blasting process of the PAS processed module. The lower roughness may be an important feature for using thin film materials on the surface.

* fon: +49-(0)3677-69-3430, email: michael.hintz@tu-ilmenau.de

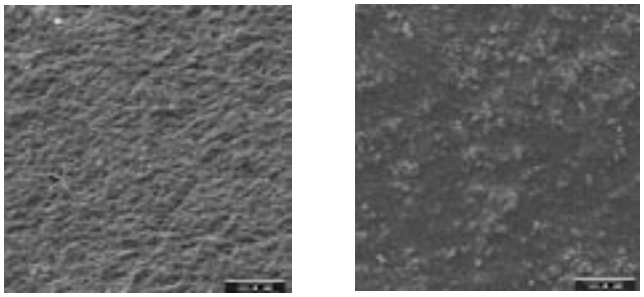

Fig. 3: Surface of free sintered (right) and PAS- processed LTCC after sandblasting (left), material A

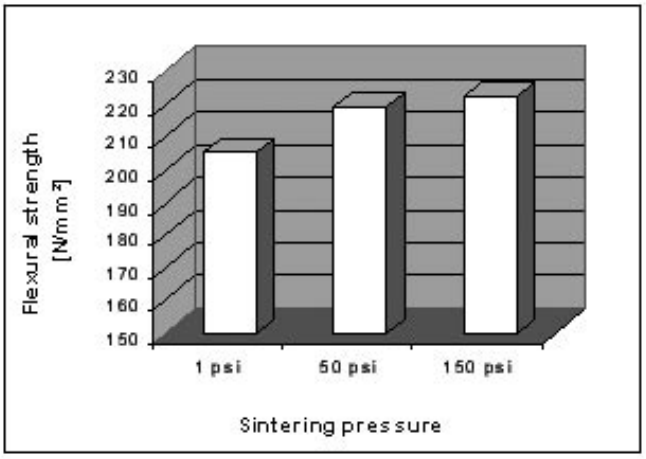

Fig. 4: Flexural strength of modules processed at different sintering pressures (material A)

The mechanical strength of PAS and PLAS processed modules was determined by 3-point tests. It is comparable to the strength of freely sintered modules but is also influenced by sand blasting. A problem of the breaking strength of LTCC substrates is the high spread caused by the inhomogeneous composition of glass ceramic composites. In this case, PLAS and PAS processed structures show a slightly better behaviour. Beside this, for PAS the flexural strength rises with higher pressures (Fig. 4).

Full metal conductors

Today, the most discussed advantage of PAS is the advanced dimensional accuracy. In addition, this process offers some other specific advantages. The pressure during sintering allows the use of cofired structures with different TCEs and without shrinkage during sintering, such as full metallic inlays.

	Screen printing prints	Photo-imageable	Full metal
Resistivity / square (10µm thickness)	4-6 mOhm (silver)	4-6 mOhm (silver)	2 mOhm (silver)
Thickness	5 - 50µm	5- 30µm	2->80µm
Resolution	low	high	high
Roughness of edges	high	low	low
Via crossover	no problem	critical	no problem

Fig. 5: Features of different processed cofired conductors

At present, for standard LTCC- applications only screen printing is used for realising conductors. With the disadvantages given like low conductivity, limited resolution and low edge accuracy, this process narrows the application field of cofired ceramics. Most of these disadvantages could be avoided by using full metallic structures. These are structures which are not based on sintered metal particles like pastes but on platings or metal foils. Different methods of structuring of such conductors were tested or developed, for instance a process called **P**lating on **C**ofired **C**eramics (**POCC**) and metal foil structuring. The direct comparison between paste based conductors and full metal conductors shows the potential and the problems of the different technologies (Fig. 5). Advantages of such full metal structures are high electrical and thermal conductivity.

Furthermore, structures with excellent edge geometry (Fig. 6), low roughness, high aspect ratio and high resolutions are possible. In this way these technologies are qualified for new applications in the fields of radio frequency and power devices.

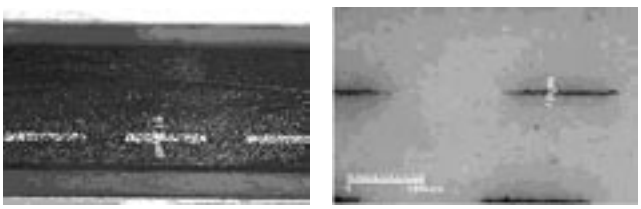

Fig. 6: Plated lines with high thickness (left) and typically screen printed lines (right)

This work has been supported by TMWFK (Az.: B609-02003)

Ultrasonic and X-ray inspection of multilayer PBC and LTCC hybrid circuits - comparison and advantages of both methods

R. Münnich[1,*], A. Sutor[2], I. Koch[1], and G.Winkler[2]
Departments of Microperipherics[1] and Design and Technology of Electronic Components[2]

The inspection of multilayer substrates and modern packaging methods is currently a necessary step in production and reliability control. A simple optical inspection is not sufficient for the evaluation of reliability of electrical connections in modern packaging systems like BGA or CSP. The question is what kind of failures is possible and which methods are available to determine production failures. The typical methods for testing such failures are X-ray microscopy and ultrasonic microscopy.

Packaging:

- At the packaging side the semiconductors are often protected with a polymer. Here, a delamination of the polymer from the chip is the worst case for the thermal conductivity. Embedded air bubbles are the second failure mechanism that has to be verified by the manufacturer of packages.
- The next connectivity level is the connection from the electronic component to the board with soldering or flip chip bonding methods. Here, different solder failures are possible ranging from dislocation to shortcuts caused by excessive solder paste or missing contacts.

Multilayer Board:
Common failure mechanism on the multilayer boards are:

- misalignment of single layers
- delamination of layers

X-ray Microscopy:
Delamination or embedded air bubbles are not easily detected by X-ray microscopy in transmission mode, because the air is not absorbing the radiation comparable to the material investigated. This method of investigation is preferred when high absorbing materials like solder bumps or conductive adhesive are tested. In LTCC technology the positioning of layers can be determined by inspection of via holes filled with conductive paste.

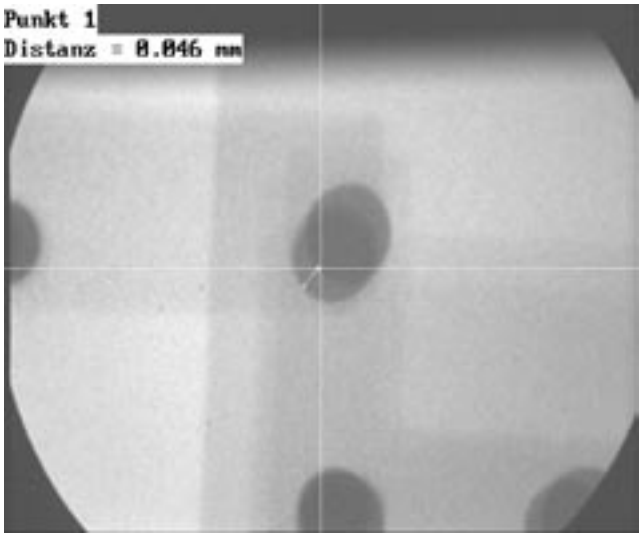

Fig. 1: Misplacement of LTCC-Vias

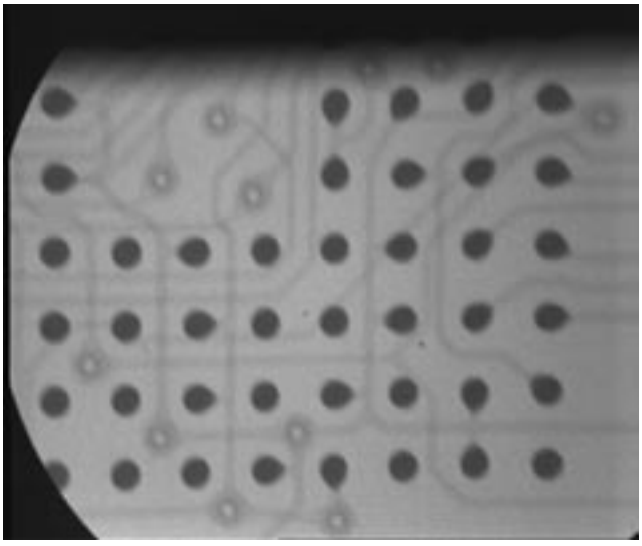

Fig. 2: Deformation of BGA-solder bumps

* fon: +49-(0)3677-69-3452, email: ralph.muennich@tu-ilmenau.de

Ultrasonic Microscopy:
Acoustic Micro Imaging is a technique that uses high frequency ultrasonic pulses to investigate hidden structures, characterize material properties, and detect defects. The ultrasonic wave can not propagate through air or vacuum, so delaminations are easily detected. On every barrier layer with different acoustic impedances the ultrasonic wave is divided in a reflected and a transmitted wave. With a gating technique for the reflected signal single layers can be detected.

Because the large differences between their acoustic impedances, ceramic and air delaminations can easily be detected. In the LTCC technology the via-connections are realised by filling a hole with a conductive paste. Captured air bubbles in these via-holes are a failure mechanism and might cause a break in the electrical contact.

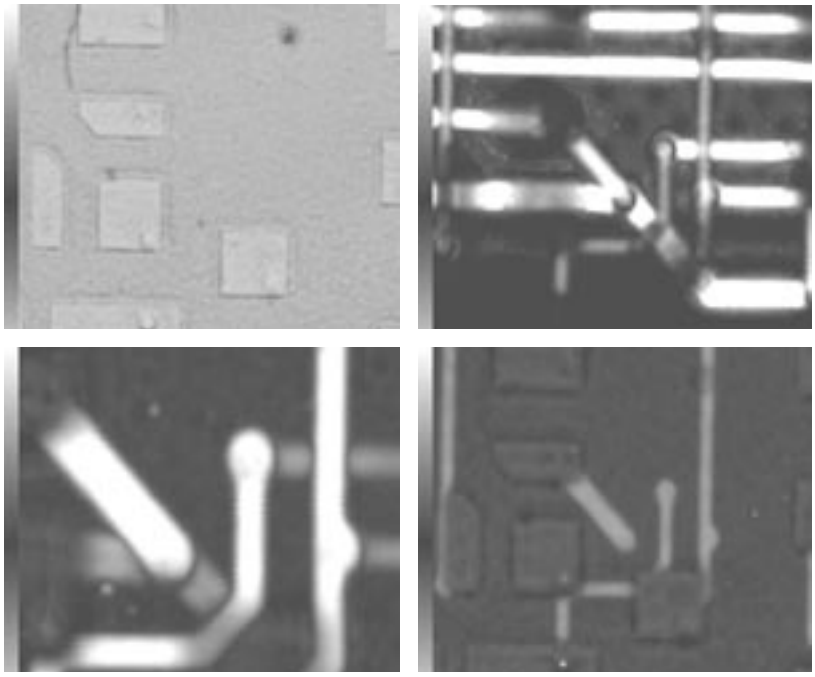

Fig. 3: Inspection of a single signal layer from LTCC substrate through gating of the echo signal

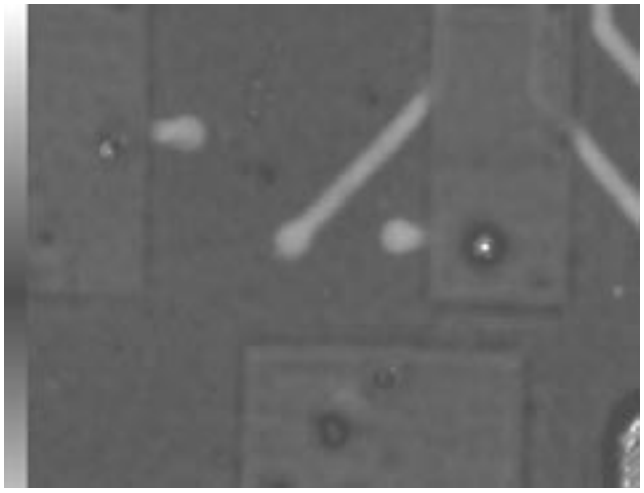

Fig. 4: Detection of a void in via-connections

Conclusion

By the selection of the appropriate method described the advantages in sensitivity and resolution can be adapted to the special applications and material combinations investigated. In the paper, the exact localization of air bubbles and incompletely filled vias with ultra sonic microscopy are demonstrated. Futhermore, the determination of misalignments in multilayer structures by X-ray microscopy has been discussed.

This work was supported by German federal ministry BMBF
research project 03GL0057

R.Muennich and H.Thust : Multilayer LTCC module for RF-applikations Symposium
"Folien- und Multilayertechnologie für funktionskeramische Anwendungen"
BAM Berlin,10.-11. April. 2003, p.53-55, Volltext auf CD

KERAMIS: 20 GHz LTCC applications for satellite communications - Challenges for design and technology

J. Trabert[1,*], R. Münnich[1], R. Perrone[1], R. Stephan[2], M. Hein[2], and H. Thust[1]
Departments of Microperipherics[1] and RF and Microwave Techniques[2]

The project KERAMIS aims at the development of innovative and low-cost components for future applications in multimedia satellite communications. The principle of operation and the potential benefits of satellite-based systems will be demonstrated.
Today the microwave circuits are built similar to a single layer printed circuit board. Connections between the components usually have to be placed on the top layer and the bottom layer is used as ground. This is a serious limitation of the complexity. Within the last years several multilayer techniques have been proposed to defeat this limitation. All these techniques are confronted with the problem that all plastic materials have rather poor dielectric properties, i.e. the losses of the dielectric layers become too large when the operating frequency exceeds several gigahertz. Only ceramic materials appear to qualify multilayer microwave circuits above 10 GHz or 20 GHz.

A variety of challenging technological problems arising from temperature stress and shrinking caused by the firing process had to be solved before the multilayer ceramics technology was prepared for production. Future microwave circuits can benefit from the LTCC (**L**ow **T**emperature **C**ofired **C**eramics) technology. The number of thick film metallization layers in this commercially available process may exceed 20. In effect, this technology is capable to improve the packing density of RF circuits dramatically.
LTCC technology offers a number of benefits such as low-cost production and assembly, light-weight, compact size, and hermetic encapsulation, which are of utmost importance for satellite-based applications. Compact and modular structured systems are realized by implementing various functions in LTCC multichip modules that are assembled on a common motherboard to provide a high functional density.

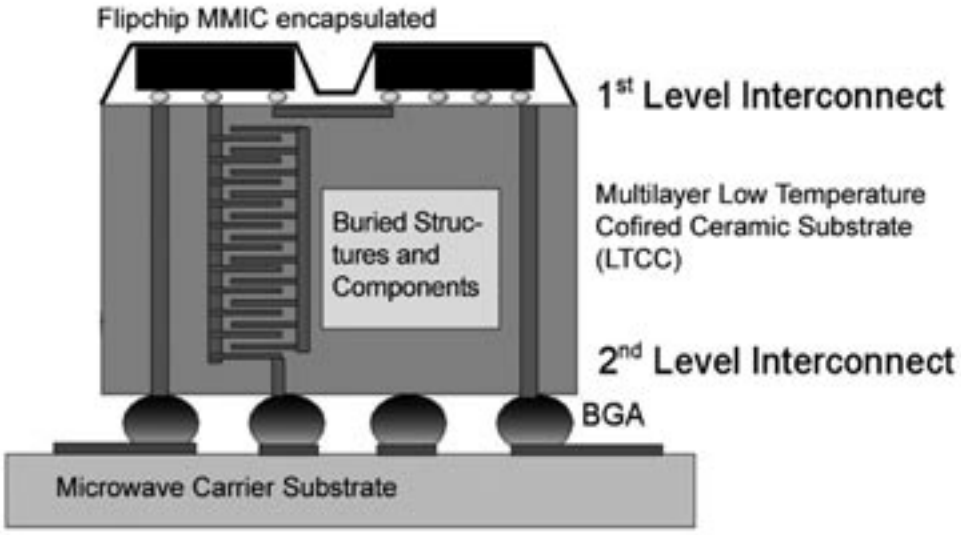

Fig. 1: Cross-section of a sophisticated LTCC-based microwave application

The rationale of the project is to exploit the possibility of integrating passive and active components and functions such as biasing networks, DC-blocks, power splitters, amplifiers, mixers, etc. in one LTCC multi-layer structure. Additional reduction of semiconductor expenses is achieved by minimizing the complexity of the semiconductor components by placing out the matching circuitry and decoupling structures on the ceramics board instead of being integrated on chip. These described benefits imply that the LTCC microwave components have to be manufactured in a reproducible high quality and with an appropriate yield. Additionally, it is obligatory to develop design rules and models for

* fon: +49-(0)3677-69-1592, email: johannes.trabert@tu-ilmenau.de

the computer aided circuit design. Furthermore, it is necessary to find promising options for the hermetic housing as well as for the signal interconnections.
Three technological milestones for Ka-band satellite applications which are used for satellite down-link purposes are under development: *a solid state power amplifier, a frequency synthesizer and a reconfigurable 4x4 switch matrix*.

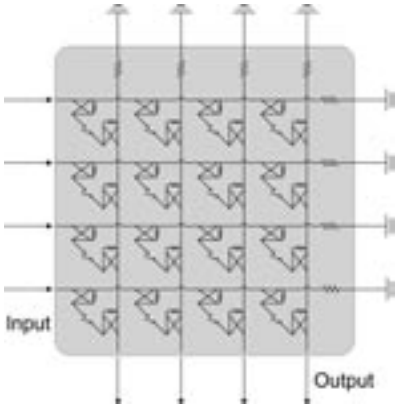

Fig. 2: Schematic diagram of a 4 x 4 switch matrix

Reconfigurable 4x4 switch matrix

A switch matrix provides digitally controllable signal paths for adaptation, reconfiguration, and functional multiplexing. Its functionality and its small size are representative for the needs of satellite-based communication systems. A realization in LTCC technology offers the desired high reconfigureability, high functional density, modular structure, light weight, low power consumption, low manufacturing costs and also high durability and reliability. As a first demonstrator the reconfigurable switch matrix is realized in a LTCC-Stack of 11 layers *DuPont®-951* AX "green"-tape with a total height of about 2.2 millimeter. The inner conductor layers are manufactured with extraordinary resolution and accuracy. This process is an aggregation of conventional silk-screen printing and a high-tech fine line photoimaging method (*DuPont® FODEL®* system). It combines the advantages of thick- and thin- film technology at moderate costs.
The active controlled switches are integrated circuits with the functionality of a single-pole four throw switch. Each single switch element (PIN-Diode) is implemented on chip in a special process which enables the incorporation of silicon pedestals that form series and shunt diodes or vias by embedding them in a low loss, low dispersion glass. This hybrid combination of silicon and glass gives these switches low loss and high isolation through K-band frequencies. The bare dies are countersinked into a cavity which is resected from the 3 top layers. These chips have gold back side metallization and are die mounted with electrically conductive epoxy. The pads on the top side of the dies are contacted by ball bonding using 1 mil diameter gold wire.

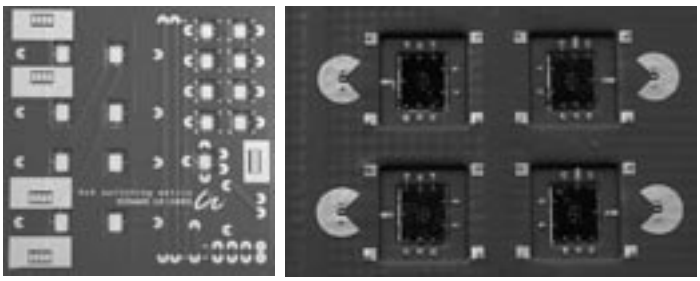

Fig. 3: Photograph of LTCC test chip and enlarged region with adhered dies (SP4T switches)

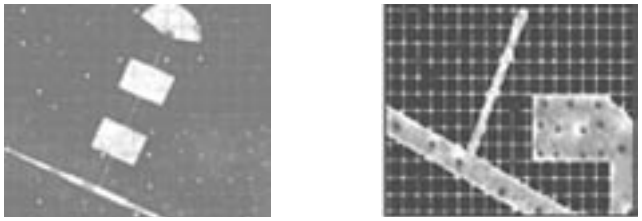

Fig. 4: Ultrasonic images of buried RF conductions, minimum line width is 40 µm

Consortium:

As well as:
Technische Universität Braunschweig, Germany
www.tu-braunschweig.de/ihf/ag/mikrowellen

RHe Microsystems GmbH, Radeberg, Germany
www.rhe.de

This work was funded and supported by DLR and BMBF.

Experimental set-up and investigations for an integrated measuring station for the examination of biological material in the nano- and picovolume range

A. Schober* , O. Ambacher, C. Buchheim, J. Burgold, V. Cimalla, Th. Doll, K.H. Drüe, M. Fischer, J. Gessner, M. Himmerlich, M. Hintz, R. Hoffmann, G. Jäger, H. Kern, G. Kittler, M. Kittler, Ch. Knedlik, S. Krischok, A. Majdeddin, E. Manske, R. Mastylo, H. Romanus, T. Sändig, J.A. Schaefer, F. Schwierz, L. Spiess, H. Thust, F. Weise, G. Winkler, H. Wurmus, and V. Yanev,
All departments of the Center for Micro- and Nanotechnologies

Introduction

Miniaturisation of analytical and technical devices for biotechnological, medical and chemical applications shows high potential for accelerating the discovery of new biological relevant substances and drugs. Especially nanotechnological approaches promise a new quality with respect to time, sensitivity, and specificity in the field of biology driven sensor technology. New sensor concepts on the nanoscale demand for new system integrative concepts including the manipulation of pico- and nanofluid volumes on chemical or structural modified surfaces and defining suitable interfaces to the macroworld.

A new laboratory with special developed measuring stations (some examples are shown in Fig.1) allow to test several integrative experimental set-ups, which contain new sensors based on AlGaN/GaN heterostructure semiconductor systems, pico- and nanofluidic dispensers based on piezo actuators, the micro periphery and the electronics for measuring biochemical assay systems (in vivo and in vitro). Iterative adaptations of e.g. surface and sensor modifications are performed to find the suitable design for testing the biological systems.

Fig. 1: (a) the experimental set-up (b) the atmospheric chamber with controlled environment by adjusting parameters like relative humidity (1...95%), pressure (±10mbar), and temperature (0...60°C).

Experimental set-up

Liquid Handling and surface modification

Active liquid handling is realised by using actuators to accelerate or to displace liquids. Different pipetting tools in the range of 50 picoliter with a frequency of 3 kHz up to 10 nanoliters with a frequency of 100 Hz have been developed see Fig. 2a). The systems are piezo driven with a bimorph construction or, alternatively, a piezo stack construction.

Hydrophilization or hydrophobization of surfaces controls the wetting behaviour of liquids and allows to define pathes and areas where liquids can be placed and controlled. For the sensor the hydrophilization of the active area has to be achieved whereas the non active surrounding should be hydrophobic. Hydrophilization is obtained by oxidation in a fast thermal process resulting in a contact angle of 45° for water (see Fig. 2b). Hydrophobization is realized by deposition and structuring of a fluorcarbonlayer which serves simultaneously as isolation of the electrical contacts. The contact angle is determined to 95° (Fig 2b). The layers are analyzed by electronspectroscopical and -microscopical measurements determining the chemical and structural parameters of the layers.

Sensorics, Frames/Peripherics and Electronics

AlGaN/GaN-heterostructure semiconductor devices were produced by plasma induced molecular beam epitaxy (PIMBE). Metallization of source- and drain contacts was realized. First sensors were constructed. The important electronic parameters e.g. the transport parameters of the $Al_xGa_{1-x}N$-layers could be simulated and identified

* A. Schober: * fon: +49-(0)3677-69-3486, email: andreas.schober@tu-ilmenau.de.

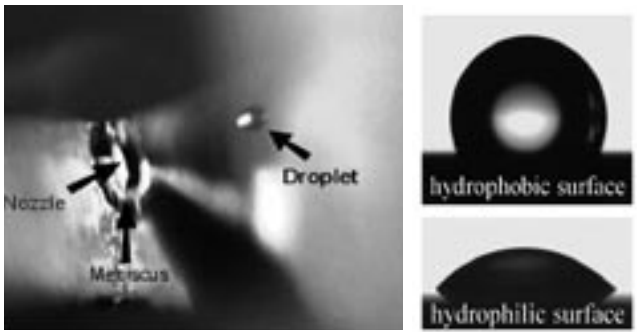

Fig. 2: Nanodroplet ejected from silicon based dispensing head (left)
The effect of surface modification (right): above a hydrophobic fluorocarbon surface and a hydrophilic AlGaN sensor surface.

by the bound/interface charge model and the two dimensional electron gas (2DEG) mobility model serving as tools for developing optimal sensor geometries.
Based on the functional requirements for the sensors, two different designs and materials of the frames for the integration have been developed.
The frame made of silicon is bonded onto a borosilicate base plate structured by micro sand blasting. The sensor will be fixed by spring clamping allowing easy replacement of the sensors. The silicon is constructed by anisotropic etching. A Titanium Gold layer enables bond and soldering processes.
The frame made of LTCC (low temperature cofired ceramics) has been constructed for fluid applications with pH values > 7. It consists of 5 layers, which

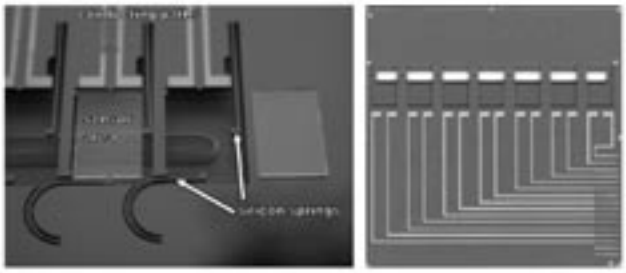

Fig. 3: Silicon frame with the spring structure (left) Frame made of LTCC (right).

have been constructed by UV Laser radiation in the green state before sintering. The lamination and sintering process was optimised with respect to crack initiation and forming, which results in suitable frame configurations for the senors (Fig. 3).

By integration of an electronic read out system (Agilent) consisting of a parameter analyser with a high power source monitor unit (SMU), two mid power SMUs and a 10 x 12 matrix switch, first measurements with the sensors have been performed (Fig. 4). The size of a water droplet is determined by the change of the source drain current with the time during evaporation of the droplet.

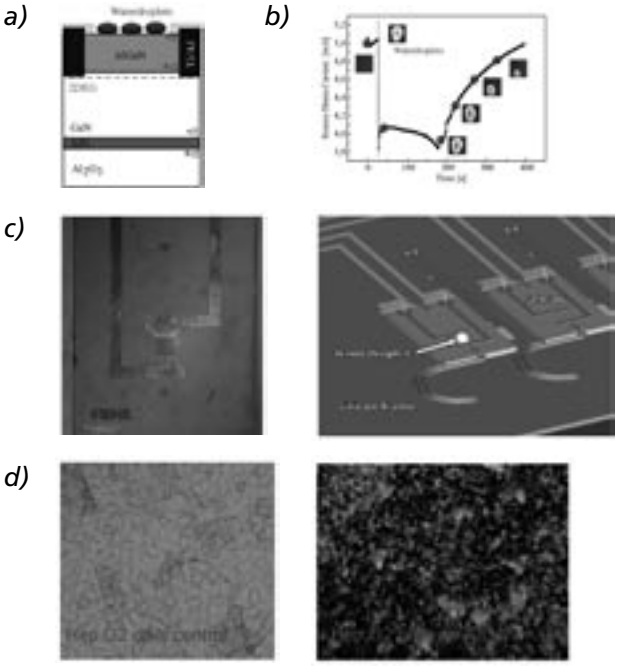

Fig. 4: a) Sensor structure, b) evaporation-measurement by the sensor, c) sensor and sketch of the sensor set-up, d) biocompatablilty experiments: (left) HepG2 cells in the petri dish as a control, (right) adherent Hep G2 cells on AlGaN.

First experiments according to the influence of AlGaN surfaces to biological materials have been performed. The biocompatability of the semiconductor heterostructure is analyzed by cell adherence. Cell growth on this material is examined and shows – as a first result – no strong interference (Fig. 4). Further investigations will be performed with different cell lines using fluorescence based viability tests.

Further research will be focused on the optimization of the sensors and the experimental set-up with respect to the biological material.

The work was partially supported by the TMWFK and the European Community (EFRE program, 6th framework program).
The collaboration with E. Gottwald and Karl-Friedrich Weibezahn IMB, Forschungszentrum Karlsruhe is greatfully acknowledged.

• Gap state absorption in AlGaN photoconductors and solar-blind photodetectors
V. Lebedev, I. Cimalla, U. Kaiser, and O. Ambacher
phys stat sol (c) 1 (2004) 233.
• Pyroelektrische AlGaN/GaN-Heterostrukturen für die Sensorik und Elektronik
O. Ambacher, V. Cimalla, V. Lebedev, G. Kittler, and M. Ali
Thüringer Werkstofftag 2004 - Vorträge und Poster,
Schriftenreihe Werkstoffwissenschaften
Bd. 18, Hrsg. L. Spiess, H. Kern, Ch. Knedlik,
Verlag Dr. Köster, Berlin 2004, p. 1 - 18.
• Trockenätzen von Siliziumkarbid
Ch. Förster, V. Cimalla, J. Pezoldt, G. Ecke, and O. Ambacher
Thüringer Werkstofftag 2004 - Vorträge und Poster, Schriftenreihe
Werkstoffwissenschaften Bd. 18, Hrsg. L. Spiess, H. Kern, and Ch. Knedlik,
Verlag Dr. Köster, Berlin 2004, p. 185 - 190.

Investigation of the metrological characteristics of the nanopositioning and nanomeasuring machine with an integrated focus sensor

R. Mastylo*, E. Manske, and G. Jäger
Department of Process Measurement

A nanopositioning and -measuring machine with a measuring range of 25 mm x 25 mm x 5 mm and a resolution of 0.1 nm has been developed at the Institute of Process Measurement and Sensor Technology of the TU Ilmenau. Additionally, an optical scanning sensor based on the principle of focusing has been developed and successfully integrated into the nanopositioning and –measuring machine as so-called null indicator [1].

Standard Nr..	Schichtdicke Mittelwert (PTB) ± U	Schichtdicke Mittelwert (NMM mit Fokussensor) ± U
C26 R18	7,4 ± 1,0 nm	7,8 ± 0,7 nm
C18 R18	21,2 ± 1,1 nm	22,1 ± 1,1 nm
C17 R27	69,1 ± 1,2 nm	68,4 ± 0,8 nm
C19 R26	294,2 ± 2,0 nm	294,7 ± 1,1 nm
C12 R01	778,36 ± 3,5 nm	777,1 ± 2,0 nm

Fig. 1: Measurement on PTB step height standards

The focus sensor is firmly built in, and all measuring operations (movement of the object of measurement) are realized by the nanopositioning and –measuring machine on the basis of the signals determined by the focus sensor. In order to enable fast dynamic measurements, the focus sensor is not permanently controlled out to zero. Instead, a permanent difference formation between the output signal of the focus sensor and the length value of the z-interferometer of the nanopositioning and –measuring machine is effected. In this case, the measuring machine supplies the low-frequency component of the measuring signal on the basis of its inertia, whereas the uncontrolled deviations of the focus signal constitute the high-frequency components of the measuring signal. This allows measurement frequencies in the scan mode up to 500 µm/s at a resolution of 1 nm. Further advantages offered by the difference measuring principle are a lower temperature and vibration sensitivity.
In order to determine the metrological characteristics of the focus sensor, step height standards calibrated at the Physikalisch-Technische Bundesanstalt (PTB) were measured. Fig. 1 shows the results recorded on five different step height standards of the PTB. All measurements were performed in the dynamic mode. The extended measuring uncertainty U has been calculated using the extension factor k = 2.

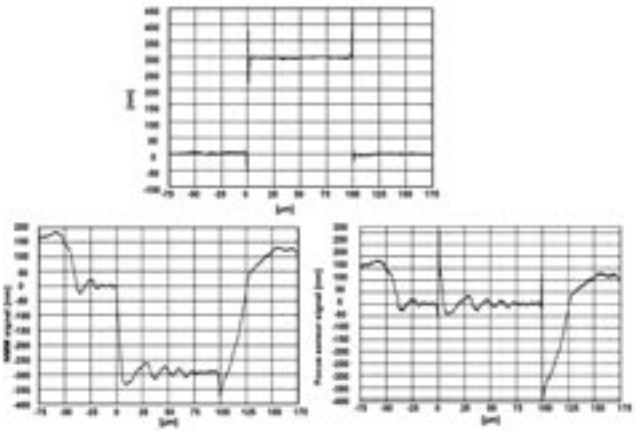

Fig. 2: Measurement made on a 294.2nm step height standard

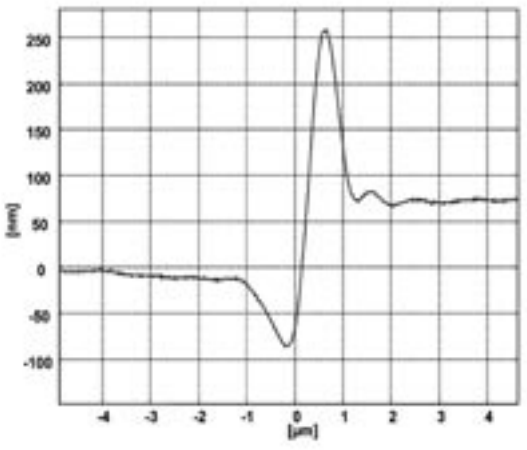

Fig. 3: Batwings effect on the step height standard

Figure 2 shows the individual measuring signals on a 294.2 nm step height standard (at the bottom left the signal of the measuring machine, at the bottom right the signal of the focus sensor), as well as the measuring result (at the top) obtained from the difference of the two signals during the scanning process. During such measurements

* fon: +49-(0)3677-69-1836, email: rostyslav.mastylo@tu-ilmenau.de

at a scan speed up to 500 µm/s no significant change of the measuring uncertainty occurs.

The overswings at the sharp edges (so-called Batwings effect) are typical phenomena occurring during the optical measurements in the nanometre range. They result from diffraction effects on the sharp edges the size of which lies in the range of the wavelength of the measuring beam [2, 3] (Fig. 3). The width of the batwing corresponds to the spot size of the focus sensor and is approximately 1 µm. By this spot size the lateral resolution of the sensor is limited. Therefore, the smallest structure width to be measured should not be less than 5 µm. The 3D-measurement made on the same 294.2 nm step height standard (Fig. 4) shows that the batwings appear to be highly reproducible, but their shape and amplitude are different on various edges.

The large Numerical Aperture (NA = 0.6) of the lens of the focus sensor allows the objects to be measured at an inclination of up to 20°. The appropriate measurements were carried out at a concave lens (Fig. 5), the measuring area amounts to 23 mm x 23 mm.
Besides the tilt angle of the measuring surface also the surface structure plays an important role. The focus sensor can be applied to almost all kinds of surfaces whose reflection factor is higher than 4 %. As mentioned above, various glass surfaces (uncoated, reflection factor about 4 %) have already been measured successfully. In addition, the measurements can also be performed on materials such as steel, aluminium, silicon, paper (black or white) and water, whereas it is always problematic to measure finely rough surfaces whose roughness amounts to some micrometers such as ceramics (non-varnished) or fine structures presenting an edge steepness between 20° and 70°.

The important advantage offered by the focus sensor developed – in combination with the nanomeasuring machine – is the possibility to perform the measurements within a very large range of X x Y = 25 mm x 25 mm and Z = 5 mm at nanometer resolution, which can be proven in the measurement of a fragment of a concave lens over 23 mm x 23 mm (Fig. 5). Furthermore, also step heights can be measured which are greater than the working range of the focus sensor characteristic line. Therefore, a special measuring algorithm has been programmed. Figure 6 shows the measurement on a step height of 1000 µm.

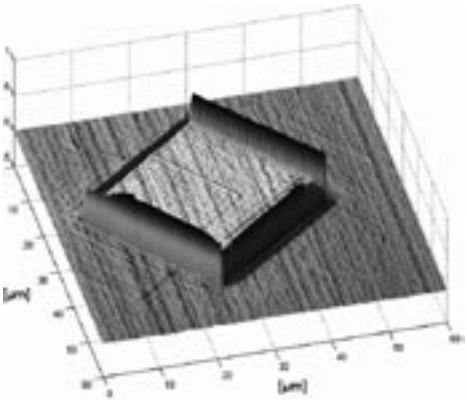

Fig. 4: 3D-measurement made on a 294.2nm step height standard

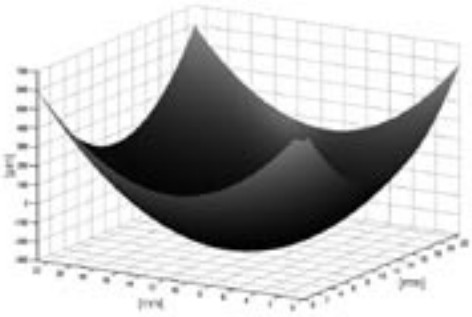

Fig. 5: Measurement on a concave lens

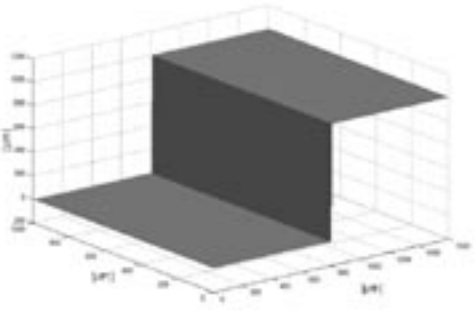

Fig. 6: Measurement on a 1000 µm step height standard

[1] Manske, E.; Mastylo, R.; Jäger, G.: Entwicklung eines Autofokussensors und Integration in die Nanopositionier- und Nanomessmaschine, Jahresbericht ZMN 2002.
[2] Harasaki, A.; Wyant, J.C.: Fringe modulation skewing effect in white light vertical scanning interferometry, Applied Optics Vol. 39, No. 13, 2000, pp 2101-2106.
[3] Czaske, M.: Strukturbreitenmessung auf photolithographischen Masken und Wafern im Lichtmikroskop: Theorie, Einfluder Polarisation des Lichtes und Abbildung von Strukturen im Bereich der Auflösungsgrenze, PTB-Bericht, Braunschweig 1997, ISBN 3-89701-011-9.

Characterization of SiC/Si heterostructures and GaN films on sapphire by infrared spectroscopic ellipsometry

C. Buchheim* **and J. Pezoldt**
Department of Nanotechnology

Infrared spectroscopic ellipsometry (IRSE) is an important tool for the characterization of semiconductors. Phonon and plasmon modes contribute to the optical response in the infrared (IR) spectral region. Plasmon modes can be used to determine free carrier parameters and phonon modes reflect crystal properties such as lattice symmetry and structural quality and internal strain. This strain is due to the lattice mismatch in pseudomorphically grown semiconductor heterostructures and different thermal expansion coefficients of the materials. The internal strain leads to dislocations. For SiC/Si heterostructures the resulting degradation of the layer properties and wafer warpage limit the use for device applications and as pseudosubstrates for group-III nitrides. Group-III nitrides, which are piezoelectric, the strain is accompanied by strong electric fields, changing the optical properties, important for light emitting diodes, laser diodes and wavelength selective detectors. Polarisation induced electric fields influencing the performance of electronic devices such as high electron mobility transistors. In this work SiC/Si heterostructures and GaN films on sapphire are investigated by IRSE.

The 3C-SiC films (d ~ 120 nm) were grown by solid source molecular beam epitaxy (MBE) on (111) *on axis* Si at 1000°C. The SiC/Si interface was modified by depositing a single monolayer of Ge on the clean Si surface at different substrate temperatures. The 1.6 µm thick GaN layer was grown by metalorganic chemical vapour deposition (MOCVD). The thicknesses were determined by spectroscopic ellipsometry in the visible and ultraviolet spectral range (not shown here). The IRSE measurements were carried out at an angle of incidence of 70° for SiC and at 60°, 65° and 70° for GaN.

Fig. 1 shows the typical spectra for Ψ and Δ for SiC on Si without Ge predeposition. The spectra are fitted by the Drude-Lorentz formalism within a four layer model, including surface roughness and an interface layer between Si and SiC, with E_{TO}, E_{LO}, ε_∞ etc. as fitting parameters. At about 790 cm^{-1} the TO phonon mode is clearly observed. The fit results for E_{TO} in dependence of the Ge predeposition temperature are summarized in Fig. 2. The obtained energetic positions are in the range between

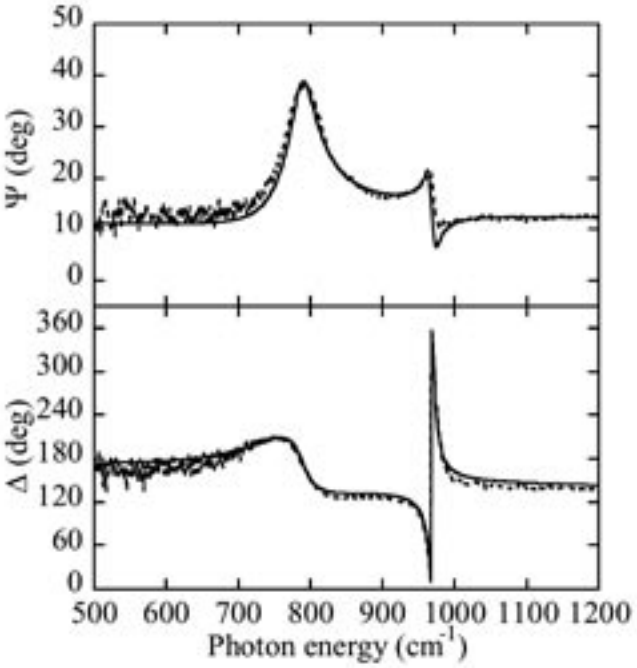

Fig. 1: Measured IRSE spectra for SiC/Si without Ge predeposition (dashed lines) and fit (solid lines) at an angle of incidence of 72°.

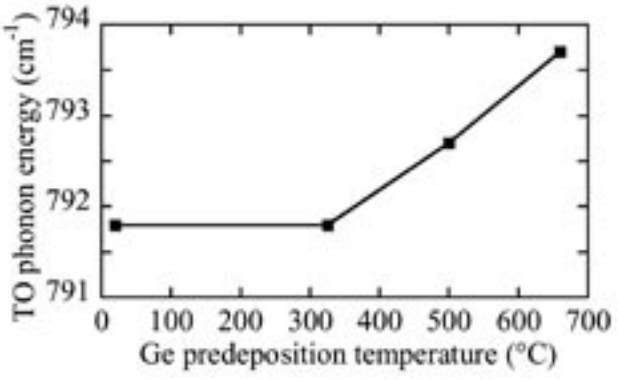

Fig. 2: TO phonon energy in dependence of the Ge predeposition temperature.

790 cm^{-1} and 794 cm^{-1} in comparison to unstrained material with E_{TO} at 796.2 cm^{-1} [1]. The lowered phonon energies indicate a tensile strain in the grown SiC layers. The energetic shift to higher energies with increasing predeposition temperature is caused by increasing incorporation of Ge into the interface between SiC and Si in agreement

* fon: +49-(0)3677-69-1172, email: carsten.buchheim@tu-ilmenau.de

with theoretical predictions [2]. The measured TO phonon energies were higher than for CVD grown SiC on Si(100) at 1330°C of similar thickness. This is in contrast to an expected residual strain for growth on Si(100), which is by a factor of two lower than for Si(111). The results are an indication for stress reduction on Si(111) in comparison to Si(100) by lowering the substrate temperature during SiC growth.

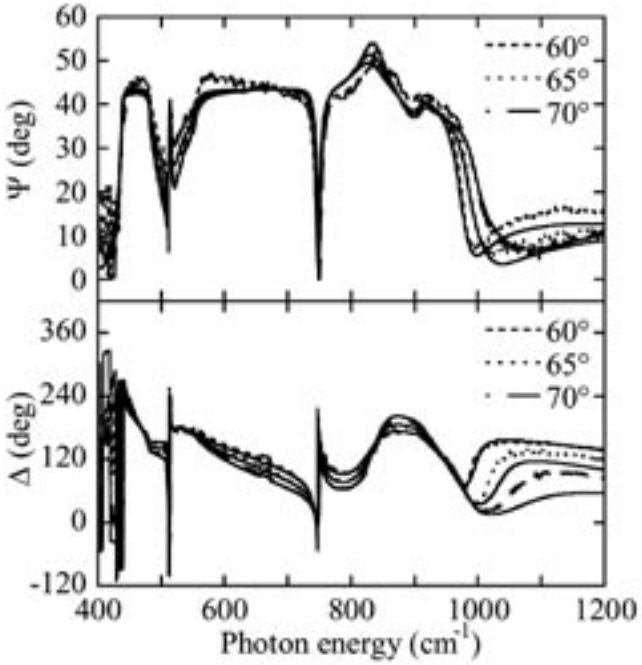

Fig. 3: Measured IRSE spectra for GaN/sapphire at different angles of incidence (dashed lines) and fit (solid lines).

For GaN on sapphire the ellipsometric data are presented in Fig. 3. The modelling of the spectra is more complicated here, because of the uniaxial anisotropy of both, film and substrate. The optical axis is in the direction of the *c-axis*, which is the growth direction in this case. For the sapphire substrate and the GaN layer there are two respective dielectric functions (DF), an ordinary $\varepsilon_{\perp}$ (in plane) and an extraordinary $\varepsilon_{\parallel}$ (out of plane). As can be seen from Fig. 3 the general line shape is reproduced

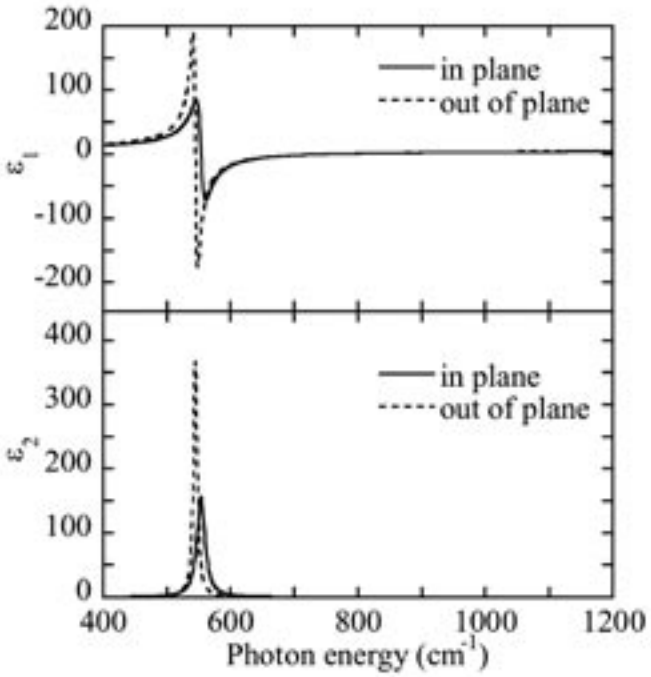

Fig. 4: Real and imaginary part of the anisotropic DF of GaN as calculated from the fit.

by the anisotropic Drude-Lorentz model. The small deviations in Ψ are due to remaining uncertainties in the substrate dielectric function and possible LO-phonon-plasmon coupling. Fig. 4 shows the real and imaginary part of the anisotropic DF as determined from the fit. $\varepsilon_{\perp}$ exhibits the E1(TO)-phonon at 554 cm^{-1}, whereas in $\varepsilon_{\parallel}$ the A1(TO)-phonon is detected at 545 cm^{-1}. The associated LO-phonons are observed at 739 cm^{-1} and 735 cm^{-1}. The obtained values are in fair agreement with values published by Kasic et al. [3]. It should be noticed, that the sensitivity of IRSE for the extraordinary DF is very low for c-plane material. For a more detailed analysis more samples with different carrier concentration and substrate material have to be investigated.

In summary, the ability of IRSE has been demonstrated to determine the anisotropic dielectric function of GaN on sapphire. For SiC films on Si(111) IRSE has been proven to be very helpful for the better understanding and the optimisation of the growth process to reduce the internal strain and to obtain layer with improved structural qualities.

[1] G. Ferro et al., Thin Solid Films 278, 22, (1996).
[2] P. Masri et al., Comp. Mater. Sci. 17, 544 (2000).
[3] A. Kasic et al., Phys. Rev. B 62, 7365 (2000).

Structural investigations of cubic InN

V. Cimalla[1,*], U. Kaiser[1], J. Pezoldt[1], L. Spieß[2], G. Teichert[2], O. Ambacher[1], H. Lu[3], and W. J. Schaff[3]
Departments of Nanotechnology[1], Materials for Electronics[2]
[3] Cornell University, Ithaca, USA

Cubic group III nitride binary compounds (such as InN, GaN and AlN) have attracted significant interest due to the absence of electric fields caused by spontaneous polarization present in hexagonal crystals. However, cubic 3C polytypes show thermodynamical metastability for the majority of the nitrides grown by conventional deposition methods. Consequently, the hexagonal 2H polytype is usually grown in the case of the well established epitaxial techniques of group-III nitrides on substrates like sapphire, hexagonal SiC or silicon (111). The breaking of the hexagonal surface symmetry, which is present in the former mentioned substrates, has shown to be the most successful attempt to grow cubic group-III nitrides. Typically, that has be done using cubic (001) substrates, for example (001)SiC on Si for cubic GaN [3] or (001)InAs on GaAs for cubic InN [4]. In this study we investigate the possibilities to stabilize the cubic phase of InN on a non cubic substrate by selection of a proper crystal surface.

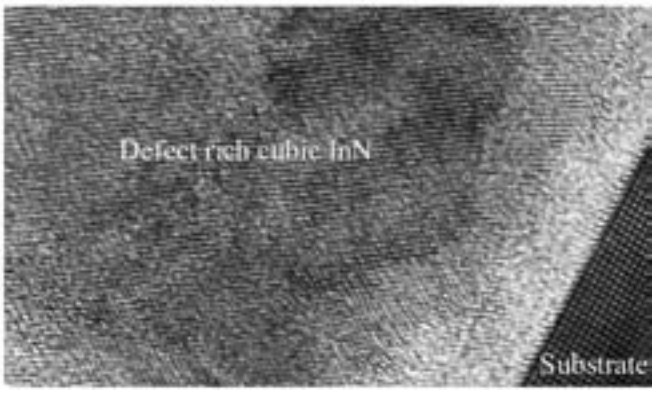

Fig. 1: TEM image of the InN layer.

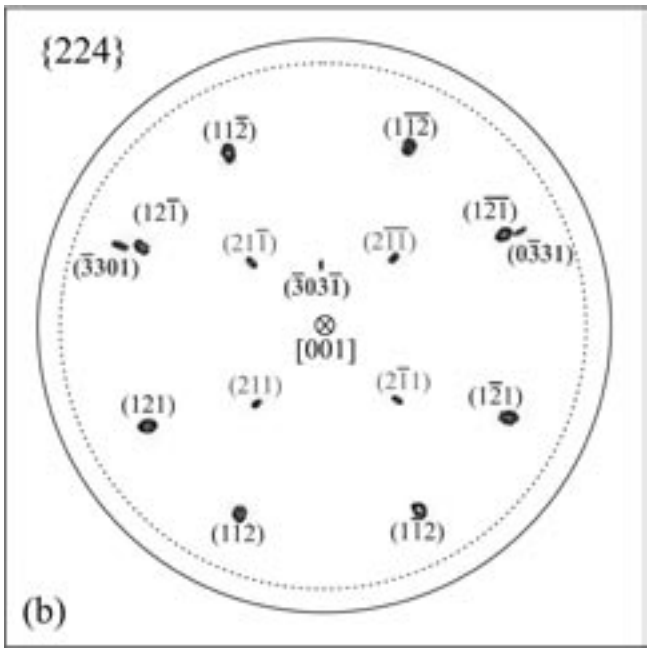

Fig. 2: Pole figures at 98.54° in the range $0° \leq \chi \leq 85°$

Up to date zinc blende InN was solely grown on a substrate with cubic crystal structure. Here we demonstrate the growth of zinc blende InN directly on a non cubic substrate – on r-plane sapphire without the use of additional buffer layers. The InN layers were grown by a Varian GEN-II gas-source molecular beam epitaxy system [5] on 3-inch $(01\bar{1}2)$ sapphire (r-plane) wafers. X-ray diffraction (XRD) and Auger electron spectroscopy validated the formation of an InN layer [6]. The structure on the sample surface was controlled by reflection high-energy electron diffraction, where in addition to a definite cubic structure spots of the hexagonal phase appeared. Interestingly, these pattern appear only in one of the four possible <111> directions of the crystal indicating a strongly preferred oriented growth of the hexagonal phase out of one of the {111} planes. Moreover, no twins were observed in the cubic InN layers. In contrast, transmission electron microscopy (TEM) revealed a high number of defects (Fig.1). The major phase was proven to be cubic, however, hexagonal inclusions with different orientations could be observed as well. To determine the exact orientation relationship and the content of the hexagonal phase XRD investigations

* fon: +49-(0)3677-69-3408, e-mail: volker.cimalla@tu-ilmenau.de

were performed. The θ-2θ scans confirmed the formation of the cubic phase of InN and the lattice constant was determined to be 4.986 Å in good agreement with the previously estimated value of a = 4.98 Å for epitaxial InN grown on InAs(001)/ GaAs substrates [4]. The pole figures of the cubic (002), cubic (224), hexagonal (0001) and hexagonal ($10\bar{1}1$) planes were measured without changing the experimental configuration. The appearance of only one (002) pole proves the practical absence of twins in the grown layer. The (224) diffractions (Fig.2) appear with a four fold symmetry as expected for a cubic crystal. The inner ring of four diffractions represents the four {224} planes at θ = 35.5 ± 0.8° (theoretical: 35.26°), and the outer ring of eight diffractions the four {422} and four {242} planes at θ = 69.5 ± 1.9° (theoretical: 69.91°). Again, no indication of twinning was found. However, additional diffraction peaks appeared in the (224) pole figure that could be assigned to the wurtzite InN phase. The orientation and the content of the wurtzite phase was validated by a set of θ-2θ scans and rocking curves around the (0002)InN diffraction peak in dependence on the substrate orientation. These measurements confirmed a highly oriented hexagonal phase parallel to just one (111) plane of the zinc blende InN and a high content of the 2H phase up to 30% close to the surface of the InN layer and a decreasing content towards the InN/sapphire interface. Thus, we conclude that initially the zincblende InN is grown on the sapphire surface and the wurtzite phase appears as a defect during the proceeding growth.

Based in these results we propose the following epitaxial relationship for the direct growth of cubic InN on sapphire: $(001)_{c\text{-InN}} \| (01\bar{1}2)_{Al_2O_3}$ and $[010]_{c\text{-InN}} \| [2\bar{1}\bar{1}0]_{Al_2O_3}$. The lattice mismatch between InN is different for the two orientations: 5% in $[2\bar{1}\bar{1}0]_{Al_2O_3}$, and just 2.5% in the $[0\bar{1}10]_{Al_2O_3}$ direction, assuming the formation of a coincidence lattice 3:1. The proposed relationship is shown in Fig.3. In conclusion, the metastable, cubic phase of InN has been grown for the first time on a non cubic substrate, on r-plane sapphire. An epitaxial relationship was proposed where this unusual behavior is stimulated by the reduced lattice mismatch between $(01\bar{1}2)$ sapphire and zinc blende (001)InN compared to the growth of wurtzite InN. However, to grow a single crystalline InN in the metastable cubic modification the deposition conditions have to be controlled more carefully to avoid the creation of hexagonal nucleation centres.

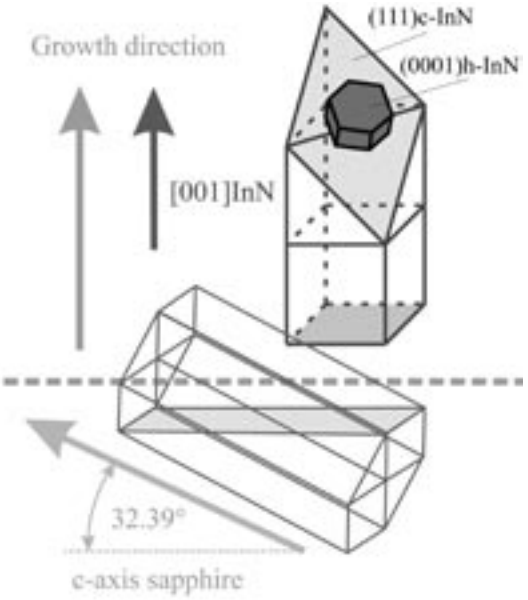

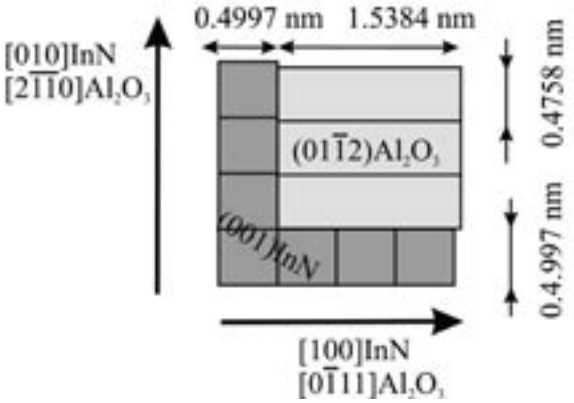

Fig. 3: Proposed epitaxial relationship between the sapphire substrate, the 3C-, and 2H-InN.

[1] T. L. Tansley and C. P. Foley, J. Appl. Phys. 59, 3241 (1986).
[2] C. Förster, TU Ilmenau, unpublished results.
[3] D.J. As, T. Frey, D. Schikora, K. Lischka, V. Cimalla, J. Pezoldt, R. Goldhahn, S. Kaiser, and W. Gebhardt; Appl. Phys. Lett. 76, 1686 (2000).
[4] A.P. Lima, A. Tabata, J.R. Leite, S. Kaiser, D. Schikora, B. Schöttker, T. Frey, D.J. As, and K. Lischka, J. Cryst. Growth 201/202, 396 (1999).
[5] J. Lu, W.J. Schaff, J. Hwang, H. Wu, W. Yeo, A. Pharkya, and L.F. Eastman, Appl. Phys. Lett. 77, 2548 (2000).
[6] V. Cimalla, J. Pezoldt, G. Ecke, R. Kosiba, O. Ambacher, L. Spieß, G. Teichert, H. Lu, and W. J. Schaff; Appl. Phys. Lett. 83, 3468 (2003).

Determination of dopands and polytypes of SiC by Auger Electron Spectroscopy

G. Ecke*, R. Kosiba, P. Weih, and J. Pezoldt
Department of Nanotechnology

It is known from theory that the spectroscopy of the kinetic energy of Auger electrons provides information about the Fermi energy of a semiconductor with respect to the vacuum level. Therefore it should be possible to see differences in doping or in the polytypes of SiC. However, only a few publications on the distinction of p- and n-type silicon by AES can be found in literature [1, 2] even though the Thermo VGScientific company advertises in their offers with this possibility. They present a Si related Auger peak position difference of 0.6 eV between n- and p-type silicon after sputtering by Ar^+ ions.

We tried to distinct between n- and p-type conduction and different polytypes of silicon carbide by Auger electron spectroscopy. Accompanied by a change in doping and conduction is a variation of the Fermi level. As a consequence of a change of SiC polytype the band gap is varied by up to 600 meV. Doping as well as band gap variation should effect the difference in energy between the Fermi and the vacuum level. Nitrogen donators create two different energetic states in 6H-SiC, which are 100 and 155 meV below the conduction band edge, respectively. Aluminium acceptors create two states of 239 and 249 meV above the valence band,

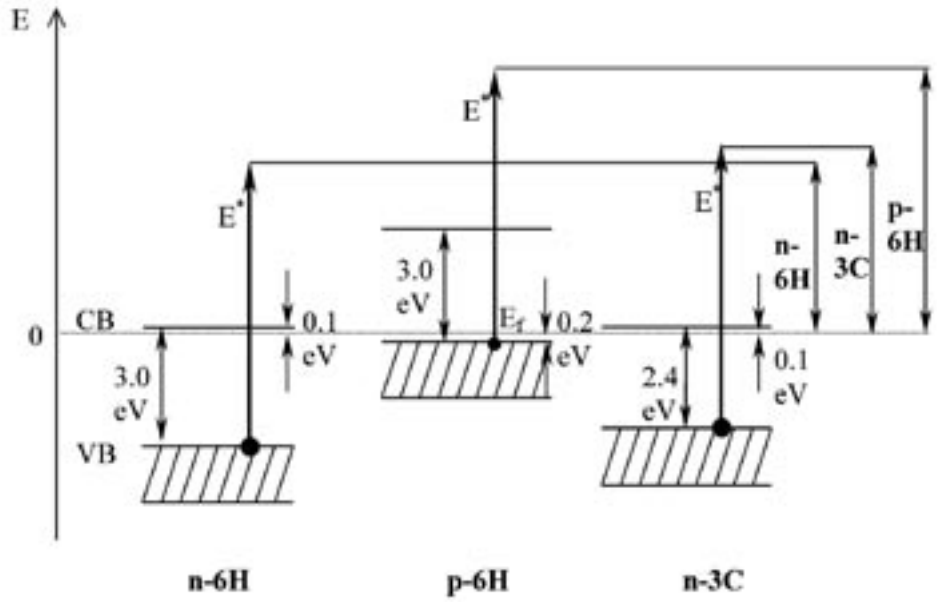

Fig. 1: Scheme of an Auger electron emission with the energy E^* from the valence band of n-6H-, p-6H- and n-3C Silicon carbide; Energy differences are valid for all other emitting levels.

respectively [3]. Cubic 3C-SiC is always n-type conducting because of intrinsic defects. At T = 0 K the position of the Fermi level is centred between the states of the dopands and the band edge. Furthermore the position of the Fermi level depends on the concentration of dopands in the semiconductor. In the following we assume the Fermi level to be 0.1 eV below the conduction band in n-type and 0.2 eV above the valence band in p-type SiC. Whereas the band gap of 6H-SiC is 3.0 eV, 3C-SiC has a band gap of 2.4 eV, respectively. Fig.1 shows the band diagram of n-type and p-type 6H-SiC as wellas of 3C-SiC.

With these values we should measure the following Si and C related Auger peak positions:

1) n-type 6H-SiC should have the lowest Auger peak energies,
2) shifted by 0.6 eV towards higher peak energy n-type 3C-SiC should follow,

* fon: +49-(0)3677-69-3407, email: gernot.ecke@tu-ilmenau.de

3) p-6H-SiC should have the highest peak energy (about 2.7 eV higher in comparison to n-type 6H-SiC).

Up to now we have discussed the Auger electron emission of as grown, not destructed single crystalline SiC. But during surface analysis and depth profiling one has to apply ion beam sputtering in order to remove adsorption layers, which cover the SiC surface and influence the Auger peak positions and shapes by creation of chemical bonds. After sputtering, the crystalline structure is damaged and partially amorphous. The degree of surface destruction, i.e. the number of electron traps generated is independent on the conduction type or polytype. The influence of the dopands is now negligible, because their concentration is much smaller than those of the ion induced defects. But if all these electron traps are filled with electrons by the electron beam, the resulting charging should be independent on the conduction type and polytype, as well. As a consequence, the band bending at the solid surfaces should be the same for n- and p-type 6H as well as for 3C-SiC and the relative peak shifts can be the same as expected for a not sputtered single crystals.

For the measurements we selected (i) a n-type 6H-SiC wafer, (ii) an Al doped p-type homoepitaxial 6H-SiC layer and (iii) a 3C-SiC heteroepitaxial layer grown on Si substrate. The carrier densities were determined to be about 3×10^{18} cm^{-3}. All these samples have been measured by AES using a cylindrical mirror analyser of an energy resolution of 0.3%. Sputter cleaning has been carried out with Ar^+ ions with an energy of 0.4 and 2 keV under 80° glancing incidence. The

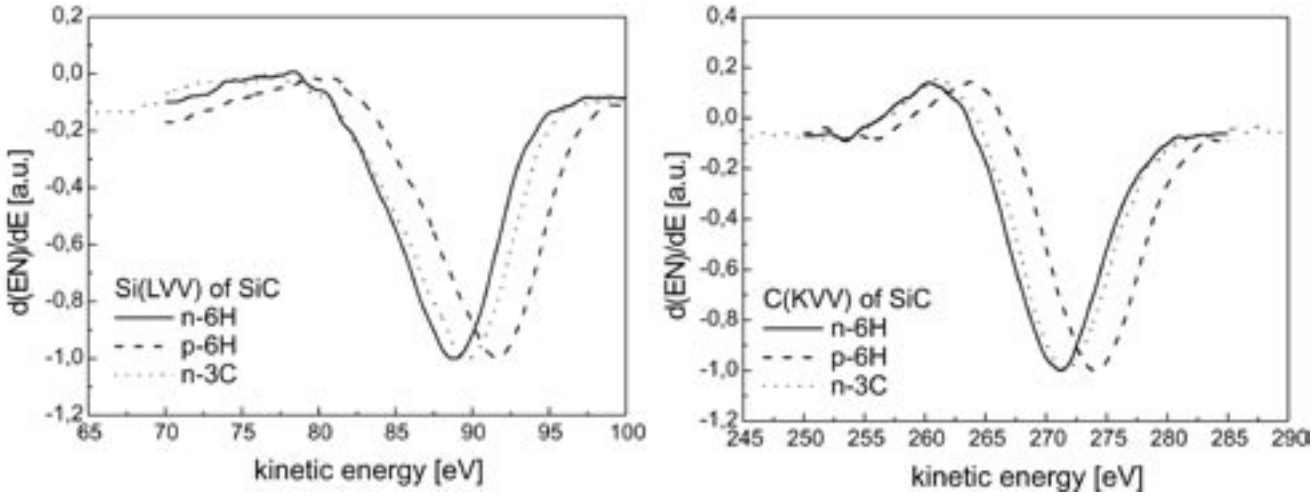

Fig. 2: Normalized (a) Si(LVV)- und (b) C(KVV)-Auger spectra of n-type , p-type 6H-SiC and n-type 3C-SiC single crystals after sputtering by 2 keV Ar^+ under 80°.

Si(KLL), Si(LVV), C(KVV) and the O(KLL) Auger peaks have been recorded. Measurements have shown, that differences in the peak position between n- and p-type 6H-SiC are not heavily influenced by the sputtering energy. Only the Si(LVV) peak shows a slight deviation between the 2 keV sputtered SiC samples compared to those sputtered with 0.4 kV. Thus we can conclude, in agreement with Ref. [1, 2], that doping of semiconductors can be distinguished by AES even for sputtered surfaces. Results for all three SiC types (n- and p-type 6H-SiC and n-type 3C-SiC), sputtered by Ar^+ ions of 2 keV under 80° the Auger peaks of the Si(LVV) and the C(KLL) are shown in Fig. 2.

In case of Si(LVV) and C(KLL) Auger transitions we found peak positions differences for n- and p-type 6H-SiC as well as for 3C-SiC like expected (Fig.1) within the accuracy of the spectrometer. For the Si(KLL) Auger transition the absolute energy resolution of our spectrometer and the analyser voltage stability is unsufficient, so that the accuracy of the measured variation in peak position are slightly smaller.

In conclusion we have proven, that Auger electron spectroscopy is able to distinguish between different kinds of doping as well as polytypes of SiC, even if the surfaces are cleaned by ion beam induced sputtering. As a consequence AES is a helpful tool to analyse vertical SiC polytype heterostructures and to identify doped regions in SiC devices with lateral design.

The authors would like to acknowledge a financial support by the TMWFK (B 607 02006)

[1] M.G. Vasilyev, D.V. Klyachko, V.G. Krigel, I.V. Razumovskaya, Poverchnost' N1 (1985) 97.
[2] V.G. Kesler, L.M. Logvinsky, I.P. Petrenko, K.K. Svitashev, Proc. of the 6th European Conference on Applications of Surface and Interface Analysis, H.J. Mathieu, B. Reihl, D. Briggs (Ed.) p. 288
[3] G.L. Harris, Ed., Properties of Silicon Carbide, INSPEC, London (1995), p. 88.

Organic field effect transistors: the molecule-metal interface

M. Eremtchenko[1], F.S. Tautz[2], and J.A. Schaefer[1,*]
[1] Department of Technical Physics,
[2] School of Engineering and Science, International University Bremen

Since the discovery of organic semiconductors, the development of electronic devices based on these materials attracts high interest. Organic electronic devices promise a number of new applications; they should be cheaper, flexible, and multifunctional. For technological applications, the performance of these devices is crucially dependent on the molecular structural order, which is defined on specific properties of the molecule-substrate interface. Therefore, fundamental studies of the interfaces between the organic molecules and oxide as well as metal surfaces are key issues related to the needs of modern technology.

The3,4,9,10-perylene-tetracarboxylicacid-dianhydride (PTCDA) is a kind of a model object for molecular growth studies. It is well known, that the molecules form a commensurate epitaxial monolayer on Ag(111) in the so called herringbone structure (Fig.1).

The ordering of these large organics (every molecule covers about fifteen unit cells of the substrate) is a result of a complicated molecule-molecule and molecule-substrate interaction. PTCDA has an intrinsic quadrupole moment which obviously produces an attraction between the middle part of the molecule and the oxygen atoms at the ends of neighbouring molecules (see Fig.1), leading to the observed herringbone structure by an electrostatic interaction. However, the commensurability between molecular and substrate order does not follow from the trivial analysis.

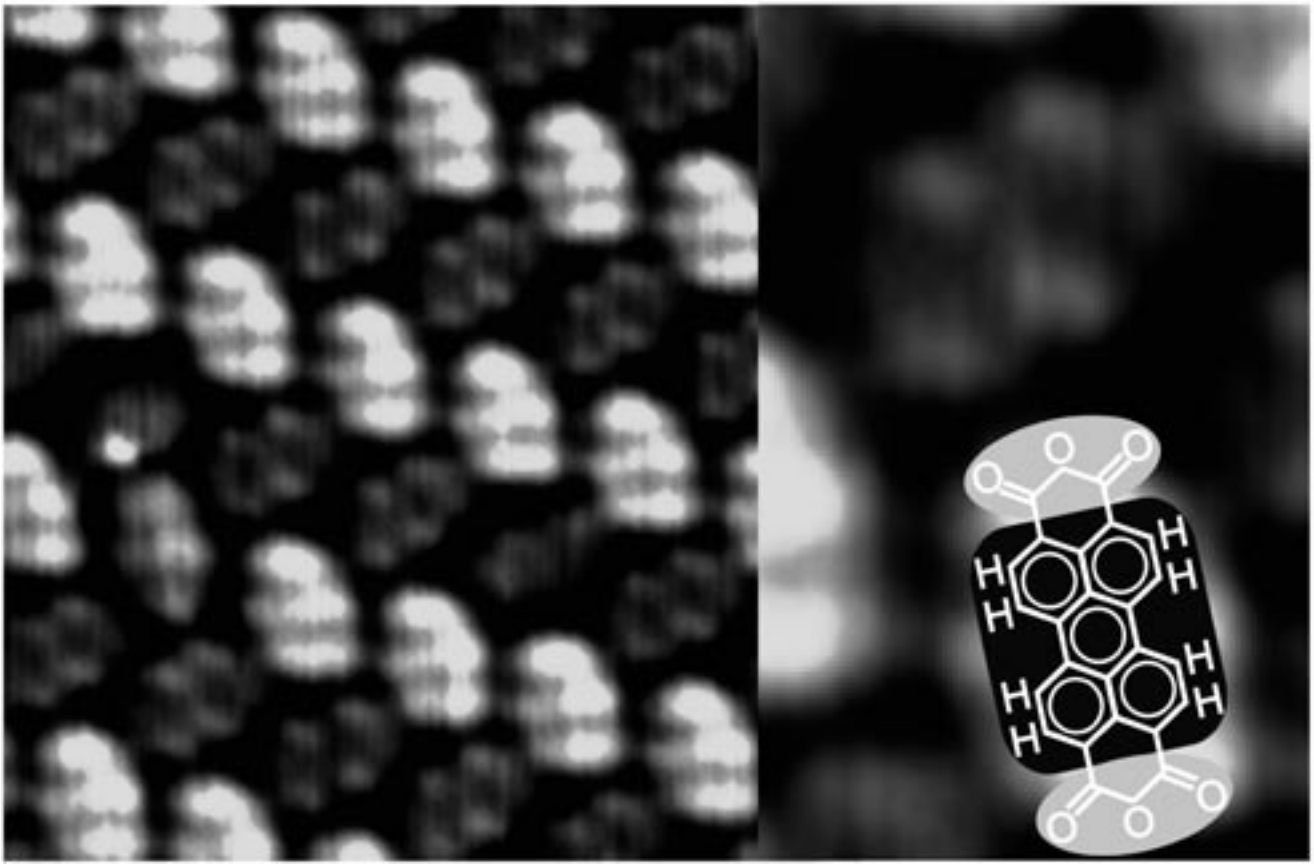

Fig. 1: "Organic epitaxy of PTCDA on the Ag(111) surface" Main image: STM image of PTCDA 'herringbone' layer on Ag(111), image area 7x7 nm^2 (tunnelling parameters: I=0.46nA, U=-2.3V). Right: chemical structure of PTCDA with schematic indication of intramolecular charge distribution (black=positive, grey=negative partial charges).

* fon: +49-(0)3677-69-3608, email: juergen.schaefer@tu-ilmenau.de

The formation of a commensurable layer is only possible if the interaction between PTCDA and the substrate is comparatively strong, otherwise, this interaction should not restrict the mobility of the molecules for the ordering. A fixation of PTCDA to the Ag(111) by some active centre, which allows almost free rotation of adsorbed molecules around the centre would explain the observed structure. However, the existence of only a single adsorption site for such a big molecule was unlikely.
Following our previous spectroscopic studies of PTCDA layers, the analysis of registered spectral features, so called Fano resonances (grey peaks in Fig.2a), in the PTCDA/Ag(111) spectra shed light to

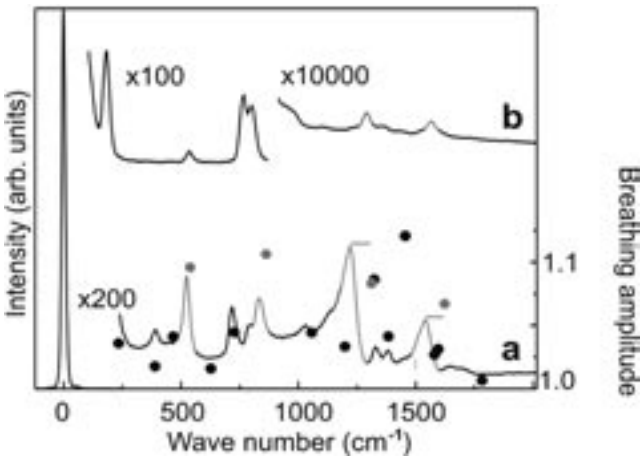

Fig. 2: "Spectroscopic signature of epitaxial site recognition". High resolution electron energy loss spectra (HREELS) for: a 0.3 monolayers PTCDA/Ag(111). Circles indicate the normalised breathing amplitude of the central carbon ring in PTCDA as calculated from density functional theory of the free molecule. Gray circles: Modes for which both the breathing amplitude is large and the charge modulation in the central ring is uncompensated. Black circles: remaining modes. b Perylene on Ag(111) also shows a slight activation of two Raman modes (grey peaks). Shown is a spectrum for a nominal coverage of a few monolayers. Additional data unambiguously prove that the gray peaks derive from molecules in the first layer.

molecule-substrate interaction. It was shown, that an interfacial dynamical charge transfer takes place in the system and one can interpret the interaction between the molecule and a metal substrate as a kind of electron doping. It was shown, that two totally symmetric Raman vibrational modes are strongly coupled to the substrate and the coupling produces the dipole activity of these modes [1].

The further analysis involves a combination of spectroscopic data, microscopy and quantum chemical calculations. It was found, that four totally symmetric modes related to the breathing of the central carbon ring are coupled to the substrate, while all others are not (see Fig.2a, note here, that two modes with high breathing amplitude of the central ring are not enhanced due to symmetry of the molecule). This observation indicates that only the central ring is strongly bonded to the substrate and it is an adsorption centre of PTCDA [2].
The model was proved by a study of an adsorption of perylene $C_{20}H_{12}$ which is the backbone of PTCDA and has the same configuration of carbon atoms. Similar analysis shows, that the molecule is also bonded to Ag(111) by the central ring, but the interaction strength is about 300 times weaker, as follows from spectroscopic peak intensities (see Fig. 2). The molecule-substrate interaction was probed by STM. Nevertheless we could not get any images of the perylene molecules, the substrate structure was resolved through perylene. Surprisingly, the corrugation depth between Ag atoms in this case is about 10 times bigger than for the clean substrate. The observation can be explained by molecular jumping between adsorption sites induced by the STM tip. The properties of perylene demonstrate the influence of carboxyl groups to the activity of the central carbon ring.
Our research related to molecular-metal interfaces allows to understand the interaction at an intramolecular scale and the influence of some parts or chemical groups to the bonding character. The analysis opens an opportunity for the engineering of the molecular interfaces [3]. It is shown how the bonding can be modified by changing the chemical composition and the role of derivatives in the processes.

1. F.S.Tautz, M.Eremtchenko, J.A.Schaefer, M.Sokolowski, V.Shklower, and E.Umbach, Physical Review B 65 (2002), p. 125405.
2. M. Eremtchenko, D. Bauer, J.A. Schaefer, and F.S. Tautz, New Journal of Physics, 6 (2004), 4.
3. M. Eremtchenko, J.A. Schaefer, and F.S. Tautz, Nature, 425 (2003), p.602.

Defect related absorption and emission of AlGaN based UV photodetectors

V. Lebedev*, I. Cimalla, R. Wagner, G. Ecke, V. Cimalla, U. Kaiser, and O. Ambacher
Department of Nanotechnology

The unique intrinsic properties and remarkable progress in the epitaxial growth of high-quality GaN films have given rise to successful commercialisation of group III nitride based optoelectronic devices. In particular, a large variation in the band gap energies and the ability to form heterojunctions have made $Al_xGa_{1-x}N$ alloys the most adequate and flexible solution for UV light detection. Despite of the rapid development in the growth techniques, the major problem of AlGaN layers is the presence of defects in large quantities, which are generated during the heteroepitaxy and post-epitaxial treatment. The detailed knowledge of the defect structure is highly desirable for improvements of AlGaN based devices. In this work, a combination of room temperature in-situ cathodoluminescence (CL), photocurrent spectroscopy (SPC) and spectral ellipsometry (SE) have been applied to study defect-related absorption and emission in AlGaN-based photodetectors designed for a high responsivity in a narrow spectral range (240-300 nm, λ_{peak} = 280 nm). Nominally undoped epitaxial $Al_xGa_{1-x}N$ heterostructures were grown on c-Al_2O_3 substrates by molecular beam epitaxy. Firstly, an $Al_{0.67}Ga_{0.33}N$ optical filter layer (E_g ~ 4.8 eV, d ~ 0.2 µm) has been grown on sapphire coated with an AlN nucleation layer (d ~ 40 nm). This layer is absorbing photons with energies above 4.8 eV and acts as a high photon energy filter. An AlN epilayer (d ~ 100nm) was grown as an insulating barrier (E_g = 6.2 eV) on top. Finally, a 0.3 µm thick $Al_{0.48}Ga_{0.52}N$ capping layer (E_g ~ 4.4eV) has been grown acting as UV photoconductor collecting photons with energies in the range of 4.4 to 4.8 eV. UV-detectors based on Si(111) substrates have been deposited at similar growth conditions and consisted of the buffer and detector layers without the integrated filter. Surface-related silicon has been detected by AES, while the residual Si doping was measured in the bulk by SIMS. The detector devices were processed by a conventional photolithography. Samples with Ti/Al (20/80 nm) finger contacts with a contact spacing ranging from 200 to 400 µm have been used for electronic measurement. In Fig.1(a, b) the CL, SPC and SE curves measured on UV-detectors are presented. Despite of the UV/visible contrast of more than four orders of magnitude, the obvious responsivity has been observed in the SPC spectra well below the band gap (< 4 eV). The low-energy SPC absorption is dominant by a broad photoionization shoulder with an onset of ~ 2.5 eV usually attributed to the transitions from various deep defect states to the levels above the mobility edge of the conduction band (Fig.1a, zone II) as well as a resonant SPC peak at ~ 2.25 eV (Fig.1a, zone I). The latter peak correlates well with the CL peak at the same energy position. It is usually associated with transitions from a shallow donor (SD) to a very deep acceptor (DA). Due to its resonance nature, the SPC peak centred at 2.25 eV cannot be attributed to the direct photoionization. It contributes to the SPC by means of the internal optical excitation between a mid-gap state and a localized SD state with E_A ~ kT at 300 K followed by the thermal ionisation. An acceptor character at least of some of the very

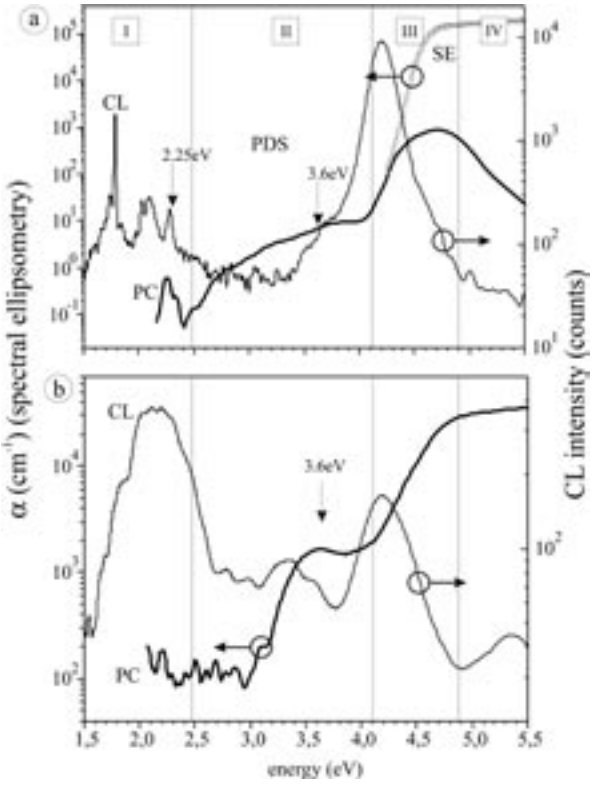

Fig. 1: Room temperature SPC (thick line) and in-situ CL spectra of (a) the detector structure grown on sapphire, and (b) the detector layer grown on Si(111). The curve marked by open triangles represent the absorption coefficient α given by spectral ellipsometry.

* fon: +49-(0)3677-69-3410, email: vadim.lebedev@tu-ilmenau.de

deep levels (V_{Ga}, carbon) has been predicted. Because the acceptor levels in n-type nitrides have been never experimentally observed, we can relate this resonance peak to DA transitions with E_A ~ 2.2 eV. The effective value of the activation energy for the shallow level is E_A = 86 ± 5 meV. Dominant donors in intentionally undoped III-nitrides are Si and O. Oxygen is a dominant impurity in the undoped $Al_xGa_{1-x}N$ epilayers. Theoretical calculations predict that oxygen can occupy a substitutional nitrogen site O_N forming a localized shallow donor state (E_A ~ 14 meV for x ~ 0.4). In the AlGaN/AlN/Si heterostructures, unintentional silicon doping is of great importance due to the strong silicon out-diffusion and channelling via the grain boundaries between AlN domains. Si also creates a SD level corresponding to the Si localized state with a DX-center behaviour with E_A ~ 30 meV for x ~ 0.5. Taking into account the spreading of the localized states due to the potential fluctuations and alloy effects, we conclude that both states (O_N and Si^{DX}) can contribute to the resonance SPC peaks at 300 K.

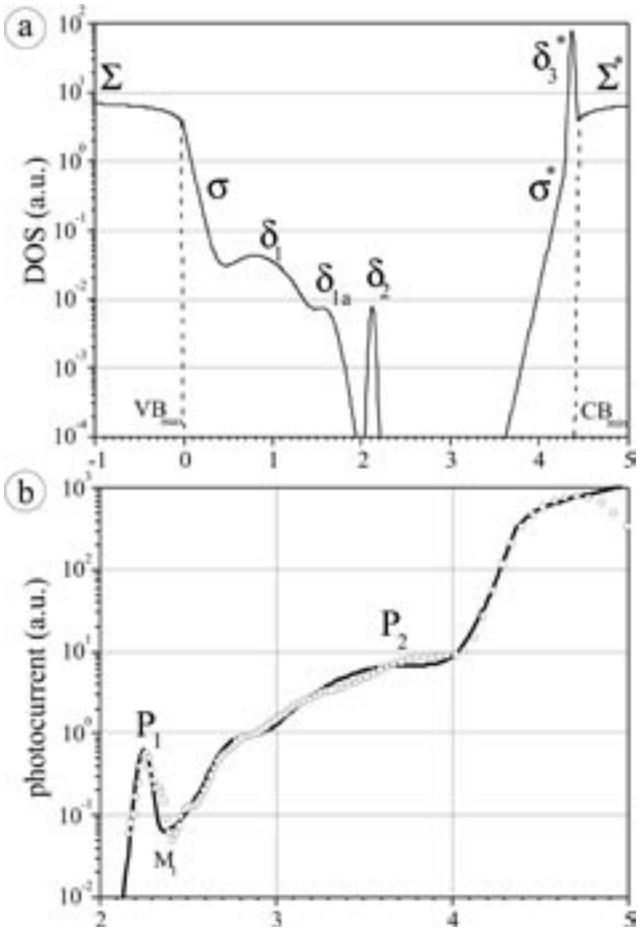

Fig. 2: (a) Proposed non-equilibrium DOS model for AlGaN. Empty states are indicated by (*). (b) SPC absorption fit for the layer grown on sapphire, (open circles: SPC experiment, solid line: simulation).

A broad SPC shoulder with an onset of ~2.5eV (Fig.1a, zone II) can be described as a photoionization process from the impurity related deep levels either onto SD level or into the CB. Due to the large activation energies and residual n-type conductivity of the epilayers, it can be attributed to the wide DA band. SPC spectra of high quality samples grown on sapphire do not show any remarkable features in this spectral region (Fig.1a) except an unpronounced shoulder with an onset of ~3.5 eV. On the other hand, SPC and CL spectra measured on the AlGaN/AlN/Si structures reveal that the second resonance peak centred at the same position (~3.6eV) dominates the subband absorption and emission (Fig.1b). The resonance nature of the absorption peak is also obvious, similar to the absorption peak at 2.25 eV assuming the existence of at least two localized states: already mentioned SD (Si^{DX} or O_N) and DA with a hole activation energy of ~0.8 eV. It was also predicted that carbon incorporated substitutional on the nitrogen site gives rise to an acceptor in GaN and AlN. In the latter case, C_N becomes a deep acceptor introducing the localized energy level at ~0.9 eV above the valence band. These predictions are in a good agreement with our spectral and AES observations allowing to consider C_N related states participating in the absorption shoulder (onset of ~3.5eV, Fig.1a, zone II). The AlGaN sub-band absorption and emission are extremely difficult for interpretation due to the large number of the bands involved in the SPC and CL transitions. However, at least a qualitative density of states (DOS) model can be derived from our SPC measurements based on the positions of the resonance features observed (see Fig. 2). The simulation shows very good fit to the experimental data.

Thermal stability of polycrystalline and epitaxial Indium Nitride layers

R. Wagner[1,*], V. Cimalla[1], H. Romanus[2], H. Lu[3], W. Schaff[3], and O. Ambacher[1]
Departments of Nanotechnology[1], Materials for Electronics[2]
[3] Cornell University, Ithaca, USA

Recently the group III-nitride compound Indium Nitride received an increased interest mainly forced by the development of light emitting and laser diodes basing on alloys of GaN and InN. The main difficulties to prepare In-rich InGaN compounds arose from the low sublimation temperature of InN and the resulting decomposition and phase separation effects. In case of pure InN, only polycrystalline material was obtained by sputtering techniques and most of the physical properties of this compound were determined by those non-perfect layers. The improvement of the growth techniques resulted in the preparation of the first epitaxial thin layers of InN in the late ninetieth. It turned out, that a variety of the estimated material properties required a revision, the most striking was the estimation of a band gap energy as low as 0.7 eV for epitaxial InN instead of the tabulated value of 1.9 eV for polycrystalline InN [1]. A weighty part of the discussion about the reasons for these differences in band gap energy focused on the incorporation of oxygen into the polycrystalline material and metallic indium inclusions in the epitaxial layers. The origin of oxygen incorporation could be the diffusion into the layer along dislocations as well as contamination of the process gas an In target during the sputter process. On the other side, metallic indium inclusion could be formed due to the instability of InN resulting in nitrogen loss at elevated temperatures. Thus, the knowledge about the stability of the layers and the amount of incorporated oxygen are prevailing conditions for the preparation of InN and indium-rich InGaN alloys.

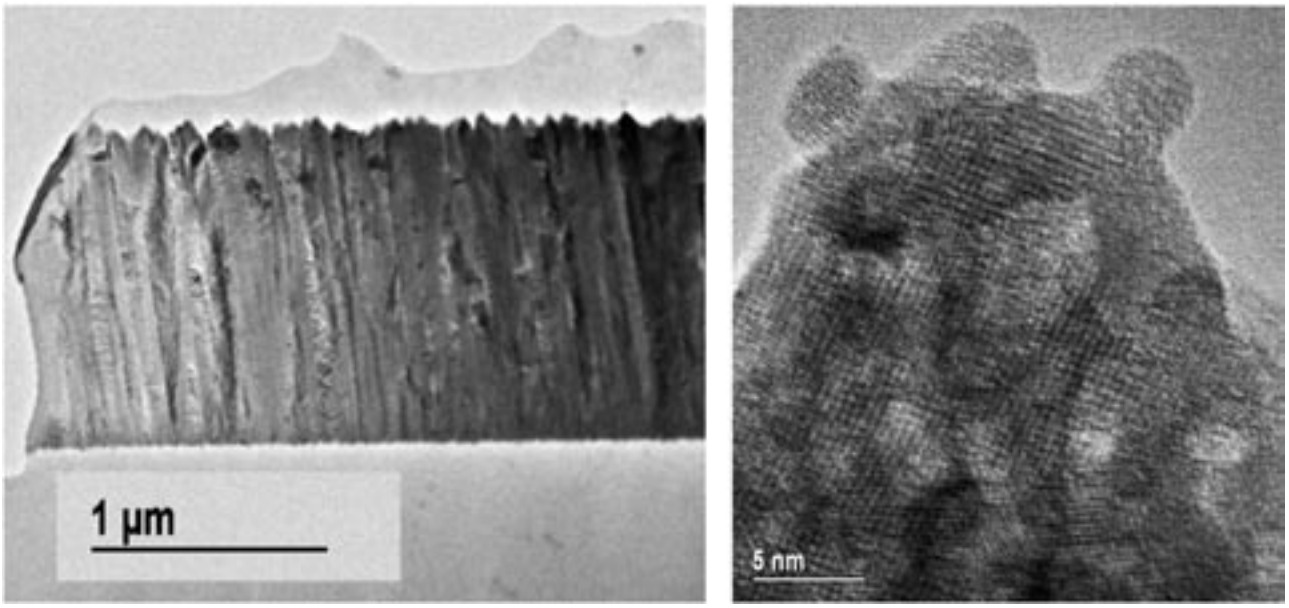

Fig. 1: Transmission electron microscopy images of a polycrystalline InN layer: (a) cross section along the layer, (b) cross section of a single column.

In this work we compare thin InN layers grown epitaxially on GaN layers and polycrystalline InN films deposited by reactive sputtering. All InN samples have wurtzite structure with the c-axis oriented normal to the surface. However, the lattice constant c is spreaded over a wide range between 5.69 Å and 5.77 Å indicating high differences in internal strain. A thick, relaxed, epitaxial InN layer with a low electron density of $8x10^{17}$ cm^{-3} is used as a reference. The polycrystalline layers have a columnar structure composed of nanocrystallites with a typical size of 5 nm, (Fig. 1). AES investigations have proved oxygen contaminations of up to 20 vol%, corresponding to a simple model, where

* fon: +49-(0)3677-69-3408, email: ronny.wagner@stud.tu-ilmenau.de

InN polycrystallites are oxidized only close to their surface. As a consequence, epitaxial InN layer show much lower oxygen contaminations due to the limited surface which is exposed to air.
The thermal stability of these two types of indium nitride layer were compared by thermal desorption spectroscopy (TDS). The set up contains three main components: the evaporation unit, a vacuum pump and a mass spectrometer. To study the thermal induced desorption behavior of nitrogen, the equipment was calibrated by a well known GaN sample with a definite volume [2]. The InN samples (typical size 5x5 mm², 1 µm thick) were loaded without any pre treatment into the evaporation chamber. The set-up was pumped down to a background pressure of < 10^{-7} mbar. The starting point for each experiment was room temperature. We choose a linear temperature ramp of 20 K per minute up to 1050°C in order to calculate the effective activation energy of nitrogen desorption.

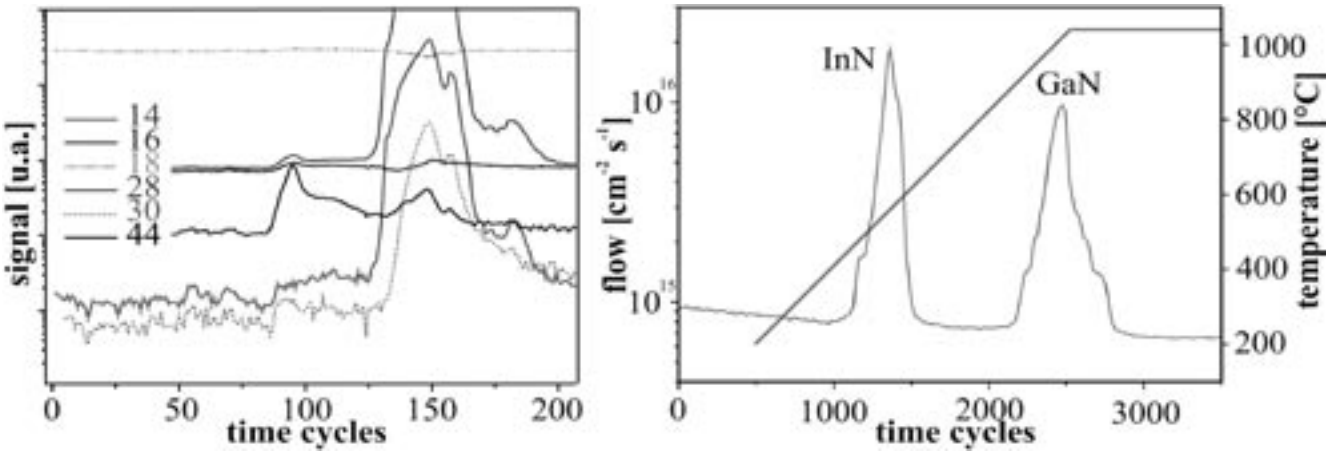

Fig. 2: TDS signals for an epitaxial InN layer grown on GaN:
(a) partial pressure of desorbed masses versus time,
(b) nitrogen flux from the surface in dependence on temperature.

The main atoms and molecules desorbed from the InN surface are H (1, 2 amu) N (14, 28 amu), H_2O (17, 18 amu) NO (30 amu) and CO_2 (44 amu) (Fig. 2a). On both types of InN no molecular oxygen (amu 32) and only traces of atomic oxygen (amu 16) were observed. But the measured partial pressure of NO indicates an oxidation of the InN and the formation of a non stoichiometric Indiumoxid or -oxynitride.

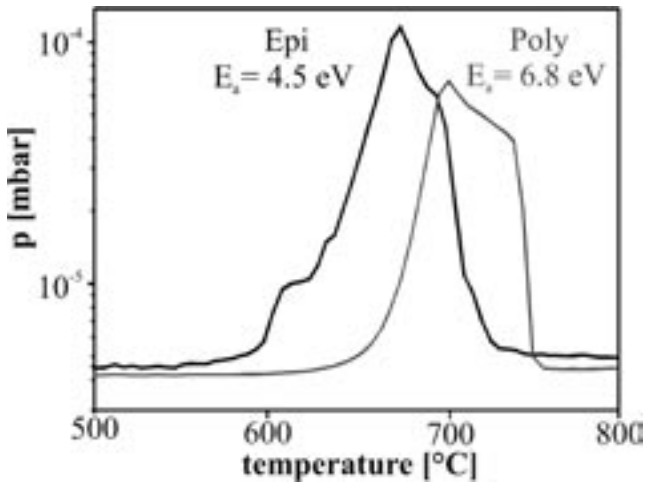

Fig. 3: Partial pressure of nitrogen which is desorbed from surfaces of epitaxial and polycrystalline InN.

Focussing on the thermal stability of InN, we analyzed the nitrogen flux from the surface as a measure of the decomposition temperature. The total flux of nitrogen, was determined by integration of the nitrogen signal over time and calibrated by the loss in InN layer thickness (Fig. 2b). We observe two clear desorption peaks corresponding to the InN and the more stable GaN beneath. The onset of the observed nirtrogen desorption is clearly shifted towards higher temperatures in the case of polycrystalline InN (Fig. 3) indicating a higher thermal stability. Moreover, a higher effective activation energy was estimated from an Arrhenius plot. Taking into account the higher stability of In_2O_3 and the observed NO_2 desorption we can conclude that the InN nanocrystals are sealed by a thin InO_x which is in agreement with the high oxygen concentration measured by AES.

[1] V. Yu. Davydov, A. Klochikhin, R.P. Seisyan et. al., phys. stat. sol. (b), 229, R1 (2002)
[2] O. Ambacher et. al.: J. Vac. Sci. Technol. B 14(6), 3535, (1996).

Plasma deposited fluorocarbon films as anti-wetting and structurable coatings for applications in nano- and picofluidic sensors

V. Yanev, M. Himmerlich, S. Krischok, and J.A. Schaefer*
Department of Technical Physics

For applications in nano- and picofluidic systems the protection of different sensor areas as well as the control of the wetting behaviour of surfaces is very important [1]. In this context, fluorocarbon (FC) thin films are attractive for surface passivation, patternable protective and anti-wetting coatings.
FC films were deposited in a conventional reactive ion etching system (Type STS 320 PC). The FC plasma polymerisation was performed on Si(111) using the process gas trifluoromethane (at 25 °C, pressure 130 mTorr, flow rate 25 sccm). Various power values (35 W, 80 W and 120 W) were used to determine their influence on the chemical composition of the deposited FC-films [2].

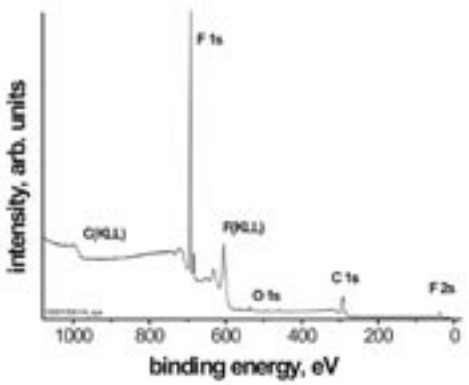

Fig. 1: XPS-survey spectrum of fluorocarbon films deposited at 35W on Si(111).

X-ray photoelectron spectroscopy (XPS) has been successfully employed to provide useful surface analyses including chemical composition and local binding properties of nearly every type of material. The examination of the C(1s) core-levels of FC-polymers allows to discriminate between
$-CF_3$, $-CF_2$, -CF, $-C-CF_x$ type bonds. For example, $-CF_2$ bonds (more than 90 %) are present in the chemical structure of conventional poly-tetrafluoroethylene (PTFE).

Each of the survey spectra shows mainly fluorine and carbon with trace amounts of oxygen (below 2.5 %). Figure 1 shows a typical survey spectrum obtained from fluorocarbon films deposited by plasma polymerisation. The observed oxygen originates from contaminations of the residual gases in the system as well as the brief air exposure during the sample transfer to the analytic modul.

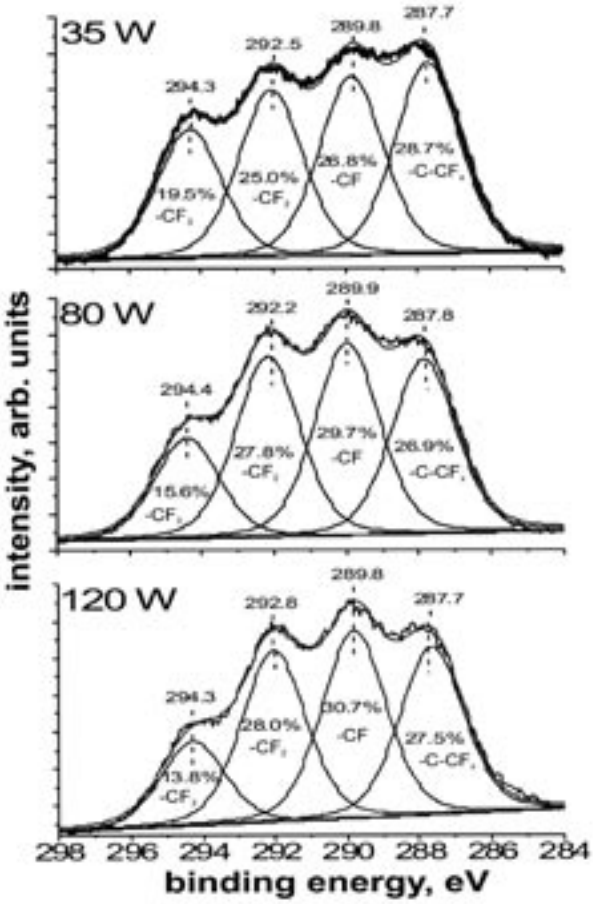

Fig. 2: C(1s) spectra of fluorocarbon films as a function of RF power.

* fon: +49-(0)3677-69-3608, email: juergen.schaefer@tu-ilmenau.de

Figure 2 shows the corresponding C(1s) spectra. The energy scale of all spectra was adjusted by setting the binding energy of the F(1s) peak to 689.0 eV [3]. Since all spectra were collected at relatively high pass energies (50 eV) and because of the fact that only trace amounts of oxygen were measured, no attempt was made to resolve any C-O bonds. All the C(1s) peaks are separated into 4 components ($-CF_3$, $-CF_2$, -CF, $-C-CF_x$). The percentage shown within each peak is the ratio of the peak area in percent with respect to the total C(1s) peak area (see fig. 2). Most evident is the fact that less $-CF_3$ type bonds are formed when films are grown using higher RF power. The amount of $-CF_3$ bonds has been associated with a strong hydrophobic behaviour of the surface [4]. Therefore, lower RF power is recommended if films with higher $-CF_3$ content are required. However, a disadvantage of low RF power during deposition is a reduction in growth rate.

Selective deposited FC coatings are useful in several microfluidic, chemical and biochemical applications [5, 6]. Therefore, the patterning of FC films is a very important task. Direct patterning of FC-films through photoresist masks is very difficult and often impossible due to the low free surface energy of the FC-polymers (the spin coated resist cannot adhere on the FC-surface). Therefore, the patterning process was optimized by varying spinning-speed and -time during spin coating using a conventional resist (AR351).

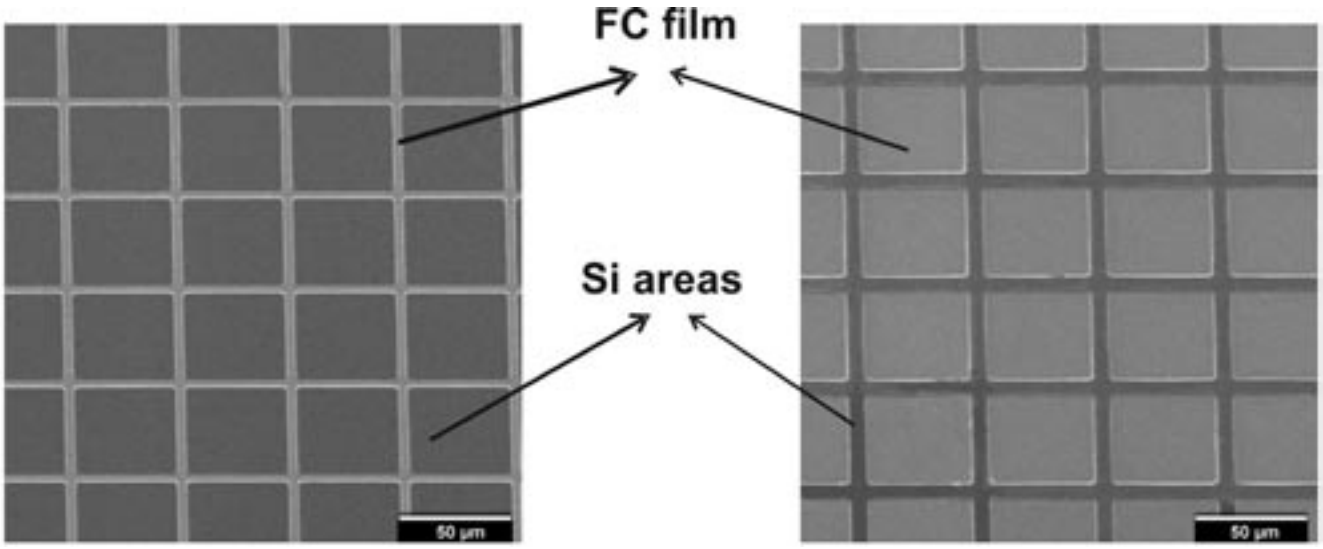

Fig. 3: SEM images of 250 nm thick, dry etched FC films

After all other lithographic steps (prebake, exposure, development) the samples were dry etched using an oxygen plasma in the same RIE-system. Figure 3 shows SEM images of FC films on Si(111) differently patterned (left: FC-squares; right: FC-stripes) using this technique. A resolution of 2 µm was obtained. Differences in the thickness uniformity of the deposited resists are below 5%. After resist stripping a significant increase of the surface energy was not observed.

[1] G. Mayer, A. Schober, J.M. Köhler: Nanotiterplates for combinatorial Chemistry, Reviews in Molecular Biotechnology 82 (2001) 137-159.
[2] V. Yanev, S. Krischok, A. Opitz, H. Wurmus, J.A. Schaefer, N. Schwesinger, S.I.U. Ahmed, Surf. Sci., accepted, (2004).
[3] G. Beamson and D. Briggs, High Resolution XPS of Organic Polymers – The Scienta ESCA300 Database, John Wiley & Sons, Chichester (1992).
[4] J.-H. Wang, J.-J. Chen, R.B. Timmons, Chem Mat. 8 (1996) 2212.
[5] M. McNeely, M. Spute, N. Tusneem, A. Oliphant, Hydrophobic Microfluidics, SPIE Microfluidic Devices & Systems II, Vol. 3877, Sept., (1999).
[6] W. Ehrfeld, V. Hessel, H. Löwe, Microreactors: new technology for modern chemistry, Wiley-VCH, Weinheim (2000).

Publications and Conference Contributions

Materials Science

Department of Metallic Materials and Composite Materials

Potenzialunterstützte Herstellung von Metall-Keramik-Verbundschichten
A. Knote, U. Schindler, H.-G. Krüger, and H. Kern, Materialwissenschaft und Werkstofftechnik 34 (2003) 608.

Nanokomposite für die Herstellung oxidischer Matrices keramischer Faserverbundwerkstoffe
C. Georgi, U. Schindler, H.-G. Krüger, and H. Kern, Materialwissenschaft und Werkstofftechnik 34 (2003) 623.

Transluzente oxidfaserverstärkte Glasmatrix-Verbundwerkstoffe
P. Fehling, D. Hülsenberg, D. Raab, T. Mache, V. Winkler, H. Kern, S. Stöckel, K. Weise, and G. Marx, Materialwissenschaft und Werkstofftechnik 34 (2003) 671.

The fabrication of coatings by means of electrophoretic deposition and galvanic methods
H.-G. Krüger, A. Knote, U. Schindler, H. Kern, and A. R. Boccaccini,
Electrochemical Society Proceedings 2002-21 (2003) 159.

Innovative Werkstoffkonzepte
H. Kern,
Materialwissenschaft und Werkstofftechnik 7 (2003).

Herstellung oxidischer faserverstärkter Verbund-werkstoffe durch elektrophoretische Infiltration
C. Georgi, H.-G. Krüger, and H Kern,
14. Symposium Verbundwerkstoffe und Werkstoff-verbunde der Deutschen Gesellschaft für Material-kunde (DGM), Wien (2003) Poster.

Oxide-oxide CMCs prepared by electrophoretic infiltration (EPI) of Nextel performs
C. Georgi, H.-G. Krüger, and H. Kern,
14th International Conference on Composite Materials (ICCM 14), San Diego, USA. (2003).

Department of Materials for Electronics

Simulation of layer sequence of Ni-Zn ferrite thin films and multilayers for EMC applications >1000 MHz
F. Gräbner, G. Teichert, Ch. Knedlik, S. Hildenbrand, H. Romanus, A. Hungsberg, and M. Koledintseva, Materialwissenschaft und Werkstofftechnik 34 (2003) 603.

Preparation of multiwalled carbon nanotubes by DC arc discharge under a nitrogen atmosphere
S. Cui, P. Scharff, C. Siegmund, L. Spieß, H. Romanus, J. Schawohl, K. Risch, D. Schneider, and S. Klötzer,
Carbon 41 (8) (2003) 1648.

Interface behaviour in nickel composite coatings with nano-particles of oxidic ceramic
F. Erler, C. Jakob, H. Romanus, L. Spieß, B. Wielage, T. Lampke, and S. Steinhäuser,
Electrochimica Acta 48 (20-22) (2003) 3063.

Growth of cubic InN on r-plane sapphire
V. Cimalla, J. Pezoldt, G. Ecke, R. Kosiba, O. Ambacher, L. Spieß, G. Teichert, H. Lu, and W.J. Schaff,
Appl. Phys. Lett. 83 (17) (2003) 3468.

Study of Annealed NiO Thin Films Sputtered on Unheated Substrate
I. Hotovy, J. Liday, L. Spiess, H. Sitter, and P. Vogrincic,
Jpn. J. Appl. Phys. 42 (10A) (2003) 1178.

The influence of the process parameters and an-neealing temperature on the physical properties of sputerred NiO thin films
I. Hotovy, J. Huran, L. Spiess, J. Liday, H. Sitter, and S. Hascik,
Vaccum 69 (2003) 237.

Nutzung von Werkstoffstrukturgrößen als Mess-normale
L. Spieß and Ch. Knedlik,
Materialwissenschaft und Werkstofftechnik 34 (2003) 648.

Tungsten Carbide layers for Nanomeasuring Systems
L. Spiess, M. Gubisch, H. Romanus, M. Breiter, Ch. Müller, V. Cimalla, G. Ecke, Y. Liu, and Ch. Knedlik,
MICRO.tec 2003, München (2003) Proceedings 165.

Investigation of preparation of carbon nanotubes by DC arc discharge under helium atmosphere
S. Cui, P. Scharff, C. Siegmund, L. Spieß, H. Romanus, J. Schawohl, K. Risch, D. Schneider, and S. Klötzer,
Carbon 2003, Oviedo, Spain (2003).

Technology

Department of Microsystems Technology

Magnetic micro components for micro reaction technology
B. Halbedel, A. Albrecht, Th. Frank et al.,
Materialwissenschaft und Werkstofftechnik 34 (2003) 677.

Magnetische Mikroaktuatoren
M. Kallenbach,
Elektormagete, E. Kallenbach, T. Ströhla, P. Quendt, R. Eick, M. Kallenbach, Teubner Verlag (2003).

Grenzen der Schnellwirkung von Antriebssystemen
M. Kallenbach et al.,
VDI-Berichte 1723 (2003).

Alternative Ansätze zur Herstellung hochstromtragfähiger Leiter in LTCC
A. Albrecht, J. Botiov, M. Fischer, K.-H. Drüe, M. Hintz, U. Schmidt, H. Thust, and H. Wurmus,
IMAPS-Deutschland, München (2003) Proceedings.

Alternative way to high current structures in LTCC
A. Albrecht, J. Botiov, M. Fischer, K.-H. Drüe, M. Hintz, and H. Wurmus,
Europ. Microelectron. Packaging Conf., Friedrichshafen (2003) Proceedings.

Alternative way to high current structures in ceramics
A. Albrecht, J. Botiov, M. Fischer, K.-H. Drüe, M. Hintz, and H. Wurmus,
Microsystems Technologies, München (2003) Proceedings.

Department of Nanotechnology

Growth of a-plane InN on r-plane sapphire with a GaN buffer by molecular beam epitaxy
H. Lu, W. J. Schaff, L. F. Eastman, J. Wu, W. Walukiewicz, V. Cimalla, and O. Ambacher,
Appl. Phys. Lett. 83 (2003) 1136.

Analysis of field effect devices bases on poly (3-octylthiophene)
S. Scheinert and W. Schliefke,
Synth. Met. 139 (2003) 501.

Photoreflectance studies of N- and Ga-face AlGaN/GaN heterostructures confining a polarisation induced 2DEG
A.T. Winzer, R. Goldhahn, C. Buchheim, O. Ambacher, A. Link, M. Stutzmann, Y. Smorchkova, U.K. Mishra, and J.S. Speck,
phys. stat. sol. (b) 240 (2003) 380.

Auger investigations of sputter induced altered layers in SiC by low energy sputter depth profiling and factor analysis
R. Kosiba, G. Ecke, J. Liday, J. Breza, and O. Ambacher,
Appl. Surf. Sci. 220 (2003) 304.

Sputtering of SiC with low energy He and Ar ions under grazing incidence
R. Kosiba, G. Ecke, O. Ambacher, and M. Menyhard,
Radiat. Eff. and Def. in Solids 158 (2003) 721.

Freestanding GaN-Substrates and Devices
C. R. Miskys, M. K. Kelly, O. Ambacher, and M. Stutzmann,
phys. stat. sol. (c) 0 (2003) 1627.

Electronics and Sensors Based on Pyroelectric AlGaN/GaN Heterostructures
Part A: Polarization and Pyroelectronics
O. Ambacher, M. Eickhoff, A. Link, M. Hermann, M. Stutzmann, F. Bernardini, V. Fiorentini, Y. Smorchkova, J. Speck, U. Mishra, W. Scharff, V. Tilak, and L. F. Eastman,
phys. stat. sol. (c) 0 (2003) 1878.
Part B: Sensor Applications
M. Eickhoff, J. Schalwig, O. Weidmann, L. Görgens, R. Neuberger, M. Hermann, G. Steinhoff, B. Baur, G. Müller, O. Ambacher, and M. Stutzmann,
phys. stat. sol. (c) 0 (2003) 1908.

Preparation of Epitaxial Templates for Molecular Beam Epitaxy of III-Nitrides on Silicon Substrates
V. Lebedev, J. Pezoldt, V. Cimalla, J. Jinschek, F. M. Morales, and O. Ambacher,
phys. Stat. Sol. (c) 1 (2003) 183.

Tight-Binding Simulation of an InGaN/GaN Quantum Well with Indium Concentration Fluctuation
J. Gleize, A. di Carlo, P. Lugli, J. M. Jancu, R. Scholz, O. Ambacher, D. Gerthsen, and E. Hahn,
phys. stat. sol. (c) 1 (2003) 302.

Theoretical Evaluation of the Interface Modification for Aluminium Nitride Growth on Si
P. Masri, V. Cimalla, J. Pezoldt, J. Camassel, B. Gil, and M. Averous,
phys. stat. sol. (c) 1 (2003) 355.

Two dimensional electron gas effects on the photoluminescence form a non intentionally doped AlGaN/GaN heterojunction
G. Martinez-Criado, A. Cros, A. Cantarero, U. Karrer, O. Ambacher, C. R. Miskys, and M. Stutzmann,
phys. stat. sol. (c) 1 (2003) 392.

Growth of cubic InN on r-plane sapphire
V. Cimalla, J. Pezoldt, G. Ecke, R. Kosiba, O. Ambacher, L. Spieß, G. Teichert, H. Lu, and W. Schaff,
Appl. Phys. Lett. 83 (2003) 3468.

Energy gap and optical properties of $In_xGa_{1-x}N$
F. Bechstedt, J. Furthmüller, M. Ferhat, L. K. Teles, L. M. R. Scolfaro, J. R. Leite, V. Yu Davydov, O. Ambacher, and R. Goldhahn,
phys. stat. sol. (a) 195 (2003) 628.

AlN/diamond heterojunction diode
C. R. Miskys, J. A. Garrido, C. Nebel, M. Hermann, O. Ambacher, M. Eickhoff, and M. Stutzmann,
Appl. Phys. Lett. 82 (2003) 290.

The Transition from 2D to 3D Nanoclusters of Silicon Carbide on Silicon
Yu. V. Thrushin, K.L. Safonov, O. Ambacher, and J. Pezoldt,
Tech. Phys. Lett. 29 (2003) 663.

Dielectric function and one-dimensional description of the absorption of poly(octylthiophene)
T. Zhokhavets, R. Goldhahn, G. Gobsch, and W. Schliefke,
Sythetic Metals 138 (2003) 491.

Photoelectron emission micorscopy observation of inversion domain boundaries of GaN-based lateral polarity heterpstructures
W.-C. Yang, B.J. Rodriguez, M. Park, R.J. Nemanich, O. Ambacher, and V. Cimalla,
J. Appl. Phys. 94 (2003) 5720.

Exciton quenching in Pt/GaN Schottky diodes with Ga- and N-face polarity
S. Shokhovets, D. Fuhrmann, R. Goldhahn, G. Gobsch, O. Ambacher, M. Hermann, M. Eickhoff, and U. Karrer,
Appl. Phys. Lett. 82 (2003) 1712.

Micro-Raman Study of Electronic Properties of Inversion Domains in GaN-based Lateral Polarity Heterostructures
M. Park, J. J. Cuomo, B. Rodriguez, W. Yang, R. J. Nemanich, and O. Ambacher,
J. Appl. Phys. 92 (2003) 9542.

Auger depth profiling and factor analysis of SiC layers altered by sputtering,
R. Kosiba, G. Ecke, J. Liday, J. Breza, and O. Ambacher,
J. Electrical Engineering 54 (2003) 25.

Spin resonance of Mn^{2+} in wurtzite GaN and AlN films
T. Graf, M. Gjukic, M. Hermann, M.S. Brandt, M. Stutzmann, and O. Ambacher
Phys. Rev. B 67 (2003) 165215.

Growth and Characterization of Mn:GaN Epitaxial Films
T. Graf, M. Gjukic, L. Görgens, B. Phillip, O. Ambacher, M. S. Brandt, and M. Stutzmann,
J. Appl. Phys. 93 (2003) 9697.

Magnetotransport properties of a polarzation-doped three-dimensional electron slab
D. Jena, S. Heikman, J. S. Speck, A. Gossard, U. K. Mishra, A. Link, and O. Ambacher,
Phys. Rev. Lett. B 67 (2003) 153306.

Charge Transfer at the Mn Acceptor Level in GaN
T. Graf, M. Gjukic, L. Görgens, O. Ambacher, M.S. Brandt, and M. Stutzmann,
J. Superconductivity: Incorporating Novel Magnetism 16 (2003) 83.

Electroreflectance and Photoreflectance Studies of Electric Fields in Pt/GaN Schottky Diodes and AlGaN/GaN Heterostructures
S. Shokhovets, G. Goldhahn, G. Gobsch, O. Ambacher, I. P. Smorchkova, J. S. Speck, U. Mishra, A. Link, M. Herrmann, and M. Eickhoff, Mat. Res. Soc. Symp., Fall Meeting, Boston (2003) Proceedings.

Dielectric Function of „Narrow" Band Gap InN
G. Goldhahn, S. Shokhovets, V. Cimalla, L. Spiess, G. Ecke, O. Ambacher, J. Furthmüller, F. Bechstedt, H. Lu, and W.J. Schaff,
Mat. Res. Soc. Symp., Fall Meeting, Boston (2003) Proceedings.

Photo-Electron Emission Microscopy (PEEM) observation of inversion domain boundaries of GaN-based lateral polarity heterostructures
W.-C. Yang, B. J. Rodriguez, R .J. Nemanich, and O. Ambacher,
Mat. Res. Soc. Symp., Fall Meeting, Boston (2003) Proceedings.

Recent Advances in GaN HEMT Development
F. Schwierz and O. Ambacher,
The 11th IEEE Int. Symp. on Electron Devices for Microwave and Optoelectronic Applications (EDMO2003), Orlando, USA (2003) Proceedings 204.

Influence of metal thickness to sensitivity of Pt/GaN Schottky diodes for gas sensing applications
V. Tilak, M. Ali, V. Cimalla, V. Manivanan, P. Sanvik, J. Fedison, O. Ambacher, and D. Merfeld,
Mat. Res. Soc. Symp., Fall Meeting, Boston (2003) Proceedings.

Temperature dependent electric fields in GaN Schottky diodes studied by electroreflectance
S. Shokhovets, D. Fuhrmann, R. Goldhahn, G. Gobsch, O. Ambacher, M. Hermann, and M. Eickhoff,
E-MRS spring meeting, Strasbourg (2003) Proceedings.

Growth of non-polar a-plane and cubic InN on r-plane sapphire by molecular beam epitaxy
H. Lu, W.J. Schaff, L.F. Eastman, V. Cimalla, O. Ambacher, J. Wu, and W. Walukiewicz,
Mat. Res. Soc. Symp., Fall Meeting, Boston (2003) Proceedings.

Two-photon magnetoabsorption of the 2P exciton in GaN
C. Schweizer, D. Fröhlich, K. Reimann, O. Ambacher, and M. Stutzmann,
26th International Conference on the Physics of Semiconductors, Edinburgh (2002) edited by A.R. Long and J.H. Davies (IOP Bristol, 2003) Proceedings C4.4-17.

Design

Department of Design and Technology of Electronic Components

Modelling the Performance of Embedded Meshed Plane Structures in LTCC
G. Chen, K. L. Virga, G. Winkler, and J. L. Prince, 53rd Electronic Components&Technology Conference, New Orleans, USA (2003) Proceedings 1413.

New Materials and Technologies for Printed Circuit Boards - A development under the spell of new demands for environmentally friendly products and production steps
Gert Winkler, Gernot Bischoff, and Aneta Sutor. 27. International Conference and Exhibition IMAPS-Poland, Podlesice/Gliwice, Poland, (2003) Proceedings 88.

Devices

Department of Solid-State Electronics

On the Suitability of DD and HD Models for the Simulation of Nanometer Double-Gate MOSFETs
R. Granzner, V. M. Polyakov, F. Schwierz, M. Kittler, and T. Doll,
Physica E 19 (2003) 33.

Simulation and Optimization of EJ-MOSFETs
M. Kittler, R. Granzner, F. Schwierz, W. Henschel, T. Wahlbrink, and H. Kurz,
Solid-State Electron. 47 (2003) 1193.

Influence of Channel Width on n- and p-type Nano-Wire-MOSFETs on Silicon on Insulator Substrate
M. Lemme, T. Mollenhauer, W. Henschel, T. Wahlbrink, M. Heuser, M. Baus, O. Winkler, B. Spangenberg, R. Granzner, F. Schwierz, and H. Kurz,
Microelectron. Eng. 67-68 (2003) 810.

RF MOSFET: Recent Advances, Current Status and Future Trends
J. J. Liou and F. Schwierz,
Solid-State Electron. 47 (2003) 1881.

Transport and Complex Formation Kinetics of Polarons, Dopands and Bipolarons
G. Paasch and S. Scheinert,
Synthetic Metals 135-136 (2003) 407.

Mixing of Surface Dipole and Band Bending at Organic/Metallinterfaces in the Case of Exponentially Distributed States
G. Paasch, H. Peisert, M. Knupfer, J. Fink, and S. Scheinert,
J. Appl. Phys. 93 (2003) 6084.

Simulation of Organic Light Emitting Diodes: Influence of Charges Localized Near the Electrodes
G. Paasch, A. Nesterov, and S. Scheinert,
Synthetic Metals 139 (2003) 425.

Relevance of Organic Field Effect Transistor Models: Simulation vs. Experiment
S. Scheinert, G. Paasch, and T. Lindner,
Synthetic Metals 137 (2003) 1451.

The Influence of Bulk Traps on the Subthreshold Characteristics of an Organic Field Effect Transistor
S. Scheinert, G. Paasch, and Th. Doll,
Synthetic Metals 139 (2003) 233.

Analyzes of Field Effect Devices Based on Poly-(3-Octoylthiophene)
S. Scheinert and W. Schliefke,
Synthetic Metals 139 (2003) 501.

Modern Microwave Transistors - Theory, Design, and Performance
F. Schwierz and J. J. Liou,
John Wiley & Sons, New York (2003).

Excessive Noise in Nanoscaled DG-MOSFETs: A Monte Carlo Study
V. Polyakov and F. Schwierz,
13th Int. Conf. on Nonequilibrium Carrier Dynamics in Semiconductors HCIS13 (2003) Proceedings P Tu 3-9.

Recent Advances in GaN HEMT Development
F. Schwierz and O. Ambacher,
EDMO (2003) Proceedings 204.

Expert System for Gas Sensor Array Configuration and Scenario Management
R. Traute, F. Haase, O. Kiesewetter, G. Müller, and T. Doll,
Eurosensor XII, Guimaraes, Portugal (2003) Proceedings 727.

Modules

Department of Microperipherics

Photostrukturierte Elemente und Leitungen in LTCC
R. Perrone, M. Hintz, K.-H. Drüe, and H. Thust,
PLUS, (2003) 126.

Embedded Components and Functions in LTCC- Review and Prospect
H. Thust,
Conf. on Ceramic Interconnect Technology: The Next Generation, Denver, USA (2003).

Manufacturability and Reliability of Trimmed Buried Resistors
W. Ehrhardt, H. Thust, and J. Müller,
Conf. on Ceramic Interconnect Technology: The Next Generation, Denver, USA (2003).

Behaviour of Sheet Resistors by Impulse Capacitor Discharge
W. Ehrhardt and H. Thust,
14th EMPC Conf., Friedrichshafen (2003) Proceedings 148.

Laser Processing of LTCC with different Machine Concepts
K.-H. Drüe, Th. Thelemann, and H. Thust,
14th EMPC Conf., Friedrichshafen (2003) Proceedings 248.

LTCC with Integrated Passives for Telecom Applications
F. Bechthold, J.P. Bertinet, and H. Thust
14th EMPC Conf., Friedrichshafen (2003) Proceedings 298.

Alternative Way to High Current Structures in LTCC
A. Albrecht, J. Botiov, M. Fischer, M. Hintz, K.-H. Drüe, and H. Wurmus,
14th EMPC Conf., Friedrichshafen (2003) Proceedings 408.

Photostrukturierte Elemente und Leitungen in LTCC
R. Perrone, M. Hintz, K.-H. Drüe, and H. Thust, Deutsche IMAPS Konf. 2003, München (2003)

Embedded Components in LTCC-Review and Prospect
H. Thust,
48. Intern. Wiss. Koll., Ilmenau (2003) Proceedings 153.

Highly Integrated Power Distribution Network on Multilayer LTCC for Ka- band Multiple-beam Phased Array Antennas
J. Kassner, R. Kulke, P. Uhlig, P. Waldow, R. Münnich, and H. Thust,
IMAPS–Nordic Annual Conf. 2003, Espoo, Finland (2003) Proceedings 51.

Advanced Electrical and Stability Characterisation of Untrimmed and Pulse Voltage Trimmed Thick Film Resistors
A. Dziedzic, A. Janek, A. Kolek, W. Ehrhardt, and H. Thust,
27. Intern. Conf. and Exib. IMAPS-Poland, Podlesice/Gliwice, Poland (2003) 50.

Systems

Department of Process Measurement

Präzision mit Laserlicht
W. Schott, W. Pöschel, S. Ecke, G. Jäger, R. Grünwald, H.-J. Büchner, and E. Manske, Fachzeit Laser + Photonik 4 (2003) 31.

An optical standing-wave interferometer for displacement measurements
H.-J. Büchner, H. Stiebig, V. Mandryka, E. Bunte, and G. Jäger,
Measurement Science and Technology 14 (2003) 311.

Standing wave detection by thin transparent n-i-p diodes of amorphous silicon
H. Stiebig, H.-J. Büchner, E. Bunte, V. Mandryka, D. Knipp, and G. Jäger,
Thin solid films 427 (2003)152.

Nanomess- und Positioniertechnik
G. Jäger,
Buchbeitrag in F. Klocke, G. Pritschow, Springer Verlag Berlin, Heidelberg, New York (2003).

Nanopositionier- und Nanomessmaschinen
G. Jäger,
VDI/VDE-Fachtagung Metrologie in der Mikro- und Nanotechnik, Stuttgart, VDI-Berichte 1669 (2003) 127.

Standing wave interferometer for length measurement
H.-J. Büchner, H. Stiebig, V. Mandryka, E. Bunte, and G. Jäger,
Euspen Aachen, Volume 2 (2003) 387.

Interference-optical force sensor for small forces
G. Jäger and R. Füßl,
XVII. IMEKO World Congress Dubrovnik, Croatia, (2003) Proceedings 32.

Miniature interferometers for applications in micro- and nanotechnology
G. Jäger, E. Manske, T. Hausotte, R. Füßl, R. Grünwald, H.-J. Büchner, W. Schott, and D. Dontsov,
SPIE-Symposium San Diego, USA, 5190 (2003) Proceedings 185.

Miniature interferometers developed for applications in nano-devices
G. Jäger, E. Manske, T. Hausotte, R. Füßl, R. Grünwald, H.-J. Büchner, W. Schott, and D.Dontsov,
7. International Conference on Mechatronic Technology 2003 (ICMT), Taipei, Taiwan (2003) Proceedings 41.

Miniature interferometers developed for applications in nano-devices
G. Jäger,
National Yunlin University of Science & Technology, Toulin, Taiwan (2003).

Nanometrology – Nanometer Devices
G. Jäger,
National Huwei Institute of Technology, Huwei, Taiwan (2003).

Miniature interferometers developed for applications in nano-devices
G. Jäger,
Nano Technology Research Center, ITRI, Hsinchu, Taiwan (2003).

Nanopositioning and Nanomeasuring Machines
G. Jäger,
Center for Measurement Standards, ITRI, Hsinchu, Taiwan (2003).

Analytics

Department of Technical Physics

Understanding and tuning the epitaxy of large aromatic adsorbates by molecular design
M. Eremtchenko, J. A. Schaefer, and F. S. Tautz,
Nature 425 (2003) 602.

The effect of wetting on the microhydrodynamics of surfaces lubricated with water and oil
W. Hild, J. A. Schaefer, A. Opitz, and M. Scherge,
Wear 254 (2003) 871.

Nanofriction of silicon oxide surfaces covered with thin water films
A. Opitz, S.I-U Ahmed, J. A. Schaefer, and M. Scherge,
Wear, 254 (2003) 924.

Ionization and solvation of CsCl interacting with solid water
A. Borodin, O. Höfft, S. Krischok, and V. Kempter,
Journal of Physical Chemistry B,
107 (35) (2003) 9357.

Interaction of alkali atoms with water multilayers adsorbed on TiO_2 (110): A study with MIES and UPS
S. Krischok, O. Höfft, and V. Kempter,
Surface Science, 532-535 (2003) 370.

The chemistry of alkali atoms on solid water: A study with MIES and UPS
S. Krischok, O. Höfft, J. Günster, R. Souda, and V. Kempter,
Nuclear Instruments and Methods in Physics Research B, 203C (2003) 124.

The interaction of CsCl molecules with films of solid water
A. Borodin, O. Höfft, S. Krischok, and V. Kempter,
Nuclear Instruments and Methods in Physics Research B, 203C (2003) 205.

Integrating Friction and Wear research
M. Scherge and J. A. Schaefer (edts.),
280. WE-Heraeus-Seminar 2002, Ilmenau,
Wear, 254 (2003) 799.

Load Dependence and Lifetime Studies of Self Assembled Monolayers
W. Hild, G. Hungenbach, S.I.-U. Ahmed,
M. Scherge, and J.A. Schaefer,
Proceedings Symposium TRIMIS 2003:
Microtribology-Tribology in Microsystems,
Neuchâtel, Switzerland (2003).

Einfluss von tribologischen Eigenschaften auf die Positioniergenauigkeit
W. Hild, G. Hungenbach, Y. Liu, A. Opitz,
P. Jaschinsky, M. Scherge, and J. A. Schaefer,
DPG Frühjahrstagung, Dresden (2003)
Oral presentation.

Photoelektronenspektroskopische Untersuchungen an InN-Oberflächen
S. Krischok, M. Himmerlich, R. Kosiba, G. Ecke,
O. Ambacher, and J. A. Schaefer,
DPG Frühjahrstagung, Dresden (2003)
Oral presentation.

Pentacene/Ag (111): film growth via an accommodation layer
M. Eremtchenko, D. Bauer, S. Döring, T. Stolz,
J. A. Schaefer, and F. S. Tautz,
DPG Frühjahrstagung, Dresden (2003) Poster.

Interaction of Na with Molecular Surfaces (H_2O; CH_3OH) between 80 and 130 K
O. Höfft, A. Borodin, U. Kahnert, S. Krischok, and V. Kempter,
DPG Frühjahrstagung, Dresden (2003) Poster.

Vibrational and structural properties of the perylene / Ag(111) interface: A quasi-liquid molecular layer
M. Eremtchenko, D. Bauer, S. Döring,
J. A. Schaefer, and F. S. Tautz,
DPG Frühjahrstagung, Dresden (2003)
Oral presentation.

C_{60} growth on InP (100)
G. Cherkashinin, S. Döring, M. Eremtchenko,
G. Hartung, D. Malsch, A. Opitz, T. Stolz,
and J. A. Schaefer,
DPG Frühjahrstagung, Dresden (2003)
Oral presentation.

Growth of C_{60} on modified InP(001) surfaces
M. Eremtchenko, A. Opitz, T. Stolz, D. Malsch,
S. Döring, R. Temirov, G. Cherkashinin, S. Krischok,
and J. A. Schaefer,
14th Interdisciplinary Surface Science Conference (ISSC), Liverpool, UK (2003).

Surface science tools and their application on nanosystems like C_{60} on indium phoshide
J. A. Schaefer, G. Cherkashinin, S. Döring, M. Eremtchenko, S. Krischok, D. Malsch, A. Opitz, and T. Stolz,
NATO Advanced Research Workshop Summer School: „Frontiers in Molecular-scale Science and Technology of Nanocarbon, Nanosilicon and Biopolymer Integrated Nanosystems", Ilmenau (2003) Oral Presentation.

Pentacene on Ag(111): Film growth via an accommodation layer?
M. Eremtchenko, D. Bauer, S. Döring, T. Stolz, F. S. Tautz, V. Yanev, S. Krischok, and J. A. Schaefer,
NATO Advanced Research Workshop Summer School: „Frontiers in Molecular-scale Science and Technology of Nanocarbon, Nanosilicon and Biopolymer Integrated Nanosystems", Ilmenau (2003) Poster.

Probing weak adsorption site recognition directly with the STM
F. S. Tautz, M. Eremtchenko, and J. A. Schaefer,
12th International Conference on Scanning Tunneling Microscopy/Spectroscopy and Related Techniques (STM'03), Eindhoven, Netherlands (2003).

Investigations of MBE grown InN and the influence of sputtering on the surface composition
S. Krischok, V. Yanev, O. Balykov, M. Himmerlich, J. A. Schaefer, R. Kosiba, G. Ecke, I. Cimalla, V. Cimalla, O. Ambacher, H. Lu, W. J. Schaff, and L. F. Eastman,
22nd European Conference on Surface Science (ECOSS), Praha, Czech Republik (2003) Poster.

Influence of the RF Power on the Deposition Rate and the Chemical Surface Composition of Fluorocarbon Films Prepared in Dry Etching Gas Plasma
V. Yanev, S. Krischok, A. Opitz, H. Wurmus, N. Schwesinger, S. I.-U. Ahmed, and J. A. Schaefer,
22nd European Conference on Surface Science (ECOSS), Praha, Czech Republik (2003) Poster.

Pentacene on Ag(111): Film growth via an accommodation layer
M. Eremtchenko, D. Bauer, F. S. Tautz, V. Yanev, S. Krischok, and J. A. Schaefer,
48. Internationales Wissenschaftliches Kolloqium, Ilmenau (2003).

C_{60} structure formation on InP (001)
Th. Stolz, G. Cherkashinin, S. Döring, M. Eremtchenko, S. Krischok, D. Malsch, A. Opitz, and J. A. Schaefer,
48. Internationales Wissenschaftliches Kolloqium, Ilmenau (2003).

Viscosity effect on GaInSn studied by XPS
F. Scharmann, G. Cherkashinin, V. Breternitz, Ch. Knedlik, G. Hartung, Th. Weber and J.A. Schaefer,
10th European Conference on Applications of Surface and Interface Analysis (ECASIA), Berlin (2003) Poster.

Sputtering of InN for depth profiling procedure
R. Kosiba, G. Ecke, V. Cimalla, L. Spiess, S. Krischok, J. Schaefer, W. Schaff, and O. Ambacher,
10th European Conference on Applications of Surface and Interface Analysis (ECASIA), Berlin (2003) Oral Presentation.

Real-time PEEM observation of the growth dynamics of Ge islands on vicinal and on-axis Si (001) surfaces
M. Himmerlich, W. Yang, R. J. Nemanich, and J. A. Schaefer,
MRS Fall Meeting, Boston, USA (2003) Oral Presentation.

Plasma & Thüringen
J. A. Schaefer,
11. Bundesdeutsche Fachtagung Plasmatechnologie, Ilmenau (2003) Invited presentation with experiments.

Theses

Habilitation

Frank Schwierz (19.12.2003)
Department of Solid-State Electronics
„Modern Microwave Transistors - Theory, Design, and Performance"

PhD-Theses

Aki Shimamura (28.01.2003)
Department of Microperipherics
„Elektrische Eigenschaften von dünnen Sol-Gel Schichten"
(Electrical Characterisation of thin Sol-Ge-layers)

Yung-Cheng Wang (28.01.2003)
Department of Process Measurement
„Präzisionsprüfgerät für Nanomesstaster"

Andreas Opitz (12.02.2003)
Department of Technical Physics
„Nanotribologische Untersuchungen von ultradünnen Wasserfilmen auf hydrophoben und hydrophilen Siliziumoberfllächen"

Ralf Siemieniec, (28.02.2003)
Department of Solid-State Electronics
„Simulation von Leistungsbauelementen mit durch Bestrahlungsverfahren eingestellter Trägerlebensdauer"

Denys Dontsov (05.05.2003)
Department of Process Measurement
„Homodyninterferometer zur berührungslosen Schwingungsanalyse"

Chao-Jung Chen (27.05.2003)
Department of Process Measurement
„Development of a Traceable Atomic Force Microscope with Interferometer and Compensation Flexure Stage"

Diploma-Theses

Torsten Mülln (15.01.2003)
Department of Microperipherics
„Vergrabene Kondensatoren in LTCC für HF-Anwendungen"

Carsten Buchheim (07.03.2003)
Department of Nanotechnology
„Photoreflexion an AlGaN/GaN-Heterostrukturen mit polarisationsinduziertem zweidimensionalem Elektronengas"

Christian Müller (02.06.2003)
Department of Materials for Electronics
„Herstellung und festkörperphysikalische Charakterisierung von magnetron-gesputterten WC-Schichten"

Ingo Hörselmann (15.07.2003)
Department of Solid-State Electronics
„Dynamisches und transientes Verhalten von OFETs"

Daniel Bauer (17.07.2003)
Department of Technical Physics
„Strukturuntersuchungen von organischen Schichten auf einkristallinen Silberoberflächen"

Markus Noren (18.11.2003)
Department of Microperipherics
„Hochfrequenztaugliche Aufbau- und Verbindungstechnik von MMICs auf LTCC"

Philipp Jaschinsky (17.12.2003)
Department of Technical Physics
„Konstruktion und Demonstration eines SNOM-Messkopfes"

Student research project reports

Marcus Noren (05.02.2003)
Department of Microperipherics
„Untersuchungen zum Schrumpfungsverhalten von LTCC Strukturen"

Gabriel Kittler (28.04.2003)
Department of Nanotechnology
„Elektrische Charakterisierung von InN und AlGaN/GaN-Heterostrukturen"

Oliver Schulz (12.06.2003)
Department of Nanotechnology
„Bestimmung von Sputterausbeuten und AES-Elementempfindlichkeitsfaktoren für die Materialien von Resonanztunneldiodenstrukturen auf GaN-Basis für ausgewählte Messbedingungen"

Ronny Wagner (30.06.2003)
Department of Nanotechnology
„Thermische Stabilität und Oberflächendesorption von Gruppe III-Nitriden"

Mathias Hujo (10.12.2003)
Department of Microsystem Technology
„Stand der Technik der Tintenstrahldruckköpfe"

Jan Driesel (31.12.2003)
Department of Microsystem Technology
„Mikrotechnische Sensoren im Kraftfahrzeug"

Invited Talks and Colloquia

Dr.-Ing. Martin Eickhoff
„GaN-basierende Sensoren“
Walter Schottky Institut der Technische Universität München, 15.01.2003

Prof. Norbert Esser
„Spectroscopic Ellipsometry for characterization of Nitride layers: bulk, surface and growth properties”
Technische Universität Berlin, 29.01.2003

Dr.-Ing. P. Renzel
„Ultraschall-Messungen bei unbekannter Schallgeschwindigkeit“
Agfa NDT GmbH, Hürth, 20.02.2003

Dipl. Phys. Thomas Holz
„Die Herstellung von Nanometermultischichten und ihre Anwendungspotentiale“
AXO Dresden GmbH, 5.03.2003

Dr. Wolfgang Skorupa
„Blaue Lichtemission aus nanoclusterreichen SiO_2-Schichten: Fakten und Visionen“
Forschungszentrum Rossendorf, Dresden, 19.03.2003

Dr. Ute Kaiser
„Transmissionselektronenmikroskopie für Nanostrukturen in z.B. SiC“
Friedrich Schiller Universität Jena, 2.04.2003

Prof. Axel Scherer
„Neue Wege in der Kombination von Fluidik und optischer Sensorik“
California Institute of Technology, Pasadena, USA, 9.04.2003

Dr.-Ing. Werner Prost
„Tunneldioden: Bauelemente und Schaltungen an der Schnittstelle von Mikro-und Nanoelektronik“
Gesamthochschule Duisburg, 16.04.2003

Dr. Peter Schroth
„Bioelektrische Interfaces für Biosensoren und BioMEMS“
Forschungszentrum Jülich, 28.04.2003

Dr. Jörg Lindner
„Quantitative Transmissions-Elektronenmikroskopie zur Charakterisierung neuer elektronischer Werkstoffe“
Universität Augsburg, 30.04.2003

Dr. Stefan Zappe
„Mikrosystemtechnik in der Biologie:
Vom genetischen Code zu Struktur und Funktion“
Stanford University, Stanford, USA 26.05.2003

Dr. Herwig Döllefeld
„Halbleiter-Nanopartikel - der chemische Blick“
Technische Universität Ilmenau /
Universität Hamburg, 28.05.2003

Dr. Viton Heera
„Nanokristalline, p-dotierte SiC-Schichten hergestellt mittels ionenstrahlinduzierter Rekristallisation - Struktur und elektrische Eigenschaften“
Forschungszentrum Rossendorf,
Dresden,11.06.2003

Prof. Fred Barlow
„Electronic Packaging Research at the University of Arkansas”
University of Arkansas, USA 27.06.2003

Dr. Mirko Lehmann
„Halbleitersensoren für die Bioanalytik“
Micronas GmbH, Freiburg, 9.07.2003

Dr. Daniel Oates
„Microwave applications of high-temperature superconductor materials and other technologies”
MIT Lincoln Laboratories, Lexington, USA, 10.09.2003

Prof. Ralf Moos
„Neuartige Gassensoren für Anforderungen in extremen Atmosphären“
Universität Bayreuth, 1.10.2003

Prof. Ignaz Eisele
„Materialsysteme und Device-konzepte für die Silizium-Nanoelektronik“
Universität der Bundeswehr München, 8.10.2003

Prof. Robert Schwarzer
„Die Analyse der lokalen Textur mit Anwendungen in den Materialwissenschaften“
Technische Universität Clausthal Zellerfeld,
29.10.2003

Dr. Horst Wendrock
„Einsatz von EBSD- und FIB-Technik zur Mikrostrukturaufklärung in der Mikroelektronik“
Institut für Festkörper- und Werkstoffforschung,
Dresden, 12.11.2003

Dr.-Ing. Jörg Bischoff
„Messung von Submikrometerstrukturen mit optischen Methoden“
Tokyo Electron Deutschland, Ismaning, 26.11.2003

Dr. Andreas Schober
„Chemische und Biochemische Synthesen sowie Detektion in Biotechnologischen Anwendungen“
Institut f. Physikalische Hochtechnologie, Jena,
10.12.2003

Herwig Döllefeld, Michael Fischer, Michael Hintz, Frank Weise, Gabriel Kittler, Kirsti Schneider
„Status-Bericht Pikofluidik-Projekt“
ZMN der Technischen Universität Ilmenau, 17.12.2003

Scientific Projects

since foundation of the ZMN including the coworkers

Federal Ministry of Education and Research (Bundesministerium für Bildung und Forschung, BMBF)

Aufbau eines Aus- und Weiterbildungsnetzwerks innerhalb der Mikrosystemtechnik in Thüringen (FASIMIT), Project manager: Prof. Wurmus
Mike Stubenrauch, Verein MicroComp e.V.

Baukastensystem in LTCC-Technologie für die Steuer- und Regelungstechnik
(IMODAS), Project manager: Prof. Thust
Torsten Thelemann

Entwicklung von alternativen Fertigungstechnologien für hochstromtragfähige Induktivitäten (MIKROSYST), Project manager: Prof. Wurmus
Arne Albrecht, Julian Botiov, Lothar Dressler, Gabriele Harnisch, and Christine Lohmann

Universelles Gas-Sensor-Baukastensystem (IESSICA), Project manager: Prof. Doll
Gernot Ecke, Christian Fachmann, Frank Haase, Rastislav Kosiba, and Roman Paris

Verbundprojekt: Zentrum für Innovationskompetenz, Mikro- und Nanosysteme in Lebenswissenschaften und Informationselektronik (Leuchtturm), Project manager: Prof. Doll
Oliver Ambacher, Herwig Döllefeld, Jens Kobow, Ulrich Liebold, Christian Schippel, Kirsti Schneider, and Delf Schwerda

Nanobiotechnologie-Verbundprojekt: Kristalloides P-Protein - Prototyp bioanaloger Nanoaktuatoren; Teilprojekt 3: Prototypische Anwendungen (P-Protein), Project manager: Prof. Wurmus
Karin Friedel, Mike Stubenrauch, and Danja Voges

Simultane Mehrgrößenmikrosensorsysteme für den Präzisionsmaschinenbau
(SIMEP), Project manager: Prof. Grünwald
Holger Wurzbacher

German Science Foundation (Deutsche Forschungsgemeinschaft, DFG)

Bindung und Strukturbildung an den Grenzflächen von organischen Schichten mit Isolatoren und metallischen Kontakten
(OFET), Project manager: Prof. Schäfer
Oleg Balykov, Gernot Ecke, Jin Guo, Rastislav Kosiba, Stefan Krischok, Annette Läffert, Willy Schliefke, and Jutta Uziel

Entwicklung und Fertigung von hochauflösenden Strömungs- und Temperatursensoren (µ-Anemometer)
(Interdisziplinäre Turbolenz-Initiative), Project manager: Prof. Wurmus
Jörg Burgold, Lothar Dressler, Karin Friedel, Gabriele Harnisch, Wolfgang Kempf, and Mike Stubenrauch

Hochspannungsabgleich von vergrabenen Widerständen
(HSP Abgleich), Project manager: Prof. Thust
Karl-Heinz Drüe, Waleed Erhardt, Uwe Genatis, Regina Lenk, and Martina Sieler

Hochtemperaturverhalten elektrisch leitfähiger, hochschmelzender Metallkarbide
(HTMEC), Project manager: Prof. Knedlik
Manuela Breiter, Gernot Ecke, Maik Gubisch, Rastislav Kosiba, Elvira Remdt, Henry Romanus, and Lothar Spieß

Technologie und Charakterisierung von Polymer-Feldeffekttransistoren
(Polymer-FET II), Project manager: Dr. Scheinert
Andrej Herasimovich, Ingo Hörselmann, Silvia Klaube, Maxi Scheinert

Heteroepitaxie von Gruppe III-Nitriden auf Diamantsubstraten für optoelektronische und elektronische Anwendungen
(Diamant), Project manager: Prof. Ambacher
Dorin Cornel Cengher, and Rastislav Kosiba

Entwicklung piezoelektrischer, mit Halbleiterbauelementen integrierbarer AlGaN/Si-Nanoresonatoren für elektrokeramische Hochfrequenzsensoren
(Pi-NEMS), Project manager: Prof. Ambacher
Klemens Brückner, Christian Förster, Matthias Hein, and Ralf Stephan

Bauelementeverhalten und Transporteigenschaften organischer Feldeffekt-Transistoren: Experiment-Simulation-Theorie
Project manager: Dr. Scheinert
Andrej Herasimovich, Ingo Hörselmann, and Silvia Klaube

Wissenschaftliche Grundlagen zur Entwicklung von Positionier-, Bearbeitungs- und Messmaschinen mit einer Auflösung von < 1nm für Bewegungsbereiche von 450x450x80mm
(Nanopositionier- und Nanomessmaschinen, SFB 622), Project manager: Prof. Jäger
Oleg Balykov, Maik Gubisch, Jin Guo, Thomas Haas, Frank Haase, Stefan Krischok, Annette Läffert, Eberhard Manske, Rostyslov Mastylo, Elvira Remdt, Henry Romanus, and Lothar Spieß

Thuringian Ministry for Science, Research, and Art (Thüringer Ministerium für Wissenschaft, Forschung und Kunst, TMWFK)

Zell- und Biomolekül-Sensoren in Piko- und Nanofluidischen Systemen
(Pikofluidik), Project manager: Prof. Ambacher
Majdeddin Ali, Arne Albrecht, Falko Baier, Volkmar Breternitz, Carsten Buchheim, Jörg Burgold, Volker Cimalla, Lothar Dressler, Karl-Heinz Drüe, Michael Fischer, Karin Friedel, Uwe Genatis, Jörg Geßner, Maik Gubisch, Gabriele Harnisch, Birgitt Hartmann, Michael Hintz, Rene Hoffmann, Matthias Kallenbach, Gabriel Kittler, Mario Kittler, Ina Koch, Stefan Krischok, Regina Lenk, Rostyslav Mastylo, Christian Müller, Andreas Opitz, Elvira Remdt, Henry Romanus, Jens Schawohl, Frank Schwierz, Martina Sieler, Lothar Spieß, Mike Stubenrauch, and Frank Weise

Entwicklung und Charakterisierung von nanoskaligen Verschleißschutzschichten
(NANOVSS), Project manager: Prof. Knedlik
Elvira Remdt, Henry Romanus, Jens Schawohl, and Lothar Spieß

Entwicklung von LTCC-Schaltungen für Anwendungen bis 20GHz
(LTCC für 20GHz), Project manager: Prof. Thust
Waleed Erhardt, Uwe Genatis, Michael Hintz, Ina Koch, Regina Lenk, Ashraf Mokayyes, Ralph Münnich, Ruben Perrone, and Martina Sieler

Herstellung von organischen Mischschichten mit nanoskaligen Domänen für Solarzellen aus konjugierten Polymeren und Fullerenen
(ORSOL), Project manager: Prof. Ambacher
Volker Cimalla, Gernot Ecke, Rastislav Kosiba, Irina Popa, Sylvia Probst, Willy Schliefke, Matthias Spode, and Jutta Uziel

Inbetriebnahme der neuen technologischen Ausrüstungen, Charakterisierung der Prozesse, Kostenanalyse zur Einführung einer Kostenrechnung (ZMN- Anlaufphase),
Project manager: Prof. Ambacher (Direktor)
Oleg Balykov, Gernot Bischoff, Manuela Breiter, Volkmar Breternitz, Jörg Burgold, Volker Cimalla, Lothar Dressler, Karl-Heinz Drüe, Michael Fischer, Karin Friedel, Uwe Genatis, Maik Gubisch, Jin Guo, Gabriele Harnisch, Birgitt Hartmann, Andrej Jancura, Matthias Kallenbach, Ina Koch, Stefan Krischok, Regina Lenk, Feng Qiao, Elvira Remdt, Henry Romanus, Jens Schawohl, Martina Sieler, Lothar Spieß, Anata Sutor, Gerd Teichert, and Frank Weise

Realisierung, Charakterisierung und Optimierung von AlGaN-basierenden UV-Detektoren mit i ntegrierten Bandpassfiltern auf Siliziumsubstraten
(UVSENS), Project manager: Prof. Ambacher
Carsten Buchheim, Volker Cimalla, Gernot Ecke, Christian Förster, Rastislav Kosiba, Vadim Lebedev, Ilona Marquardt, Irina Popa, Sylvia Probst, Thomas Stauden, and Andreas Winzer

SiC-Hochfrequenztransistor mit neuen Materialien
(NEMASIC), Project manager: Prof. Doll
Gernot Ecke, Christian Fachmann, Christian Förster, Rastislav Kosiba, Ilona Marquardt, Jörg Pezoldt, Henry Romanus, Frank Schwierz, Lothar Spieß, Thomas Stauden, and Petia Weih

Technologisches line-up Polymer-FET
(Polymer-FET I), Project manager: Prof. Doll
Gernot Ecke, Frank Haase, Andrej Herasimovich, Ingo Hörselmann, Silvia Klaube, Rastislav Kosiba, Susanne Scheinert, Willy Schliefke, and Jutta Uziel
Wachstumskinetik und elektrische Eigenschaften niedermolekularer organischer Funktionsschichten für die Anwendung in Feldeffekttransistoren
(Organische Funktionsschichten),
Project manager: Prof. Schäfer
Oleg Balykov, Jin Guo, Stefan Krischok, and Annette Läffert

European Union, EU

Entwicklung von prototypischen Anwendungen für funktionelle flüssigkristalline Elastomere (FULCE), Project manager: Prof. Wurmus
Mike Stubenrauch

Herstellung und Optimierung von 3C-SiC-Schichten auf Siliziumsubstraten durch eine Kombination der Molekularstrahlepitaxie und des lichtinduzierten Ausheilens von Defekten
(FLASIC), Project manager: Dr. Pezoldt
Volker Cimalla, Gernot Ecke, Christian Förster, Rastislav Kosiba, Ilona Marquardt, Thomas Stauden, Petia Weih, and Charbel Zgheib

Office of Naval Research, ONR

Pyroelectric AlGaN/GaN HEMTs for ion, gas & polar liquid sensors
(NICOP), Project manager: Prof. Ambacher
Volker Cimalla, Gernot Ecke, Christian Förster, Rastislav Kosiba, Vadim Lebedev, Ilona Marquardt, Jörg Pezoldt, Thomas Stauden, and Petia Weih

German Academic Exchange Service (Deutscher Akademischer Austausch Dienst, DAAD)

Internationale Qualitätsnetzwerke: Ilmenauer Koordinationszentrum
(International Coordination Center, ICC), Project manager: Dr. Pezoldt
Thomas Stauden

German Federal Foundation for Environment (Deutsche Bundesstiftung Umwelt, DBU)

Polysiloxanfolie als Trägermaterial für elektronische Baugruppen
(Polysiloxanfolie), Project manager: Prof. Winkler
Gernot Bischoff, Uwe Genatis, Andrej Jancura, Regina Lenk, and Martina Sieler

German aerospace society (Deutsches Zentrum für Luft- und Raumfahrt, DLR)

LTCC-Schaltungen für Raumfahrtanwendungen (Satellitenkommunikation)
(EASTON), Project manager: Prof. Thust
Karl-Heinz Drüe, Uwe Genatis, Ralph Münnich, and Martina Sieler

Keramische Mikrowellenschaltkreise für die Satellitentechnik
(KERAMIS), Project manager: Prof. Thust
Karl-Heinz Drüe, Uwe Genatis, Matthias Hein, Ralph Münnich, Ruben Perrone, Martina Sieler, Ralf Stephan, and Johannes Trabert

Physical-Technical Federal Institute (Physikalisch-Technische Bundesanstalt, PTB)

Entwicklung eines Antastsystems für ein universell einsetzbares metrologisches Rasterkraftmikroskop
Project manager: Prof. Jäger
Nataliya Dorozhovets

Industry

Kennametall Widia GmbH & Co. KG:
Röntgenografische Spannungs- und Texturmessungen an beschichtete Hartmetallwerkzeugen (Textur- und Spannungsuntersuchungen an Schneidmaterialien), Project manager: Dr. Spieß
Jens Schawohl and Gerd Teichert

Kerafol Keramische Folien GmbH, Eschenbach:
Chemikalienfreie, strukturierte Metallisierung von schadstofffreien Leiterplatten auf Polysiloxanbasis (POLYMETA), Project manager: Prof. Winkler
Gernot Bischoff, Uwe Genatis, Regina Lenk, Martina Sieler, and Aneta Sutor

Moeller GmbH, Bonn:
Anwendung von Flüssigmetallen in Schaltern, Untersuchung des Langzeitverhaltens von Flüssigmetallen bei Schaltvorgängen
(Flüssig-Metall), Project manager: Knedlik

Thüringer Institut für Textil- und Kunststoff-Forschung e.V. (TITK) Rudolstadt/Schwarza:
Polymertransistor, Project manager: Dr. Scheinert
Andrej Herasimovich, Ingo Hörselmann, and Silvia Klaube

Fraunhofer-Gesellschaft zur Förderung der angewandten Forschung e.V.; Fraunhofer-Institut für Angewandte Optik und Feinmechanik Jena:
Entwurf und Herstellung von LTCC-Substraten für optomechatronische Anwendungen
Project manager: Prof. Thust
Uwe Genatis, Michael Hintz, Ina Koch, Regina Lenk, Ralph Münnich, Ruben Perrone, and Martina Sieler

Adresses

ZMN
Center for Micro- and Nanotechnologies
Gustav-Kirchhoff-Str. 7
98693 Ilmenau
Germany

fon: +49-(0)3677-69-3401
fax: +49-(0)3677-69-3499

e-mail: zmn@tu-ilmenau.de
URL: http://www.zmn.tu-ilmenau.de

Oliver Ambacher:
oliver.ambacher@tu-ilmenau.de
fon: +49-(0)3677-69-3723

Theodor Doll:
theodor.doll@tu-ilmenau.de
fon: +49-(0)6131-990-100

Gerd Jäger:
jaeger@mb.tu-ilmenau.de
fon: +49-(0)3677-69-2822

Heinrich Kern:
kern@tu-ilmenau.de
fon: +49-(0)3677-69-2533

Christian Knedlik:
christian.knedlik@tu-ilmenau.de
fon: +49-(0)3677-69-3611

Jürgen A. Schäfer:
juergen.schaefer@tu-ilmenau.de
fon: +49-(0)3677-69-3609

Heiko Thust:
heiko.thust@tu-ilmenau.de
fon: +49-(0)3677-69-2605

Gert Winkler:
gert.winkler@tu-ilmenau.de
fon: +49-(0)3677-69-2606

Helmut Wurmus:
helmut.wurmus@tu-ilmenau.de
fon: +49-(0)3677-69-2487

ZMN, Center for Micro- and Nanotechnologies

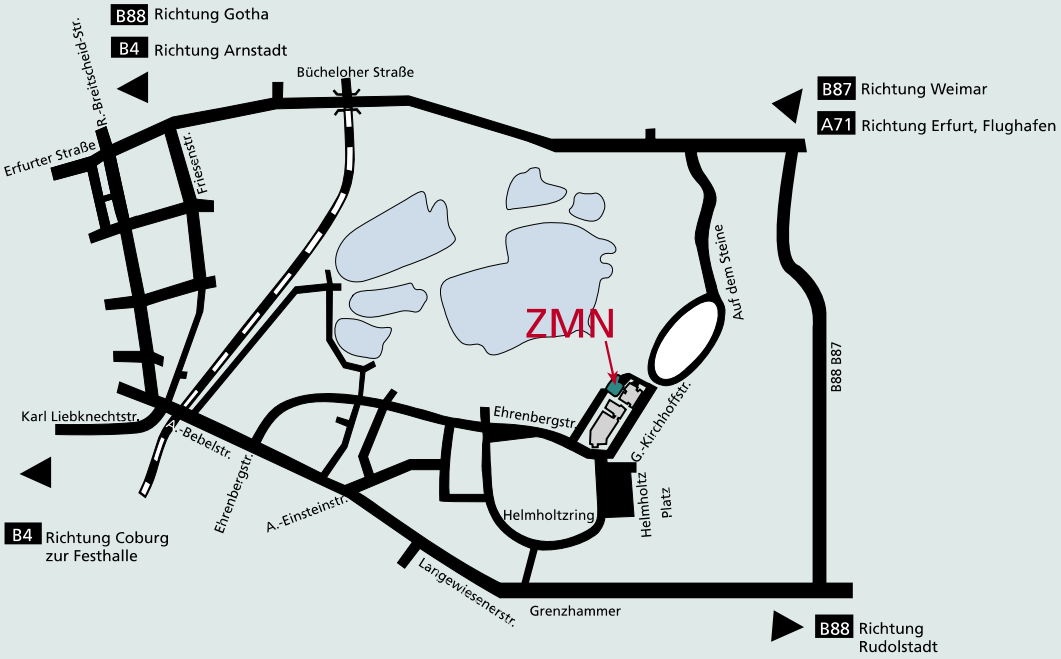

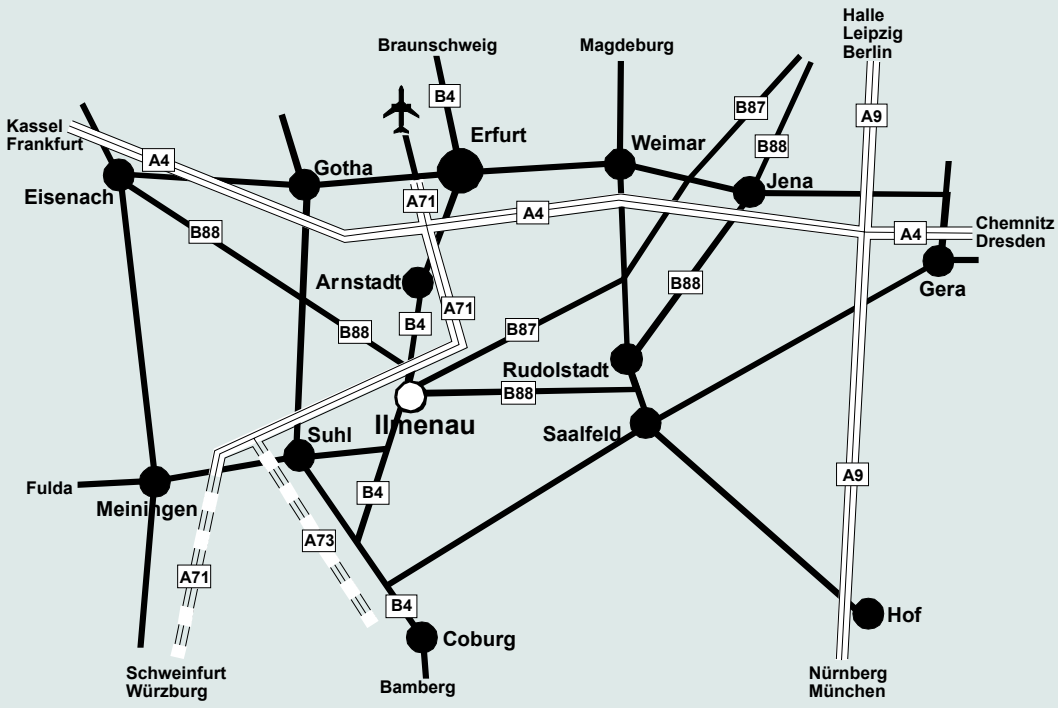

ZMN, Center for Micro- and Nanotechnologies
Gustav-Kirchhoff-Str. 7
98693 Ilmenau, Germany
fon: +49-(0)3699-69-3400
fax: +49-(0)3699-69-3499
email: zmn@tu-ilmenau.de
URL : http://www.zmn.tu-ilmenau.de

Director: Prof. Oliver Ambacher
Contact: Dr. Herwig Döllefeld